Optimization of left ventricular muscle fiber orientation

Optimization of left ventricular muscle fiber orientation

OPTIMIZATION OF LEFT VENTRICULAR MUSCLE FIBER ORIENTATION

PROEFSCHRIFT

ter verkrijging van de graad van doctor aan
de Universiteit Maastricht,
op gezag van de Rector Magnificus, Prof. mr. M.J. Cohen
volgens het besluit van het College van Decanen,
in het openbaar te verdedigen
op donderdag 11 september 1997 om 14.00 uur

door

Johannes Matthias Rijcken

geboren te Enschede in 1968

Promotores:
Prof. dr. ir. T. Arts
Prof. dr. ir. D.H. van Campen (Technische Universiteit Eindhoven)

Co-promotor:
Dr. ir. P.H.M. Bovendeerd (Technische Universiteit Eindhoven)

Beoordelingscommissie:
Prof. dr. R.S. Reneman (voorzitter)
Prof. dr. A. Huson
Prof. dr. ir. A. Hoeks
Dr. K. Nicolay (Universiteit Utrecht)
Dr. ir. A.J.G. Schoofs (Technische Universiteit Eindhoven)

Financial support by the Netherlands Heart Foundation for the publication of this thesis is gratefully acknowledged.

Cover Design by Oli4 Rijcken
Printed by Ponsen & Looijen bv, Wageningen

ISBN 90-9010880-7

Contents

Chapter 1

Introduction

Introduction

The heart is a hollow muscular structure which serves primarily to pump blood around the body. The ventricular walls of the heart consist for an important part of muscle fibers, which are oriented in the walls in a complex but highly organized manner. The heart is capable of adapting, by growth and by changes in structure, to long term changes in mechanical loading of the cardiac walls (9, 10, 12, 18, 19, 21, 22, 36, 40). It appears that in the face of a chronically altered hemodynamic load, the complex distribution of fiber orientation is maintained (6, 38). The underlying mechanisms by which cardiac structure is determined are not clearly understood. In this thesis we sought, by a combination of mathematical modeling and anatomical measurements, to gain insight into the mechanisms which determine the distribution of fiber orientation in the cardiac walls.

This chapter starts with a brief description of aspects of cardiac anatomy that are important to the heart as a load-bearing structure. Following this, aspects of cardiac mechanics are addressed that are possibly related to the heart's ability to adapt to long term changes in mechanical loading. Subsequently, the research objective of the thesis is stated and the strategy employed for its realization is expounded. The chapter is concluded with an outline of the contents of the thesis.

Basic cardiac anatomy

The heart is a hollow muscular organ that pumps blood through the vascular system. The heart consists of two pulsatile pumps which pump in phase with each other. The left heart (fig. 1) receives blood from the lungs and pumps this to the rest of the body. The right heart pumps blood that was received from the rest of the body to the lungs. Each pump consists of a low-pressure reservoir (atrium) and a high-pressure chamber (ventricle) (fig. 1). Blood collects in the atrium and passes through a valve to the ventricle. Contraction of the ventricle causes blood to be squeezed out through valves to the lungs (right heart) or the rest of the body (left heart). The valves are operated by blood pressure differences across the valve leaflets. The atrial-ventricular valves separating the atria from the ventricles are attached to the inner ventricular walls by the chordae tendinae-papillary muscle system. During ventricular contraction the papillary muscles shorten to prevent collapse of the atrial-ventricular valve leaflets.

The left ventricle resembles a thick-walled (truncated) prolate spheroid (5, 13, 43, 50, 54) (fig. 2). The internal surface of a ventricle contains many invaginations of up to one third of the wall thickness (47, 52) (fig. 1). The right

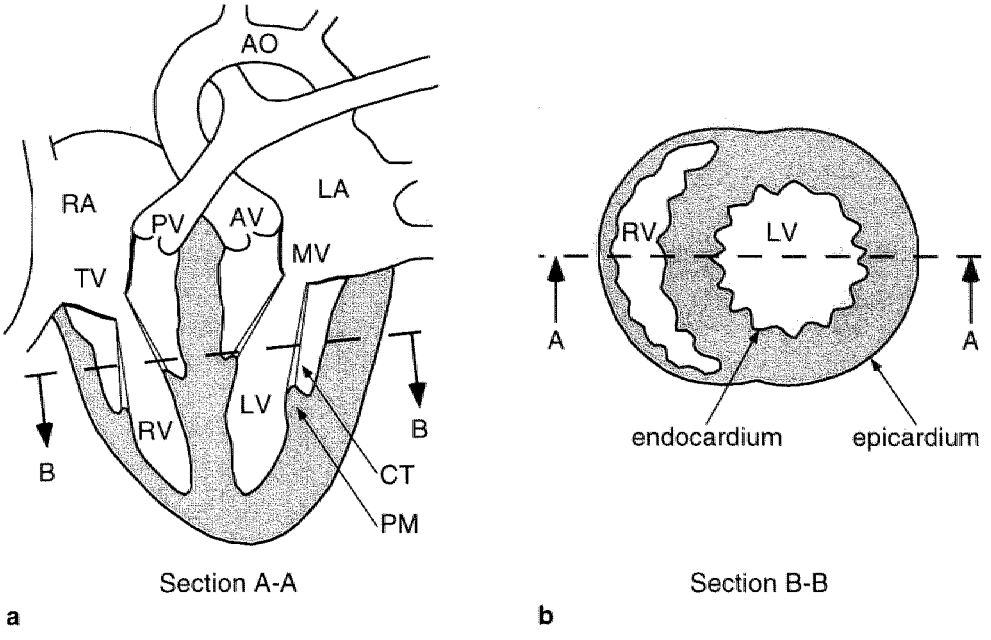

fig. 1. Schematic cross-sections of the heart. (a) Longitudinal cross-section showing left heart (LA and LV) anatomically joined to the right heart but functionally in series with it. (b) Short-axis cross-section. Symbols: AO=aorta, AV=aortic valve, CT=chordae tendinae, LA=left atrium, LV=left ventricle, MV=mitral valve, PM=papillary muscle, PV=pulmonary valve, RA=right atrium, RV=right ventricle, TV=tricuscpid valve.

ventricular wall is positioned around the left ventricle giving the right ventricular cavity a crescent shape when viewed in short-axis section (fig. 1). The right ventricular free wall is considerably thinner than the left ventricular one, owing to the higher cavity pressures prevalent in the latter ventricle (19). The septal wall separates left and right ventricles. We consider the septum as part of the left ventricle (55).

The left ventricular wall consists for an important part (approximately 70% by volume) of muscle cells embedded in interstitial fluid (30, 61). The cells are tethered by an extensive network of connective tissue fibers (7, 31), comprising 1-4% of myocardial volume (61, 62). A dense network of coronary blood vessels perfuses the cardiac tissue (7). Myocardial blood volume is estimated to make up between 10 and 20% of myocardial volume (25, 66). The short rod-shaped muscle cells (length 30-130 μm, diameter 8-20 μm) generally branch and form anastomoses with neighboring cells (51). Within this weave of muscle cells, an average muscle fiber direction can be distinguished (33).

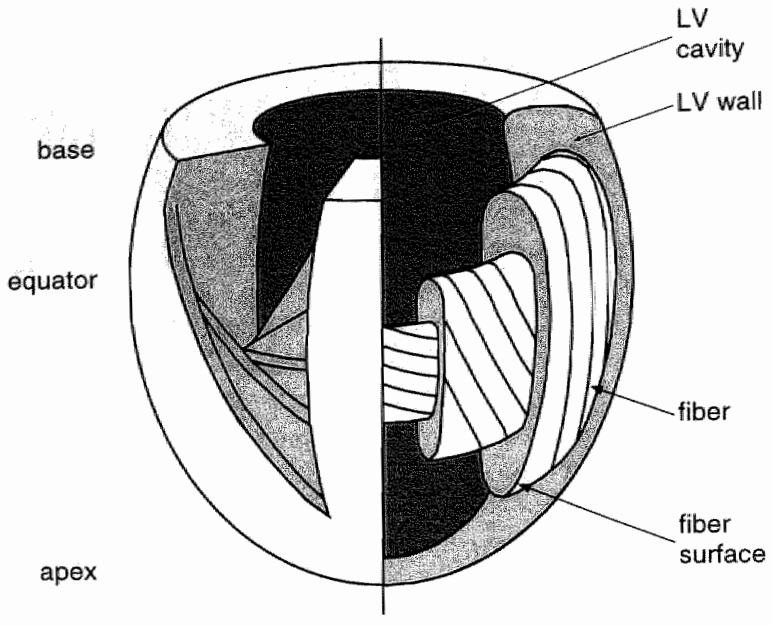

fig. 2. Schematic representations of fiber pathways in the rotationally symmetric left ventricular wall. The mitral and aortic valves in the basal plane as well as the papillary muscles are not shown. Left hand side: helical fiber pathways are represented in layers parallel to the inner and outer wall surfaces. Right hand side: fiber pathways are represented on approximately toroidal shells.

The distribution of muscle fiber direction over the left ventricular wall is rather complex. In mathematical models of the left ventricular wall, muscle fibers commonly described as being helically wound in layers parallel to the wall surfaces (1, 5, 8, 23, 28, 35) (fig. 2). Anatomical dissections (48, 52, 53, 55, 56) indicate that fiber direction also has a transmural component. Near the equator, fiber pathways were found to be almost parallel to the wall surfaces. Towards the base and apex, epicardial fibers penetrated the wall and re-appeared near the endocardial surface. Streeter and coworkers (52, 53, 56) suggested that fibers are wound on imaginary, approximately toroidal surfaces, with the pitch of winding depending on depth in the wall (fig. 2). In the middle of the wall, at the equator, muscle fibers run purely in circumferential direction. On any other toroidal surface, a fiber spirals down the epicardial side of the torus, crosses over to the endocardial side and spirals back up towards the base of the wall.

Regional cardiac mechanics

Experimental studies on the mechanical behavior of the heart focus mainly on the left ventricle. Important quantities for the description of regional mechanics are deformation and stress. To date the direct measurement of stress or force in the wall by a force transducer has proved unreliable due to regional disturbance of the tissue (26). Many methods have been developed to measure regional deformation, in the form of strain or segment length, in the cardiac walls (2, 16, 41, 45, 58, 59). In most methods, strain is determined from the relative movement of markers of various kinds that are attached to the tissue. However, there have been only a few studies in which strain measurements have been related to the local fiber direction (14, 24, 42, 59). In studies in which either fiber strain (14, 42, 59) or sarcomere length (24) were measured during the ejection phase of the cardiac cycle, regional differences were found to be not significant, except perhaps at the junction of right and left ventricles (42). Most of these measurements covered only a small extent of the left ventricular wall. The limited available experimental data suggest that fiber strain is uniformly distributed over the left ventricular wall during the ejection period.

Mathematical models of left ventricular wall mechanics have been developed to provide insight into mechanisms underlying experimental observations. In initial models many simplifying assumptions were made (for review of such models see for example (27, 65)). The left ventricular wall was initially approximated by a thin- or thick-walled sphere or cylinder, and the fibrous nature of myocardial tissue was often ignored. Advances in computer hardware and numerical methods, particularly the finite element method, have made the description of cardiac mechanics increasingly realistic. Thus, more recent models generally consider simultaneously the fibrous nature of cardiac tissue, a realistic description of wall shape, physiological stress-strain relationships and large deformations (1, 5, 23, 28).

The simulations performed with mathematical models indicate that the distributions of fiber stress and strain are sensitive to the choice of the distribution of fiber orientation, even if this choice is made within the range of anatomical findings (5, 28). In models by Huyghe *et al.* (28) and Beyar *et al.* (4) a similar transmural course of stress was predicted for a given distribution of fiber orientation, eventhough different wall geometries were used. Huyghe *et al.* (28) and Bovendeerd *et al.* (5) also showed that transmural courses of fiber orientation within the anatomical range could be chosen, that yielded transmural distributions of systolic fiber stress that were either uniform or varied by more than a factor 2.

Cardiac adaptation

Cardiac adaptation effects can occur as a result of long term changes in hemodynamic load, leading to changes in mechanical loading that are similar in all parts of the cardiac walls. In response to pressure overload (e.g. in hypertension) the left ventricular wall thickens whereas the inner diameter remains practically unchanged (concentric hypertrophy) (22, 37). In response to volume overload (e.g. due to aortic valve regurgitation) the left ventricular wall thickens and the internal diameter increases proportionally (eccentric hypertrophy) (22, 36). Despite the pressure or volume overload the fibrous structure of the left ventricle is maintained (6, 38). The adaptive tissue growth results in normalization of the mechanical load in the wall. For instance, peak wall stress during systole returns to normal following concentric or eccentric hypertrophy (22). Also, in the volume overloaded dog heart, the adaptive growth in fiber and cross-fiber directions is uniformly distributed through the wall (36). By expressing strain data from the latter study with respect to the fiber direction it can be concluded that end-systolic fiber strain referred to end diastole is distributed practically uniformly across the wall both before and after the volume overload. In the compensated stage of progressive pressure overload, removal of the overload leads to complete reversal of the hypertrophy (11). When the overload has advanced to a decompensated stage removal of the overload has been shown to lead to regression of the hypertrophy that is either partial (19, 29, 46, 64) or complete, but only after many years (49).

Adaptation effects also occur in response to direct local changes in mechanical loading of the left ventricular wall. For instance, asynchronous electrical activation of cardiac tissue in the LV wall gives rise to a redistribution of wall mass: the wall thins in regions with lowered load, near the pacing electrode, and thickens in regions with increased load (40). Also, adaptation effects are reported after transection of the chordae tendinae of a single right ventricular papillary muscle (10). The transection resulted in a local loss and disorientation of contractile proteins that was fully reversed following a repair operation.

These findings indicate that a) local differences in mechanical load may be responsible for local differences in growth and other structural adaptations, and b) the adaptations that occur tend to normalize mechanical load in the cardiac walls. It is still unclear which aspects of mechanical load serve as growth stimuli. Candidates are stress, sarcomere length, strain, strain rate, sarcomere shortening, or work done. Experiments on isolated cardiac myocytes in which static strain is applied (32, 60), indicate that strain is likely to be involved in controlling cardiac growth. Static lengthening or shortening of skeletal muscle results in series addition and removal of sarcomeres, respectively (63), indicating that deviation of

sarcomere length from a reference value may serve as growth stimulus.

Research objective

The broad objective of the studies presented in this thesis was to gain insight into the mechanisms by which the fibrous structure of the heart is determined. Mathematical models of left ventricular wall mechanics indicate that the distribution of fiber strain is sensitive to the choice of fiber orientation. Measurements indicate that fiber strain may be homogeneous over the left ventricular wall during the ejection period of the cardiac cycle. Animal experiments indicate that cardiac adaptation mechanisms exist that control mechanical loading of the walls. These observations led us to formulate the following hypothesis regarding the fibrous structure of the left ventricle: the distribution of muscle fiber orientation in the left ventricular wall is such that fiber strain is as homogeneous as possible during the ejection phase of the cardiac cycle. The objective of this thesis was to investigate whether the hypothesis embodies a realistic design principle for the fibrous structure of the heart.

Strategy

The hypothesis linking the distributions of fiber strain and fiber orientation was tested in two steps. Firstly, in a mathematical model of left ventricular wall mechanics a distribution of muscle fiber orientation was predicted that made the distribution of fiber strain as homogeneous as possible. Secondly, the predicted distribution of fiber orientation was compared with experimental data, both reported in literature and resulting from measurements described in this thesis.

The developed mathematical model of left ventricular wall mechanics incorporated realistic wall geometry, large deformations and nonlinear elastic material properties. The model was used as a tool to evaluate the distributions of stress and strain over the left ventricular wall during the cardiac cycle for a given distribution of fiber orientation. Computation of the stress and strain distributions involved the solution of partial differential equations expressing conservation of momentum in the wall. The equations express the static equilibrium of forces due to both blood pressure acting on the inner surface of the wall and forces in the myocardium. Inertial forces, i.e. associated with accelerations, do not play a significant role in the force equilibrium and may be safely ignored (34, 39). The equations were solved numerically by the finite element method (4), using the

commercial finite element package DIANA-5.1 (DIANA Analysis B.V., Delft, The Netherlands). The finite element model of left ventricular wall mechanics was incorporated in an optimization procedure in which inhomogeneities in fiber strain during ejection were minimized by adjustment of fiber orientation. Because the optimization required a lot of computational effort, attention was devoted to computational efficiency (3). The result of the optimization is a distribution of fiber orientation for which inhomogeneities in fiber strain over the left ventricular wall are minimal during ejection.

Experimental data on the distribution of fiber orientation were obtained from literature and from measurements described in this thesis. Current methods to measure fiber orientation rely on anatomical dissection (20, 35, 47, 52, 56) ultrasonic backscatter (61), or diffusion tensor imaging (17, 44). In the latter technique the local three-dimensional diffusion of water is determined. Experiments in cardiac (44) and skeletal muscle (15, 57) confirm that the direction of highest diffusivity corresponds closely to local fiber orientation, as determined by anatomical measurements. In many studies (20, 35, 47, 52), quantification of fiber orientation has concentrated on the component of fiber direction parallel to the ventricular wall surfaces. Measurements of the transmural component of fiber orientation are scarce and restricted to localized regions of the left ventricular wall (52, 56). To obtain more comprehensive and accurate data, we improved the analysis of data obtained by the diffusion tensor imaging method. Thus, the transmural component of fiber orientation in the post-mortem heart could be quantified.

Contents

In **chapter 2**, the finite element model of left ventricular wall mechanics is described. The finite element model is incorporated in an optimization procedure in which the distribution of muscle fiber orientation (described by 3 parameters) is varied to make fiber strain at beginning of ejection as homogeneous as possible. The effect of a transmural component of fiber direction on homogeneity of fiber strain is investigated. The predicted distribution of fiber orientation is compared with reported anatomical measurements. In **chapter 3**, an extended model of left ventricular wall mechanics is used to minimize regional differences in the weighted sum of mean fiber strain and fiber shortening during ejection. The effect of the weighting factor on the optimal fiber angle distribution and on the homogeneity of fiber strain during ejection is studied. Also, for a given value of the weighting factor, the uniqueness of the predicted optimal distribution of fiber orientation is studied.

This was done by evaluating homogeneity of fiber strain during ejection for many distributions of fiber orientation in a broad anatomical range. In **chapter 4** a method based on diffusion tensor imaging is described, that enables quantification of the transmural component of fiber direction in the post-mortem heart. A detailed distribution of fiber orientation (described by 12 parameters) is computed in **chapter 5**. This chapter also includes a comparison of the predicted transmural component of fiber direction with experimental data obtained in chapter 4. The thesis is concluded with a discussion of the findings in **chapter 6**.

References

1. Arts, T., and R. S. Reneman. Dynamics of left ventricular wall and mitral valve mechanics - a model study. *J Biomech* 22: 261-271, 1989.
2. Azhari, H., J. L. Weiss, W. J. Rogers, C. O. Siu, E. A. Zerhouni, and E. P. Shapiro. Noninvasive quantification of principal strains in normal canine hearts using tagged MRI images in 3-D. *Am J Physiol* 264: H205-H216, 1993.
3. Barthelemy, J.-F. M., and R. T. Haftka. Approximation concepts for optimum structural design - a review. *Structural optimization* 5: 129-144, 1993.
4. Beyar, R., and S. Sideman. Left ventricular mechanics related to the local distribution of oxygen demand throughout the wall. *Circ Res* 58: 664-677, 1986.
5. Bovendeerd, P. H. M., T. Arts, J. M. Huyghe, D. H. van Campen, and R. S. Reneman. Dependence of local left ventricular wall mechanics on myocardial fiber orientation: a model study. *J Biomech* 25: 1129-1140, 1992.
6. Carew, T. E., and J. W. Covell. Fiber orientation in the hypertrophied canine left ventricle. *Am J Physiol* 236: H487-H493, 1979.
7. Caulfield, J. B., and T. K. Borg. The collagen network of the heart. *Lab Invest* 40: 364-372, 1979.
8. Chadwick, R. S. Mechanics of the left ventricle. *Biophys J* 39: 279-288, 1982.
9. Cooper IV, G. Cardiocyte adaptation to chronically altered load. *Ann Rev Physiol* 49: 501-518, 1987.
10. Cooper IV, G., R. L. Kent, C. E. Uboh, E. W. Thompson, and T. A. Marino. Hemodynamic versus adrenergic control of cat right ventricular hypertrophy. *J Clin Invest* 75: 1403-1414, 1985.
11. Cooper IV, G., and T. A. Marino. Complete reversibility of cat right ventricular chronic progressive pressure overload. *Circ Res* 54: 323-331, 1984.
12. Cooper IV, G., W. E. Mercer, J. K. Hoober, P. R. Gordon, R. L. Kent, I. K. Lauva, and T. A. Marino. Load regulation of the properties of adult feline cardiocytes: the role of substrate adhesion. *Circ Res* 58: 692-706, 1986.
13. deKemp, R. A., and C. Nahmias. Automated determination of left ventricular long axis in cardiac positron tomography. *Physiol Meas* 17: 95-108, 1996.
14. Delhaas, T., T. Arts, P. H. M. Bovendeerd, F. W. Prinzen, and R. S. Reneman. Subepicardial fiber strain and stress as related to left ventricular pressure and volume. *Am J Physiol* 264: H1548-H1559, 1993.
15. Drost, M. R., G. C. van Donkelaar, L. J. G. Kretzers, and K. Nicolay. A comparison of local muscle fiber direction measured

by diffusion tensor imaging with muscle fiber direction as determined in an actual section. *Fifth scientific meeting of the International Society of Magnetic Resonance in Medicine*, Vancouver, 1997, p. 1717.

16. Fann, J. I., G. E. Sarris, N. B. Ingels Jr., M. A. Niczyporuk, K. L. Yun, G. T. Daughters II, G. C. Derby, and D. C. Miller. Regional epicardial and endocardial two-dimensional finite deformations in canine left ventricle. *Am J Physiol* 261, 1991.
17. Garrido, L., V. J. Wedeen, K. K. Kwong, U. M. Spencer, and H. L. Kantor. Anisotropy of water diffusion in the myocardium of the rat. *Circ Res* 74: 897-793, 1994.
18. Gerdes, A. M. Remodeling of ventricular myocytes during cardiac hypertrophy and heart failure. *J Florida MA* 79: 253-255, 1992.
19. Gerdes, A. M., L. C. Clark, and J. M. Capasso. Regression of cardiac hypertrophy after closing an aortocaval fistula in rats. *Am J Physiol* 268: H2345-H2351, 1995.
20. Greenbaum, R. A., Y. H. Siew, D. G. Gibson, A. E. Becker, and R. H. Anderson. Left ventricular fibre architecture in man. *Br Heart J* 45: 248-263, 1981.
21. Grossman, W. Cardiac hypertrophy: Useful adaptation or pathologic process? *Am J Med* 69: 576-584, 1980.
22. Grossman, W., D. Jones, and L. P. McLaurin. Wall stress and patterns of hypertrophy in the human left ventricle. *J Clin Invest* 56: 56-64, 1975.
23. Guccione, J. M., K. D. Costa, and A. D. McCulloch. Finite element stress analysis of left ventricular mechanics in the beating dog heart. *J Biomech* 28: 1167-1177, 1995.
24. Guccione, J. M., W. G. O'Dell, A. D. McCulloch, and W. C. Hunter. Anterior and posterior left ventricular sarcomere lengths behave similarly during ejection. *Am J Physiol* 272: H469-H477, 1997.
25. Hoffman, J. I. E., and J. A. E. Spaan. Pressure-flow relations in coronary circulation. *Physiol Rev* 70: 331-390, 1990.
26. Huisman, R. F., G. Elzinga, N. Westerhof, and P. Sipkema. Measurement of ventricular wall stress. *Cardiovasc Res* 14: 142-153, 1980.
27. Huisman, R. M., P. Sipkema, N. Westerhof, and G. Elzinga. Comparison of models used to calculate left ventricular wall force. *Med Biol Eng Comput* 18: 133-144, 1980.
28. Huyghe, J. M., T. Arts, D. H. van Campen, and R. S. Reneman. Porous medium finite element model of the beating left ventricle. *Am J Physiol* 262: H1256-H1267, 1992.
29. Ishihara, K., M. R. Zile, M. Nagatsu, K. Nakano, M. Tomita, S. Kanazawa, L. Clamp, G. DeFreyte, and B. A. Carabello. Coronary blood flow after the regression of pressure-overload left ventricular hypertrophy. *Circ Res* 71: 1472-1481, 1992.
30. Kass, D. A., T. A. Traill, M. Keating, P. I. Altieri, and W. L. Maughan. Abnormalities of dynamic ventricular shape change in patients with aortic and mitral valve regurgitation: assessment by fourier shape analysis and global geometry indexes. *Circ Res* 62: 127-138, 1988.
31. LeGrice, I. J., B. H. Smaill, L. Z. Chai, S. G. Edgar, J. B. Gavin, and P. J. Hunter. Laminar structure of the heart: ventricular myocyte arrangement and connective tissue architecture in the dog. *Am J Physiol* 269: H571-H582, 1995.
32. Mann, D. L., R. L. Kent, and G. Cooper IV. Load regulation of the properties of adult feline cardiocytes: growth induction by cellular deformation. *Circ Res* 64: 1079-1090, 1989.
33. McLean, M., and J. Prothero. Determination of relative fiber orientation

in heart muscle: methodological problems. *Anat Rec* 232: 459-465, 1992.

34. Moskowitz, S. E. Effects of inertia and viscoelasticity in late rapid filling of the left ventricle. *J Biomech* 14: 443-445, 1981.
35. Nielsen, P. M. F., I. J. Le Grice, B. H. Smaill, and P. J. Hunter. Mathematical model of geometry and fibrous structure of the heart. *Am J Physiol* 260: H1365-H1378, 1991.
36. Omens, J. H., and J. W. Covell. Transmural distribution of myocardial tissue growth induced by volume-overload hypertrophy in the dog. *Circulation* 84: 1235-1245, 1991.
37. Omens, J. H., D. E. Milkes, and J. W. Covell. Effects of pressure overload on the passive mechanics of the rat left ventricle. *Ann Biomed Eng* 23: 152-163, 1995.
38. Pearlman, E. S., K. T. Weber, J. S. Janicki, G. G. Pietra, and A. P. Fishman. Muscle fiber orientation and connective tissue content in the hypertrophied human heart. *Lab Invest* 46: 158-164, 1982.
39. Peskin, C. S. Fiber architecture of the left ventricular wall: an asymptotic analysis. *Commun Pure Appl Math* 42: 79-113, 1989.
40. Prinzen, F. W., E. C. Cheriex, T. Delhaas, M. F. M. van Oosterhout, T. Arts, H. J. J. Wellens, and R. S. Reneman. Asymmetric thickness of left ventricular wall resulting from asynchronous electric activation: A study in dogs with ventricular pacing and in patients with left bundle branch block. *Am Heart J* 130: 1045-1053, 1995.
41. Prinzen, T. T., T. Arts, F. W. Prinzen, and R. S. Reneman. Mapping of epicardial deformation using a video processing technique. *J Biomech* 19: 263-273, 1986.
42. Rademakers, F. E., W. J. Rogers, W. H. Guier, G. M. Hutchins, C. O. Siu, M. L. Weisfeldt, J. L. Weiss, and E. P. Shapiro. Relation of regional cross-fiber shortening to wall thickening in the intact heart. Three-dimensional strain analysis by NMR tagging. *Circ* 89: 1174-1182, 1994.
43. Rankin, J. S., P. A. McHale, C. E. Arentzen, D. Ling, J. C. J. Greenfield, and R. W. Anderson. The three-dimensional dynamic geometry of the left ventricle in the conscious dog. *Circ Res* 39: 304-313, 1976.
44. Reese, T. G., R. M. Weisskoff, R. N. Smith, B. R. Rosen, R. E. Dinsmore, and V. J. Wedeen. Imaging myocardial fiber architecture in vivo with magnetic resonance. *Magn Reson Med* 34: 786-791, 1995.
45. Rodriguez, E. K., W. C. Hunter, M. J. Royce, M. K. Leppo, A. S. Douglas, and H. F. Weisman. A method to reconstruct myocardial sarcomere lengths and orientations at transmural sites in beating canine hearts. *Am J Physiol* 263: H293-H306, 1992.
46. Roman, M. J., L. Klein, R. B. Devereux, P. Kligfield, N. W. Niles, c. hochreiter, O. W. Isom, and J. S. Borer. Reversal of left ventricular dilatation, hypertrophy, and dysfunction by valve replacement in aortic regurgitation. *Am Heart J* 118: 553-561, 1989.
47. Ross, M. A., and D. D. Streeter Jr. Nonuniform subendocardial fiber orientation in the normal macaque left ventricle. *Eur J Cardiol* 3: 229-247, 1975.
48. Sanchez-Quintana, D., V. Garcia-Martinez, V. Climent, and J. M. Hurle. Morphological changes in the normal pattern of ventricular myoarchitecture in the developing human heart. *Anat Rec* 243: 483-495, 1995.
49. Shigematsu, S., K. Hiramatsu, T. Aizawa, T. Yamada, N. Takasu, A. Niwa, Y. Miyahara, M. Tsujino, and Z. Shimizu. Regression of left ventricular hypertrophy in patients with essential

hypertension: outcome of 12 years antihypertensive treatment. *Cardiology* 77: 280-286, 1990.

50. Slinker, B. K., and S. A. Glantz. The accuracy of inferring left ventricular volume from dimensions depends on the frequency of information needed to answer a given question. *Circ Res* 56: 161-174, 1985.
51. Sommer, J. R., and B. Scherer. Geometry of cell and bundle appositions in cardiac muscle: light microscopy. *Am J Physiol* 248: H792-H803, 1985.
52. Streeter, D. D., Jr. Gross morphology and fiber geometry of the heart. In: *Handbook of physiology - The cardiovascular system I*, edited by R. M. Berne Am. Physiol. Soc., Bethesda, MD, 1979, p. 61-112.
53. Streeter, D. D., Jr., W. E. Powers, M. A. Ross, and F. Torrent-Guasp. Three-dimensional fiber orientation in the mammalian left ventricular wall. In: *Cardiovascular System Dynamics*, edited by J. Baan, A. Noordergraaf and J. Raines. Cambridge, Mass.: M.I.T. Press, 1978, p. 73-84.
54. Streeter, D. D. J., and W. T. Hanna. Engineering mechanics for successive states in canine left ventricular myocardium. 1. Cavity and wall geometry. *Circ Res* 33: 639-655, 1973.
55. Thomas, C. E. The muscular architecture of the ventricles of hog and dog hearts. *Am J Anat* 101: 17-57, 1957.
56. Torrent-Guasp, F. *The cardiac muscle.* Madrid: Fundacin Juan, 1973.
57. van Doorn, A., P. H. M. Bovendeerd, K. Nicolay, M. R. Drost, and J. D. Janssen. Determination of muscle fibre orientation using diffusion-weighted MRI. *Eur J Morphol* 34: 5-10, 1996.
58. Villarreal, F. J., and W. Y. W. Lew. Finite strains in anterior and posterior wall of canine left ventricle. *Am J Physiol* 259: H1409-H1418, 1990.
59. Waldman, L. K., D. Nosan, F. Villareal, and J. W. Covell. Relation between transmural deformation and local myofiber direction in canine left ventricle. *Circ Res* 63: 550-562, 1988.
60. Watson, P. A. function follows form: generation of intracellular signals by cell deformation. *FASEB J* 5: 2013-2019, 1991.
61. Wickline, S. A., E. D. Verdonk, and J. G. Miller. Three-dimensional characterization of human ventricular myofiber architecture by ultrasonic backscatter. *J Clin Invest* 88: 438-446, 1991.
62. Wickline, S. A., E. D. Verdonk, A. K. Wong, R. K. Shepard, and J. G. Miller. Structural remodeling of human myocardial tissue after infarction. *Circ* 85: 259-268, 1992.
63. Williams, P. E., and G. Goldspink. Changes in sarcomere length and physiological properties in immobilized muscle. *J Anat* 127: 459-468, 1978.
64. Wisenbaugh, T., and W. O'Connor. Right ventricular hypertrophy long after reversal of severe pressure overload in cats. *Am J Physiol* 254: H1099-H1104, 1988.
65. Yin, F. C. P. Ventricular wall stress. *Circ Res* 49: 829-842, 1981.
66. Yin, F. C. P., C. C. H. Chan, and R. J. Judd. Compressibility of passive myocardium. *Am J Physiol* 271: H1864-H1870, 1996.

Chapter 2

Optimization of cardiac fiber orientation for homogeneous fiber strain at beginning of ejection

J. Rijcken[1], P.H.M. Bovendeerd[2], A.J.G. Schoofs[2], D.H. van Campen[2], T. Arts[1]

[1] Department of Biophysics, Cardiovascular Research Institute, Maastricht University, Maastricht, The Netherlands,
[2] Department of Mechanical Engineering, Eindhoven University of Technology, Eindhoven, The Netherlands.

J Biomechanics (in press)

Abstract

Mathematical models of left ventricular (LV) wall mechanics show that fiber stress depends heavily on the choice of muscle fiber orientation in the wall. This finding brought us to the hypothesis that fiber orientation may be such that mechanical load in the wall is homogeneous. Aim of this study was to use the hypothesis to compute a distribution of fiber orientation within the wall.

In a finite element model of LV wall mechanics, fiber stresses and strains were calculated at beginning of ejection (BE). Local fiber orientation was quantified by helix (HA) and transverse (TA) fiber angles using a coordinate system with local r-, c-, and l- directions perpendicular to the wall, along the circumference and along the meridian respectively. The angle between the c-direction and the projection of the fiber direction on the cl-plane (HA) varied linearly with transmural position in the wall. The angle between the c-direction and the projection of the fiber direction on the cr-plane (TA) was zero at the epicardial and endocardial surfaces. Midwall TA increased with distance from the equator. Fiber orientation was optimized so that fiber strains at BE were as homogeneous as possible.

By optimization with TA=0°, HA was found to vary from 81.0° at the endocardium to -35.8° at the epicardium. Inclusion of TA in the optimization changed these angles to respectively 90.1° and -48.2° while maximum TA was 15.3°. Then the standard deviation of fiber strain (ε_f) at BE decreased from ±12.5% of mean ε_f to ±9.5%. The root mean square (RMS) difference between computed HA and experimental data reported in literature was 15.0° compared to an RMS difference of 11.6° for a linear regression line through the latter data.

Keywords: left ventricle, fibers, optimization, finite element analysis

Introduction

Within the cardiac wall, stress and strain are important determinants of the distributions over the cardiac wall of blood flow, oxygen consumption (9) and tissue adaptation effects (2). Experimental assessment of the stress and strain distributions over the wall is difficult. Strain can be accurately measured at only a limited number of sites in the wall (28, 42). The reliability of the measurement of wall stress is limited, because insertion of a force transducer damages the tissue at the site of measurement (14). In the assessment of cardiac function, stress and strain expressed with respect to muscle fiber orientation is most relevant. However, accurate knowledge of regional muscle fiber orientation is often not available.

Because of these experimental limitations, mathematical models have been developed to facilitate assessment of the distributions of stress and strain. Advances in computer hardware and numerical methods have enabled an increasing number of aspects of cardiac mechanics to be simulated. The more recent models generally consider the fibrous nature of cardiac tissue, increasingly accurate descriptions of wall shape, nonlinear stress-strain relationships and finite deformations (3, 5, 13, 15). Unfortunately the predicted distributions of fiber stress and strain disagree. Guccione *et al.* (13) used a measured wall geometry and distribution of fiber orientation and calculated an inhomogeneous distribution of fiber stress and strain. Bovendeerd *et al.* (5) and Huyghe *et al.* (15) adapted fiber orientation heuristically so that the distribution of fiber stress was more even. The thus determined fiber orientation appeared not to be significantly different from what has been measured in experiments (22, 33). The latter models indicate that the distribution of fiber stress is sensitive to the distribution of fiber orientation, even within the limits of biological variance. Combining this finding with the fact that muscle fiber contraction is most efficient for a particular combination of fiber shortening and fiber stress, we came to the hypothesis that mechanical load may be distributed evenly over the wall by proper adjustment of local fiber orientation. Various experimental findings are in compliance with homogeneous mechanical loading of the LV wall. If the distribution of mechanical load is disturbed, adaptation effects, such as growth (7, 12, 27) or changes in fiber orientation (6, 25) result in at least partial recovery to the original loading level.

In this study we predicted the orientation of muscle fibers using the hypothesis that mechanical load in the cardiac wall is homogeneous. In a finite element model of LV wall mechanics the distribution of fiber stress and strain over the wall was calculated at a single moment during the cardiac cycle for given fiber orientation and given stiffness of the fibers. In the reference state of deformation left ventricular cavity pressure was zero and wall stress was zero everywhere. The

stress state at beginning of ejection was obtained by stiffening of the fibers while pressurizing the cavity. In an optimization procedure inhomogeneity of mechanical load, defined as the variance of fiber strain at the beginning of ejection, was minimized by proper adjustment of the fiber orientation. The thus predicted fiber orientation was compared with anatomical findings.

Methods

Finite element model of left ventricular wall mechanics

Reference state . To calculate fiber stresses and strains with a finite element model a reference state must be defined. We used as a reference the state in which transmural pressure across the LV wall and the stresses in the wall were 0 kPa.

Geometry. In the reference state the LV wall is considered thick-walled and rotationally symmetric around the long axis. The center of the equatorial plane is a point of symmetry. Consequently, only the mechanics of the region between the apex and equator was considered. The shape of the LV wall in the reference state was defined by a prolate spheroidal midwall surface with a wall thickness perpendicular to the midwall. The wall shape was defined by five parameters (Appendix) whose values were chosen so that the LV had given values for: cavity volume, ratio of cavity-to-wall-volume, ratio of equatorial-to-apical-wall-thickness, and ratio of midwall-long-to-short-axes. The geometry parameters were also such that wall thickness decreased smoothly from equator to apex. For the evaluation of cavity and wall volumes it was assumed that the base extended vertically above the equatorial plane by a distance equal to half the semi-major axis of the midwall surface (37). The choice of parameter values of the finite element model, including LV wall geometry, are described in a separate section below.

Fiber orientation. Fiber orientation in the reference state was quantified by the helix and transverse fiber angles (33) measured with respect to the local transmural, circumferential and longitudinal directions (fig. 1). To be able to define the local transmural, circumferential and longitudinal directions, we first define a wall-bound coordinate system (u, v) (fig. 2); the coordinate u decreases from 0 at the equator to -1 at the apex in direct proportion with distance along the midwall surface in the equator-to-apex direction; the coordinate v increases from -1 at the endocardium to +1 at the epicardium in direct proportion with distance in the direction perpendicular to the midwall surface. The local transmural direction was then defined as the outward normal to a surface of constant v. The local longitudinal direction is orthogonal to both the transmural and circumferential directions. The helix fiber angle was defined as the angle between the local

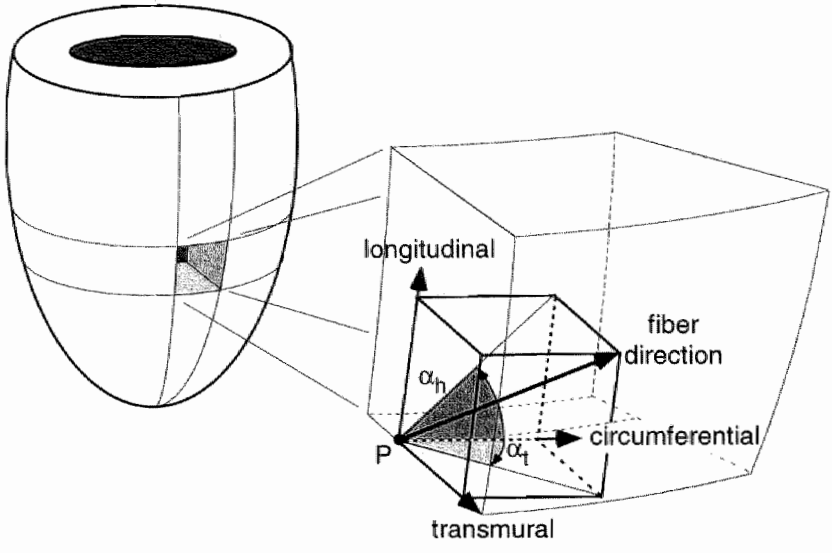

fig. 1. Illustration of the helix (α_h) and transverse (α_t) fiber angles in the rotationally symmetric LV. The fiber angles at a point P are defined with respect to the local transmural, longitudinal and circumferential directions.

circumferential direction and the projection of the fiber direction on the plane perpendicular to the local transmural direction. The transverse fiber angle determines the degree to which fibers cross over between inner and outer wall surfaces. It was defined as the angle between the local circumferential direction and the projection of the fiber direction on the plane perpendicular to the local longitudinal direction. The spatial distributions of the helix and transverse fiber angles are specified with respect to the wall-bound coordinate system (u, v). The helix fiber angle, α_h, varies with v according to (fig. 3):

$$\alpha_h(v) = p_1 + p_2\, v, \qquad [1]$$

where p_1 and p_2 are parameters whose optimal values are to be determined. The transverse fiber angle, α_t, is zero at the wall boundaries, i.e. fibers are assumed not to end here. Because the equatorial plane is a plane of symmetry, α_t is an odd function in coordinate u (35). To satisfy the latter conditions, we used the following

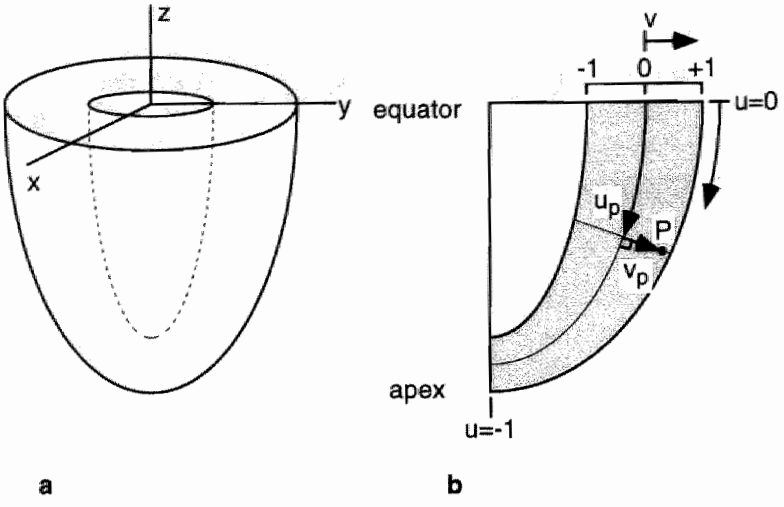

fig. 2. Diagram showing rotationally symmetric LV geometry and coordinate systems: (a) cartesian coordinate system (x,y,z) and (b) wall-bound coordinate system (u,v): point P has coordinates (u_p,v_p). Both u and v vary linearly with distance.

equation (fig. 3):

$$\alpha_t(u,v) = p_3(1-v^2)\sin(\pi u/2), \qquad [2]$$

where parameter p_3 has to be optimized.

Constitutive behavior. The aim of this section is the development of a mathematical relation between the second Piola-Kirchhoff stress and the Green-Lagrange strain for cardiac tissue. Myocardial tissue is a mixture of several components. Interlacing networks of branching muscle fibers and blood vessels are tethered by collagen fibers and surrounded by intercellular fluids. The muscle fibers contain sarcomeres, protein units capable of generating contractile force under the influence of calcium ions. In the model, myocardial tissue is assumed to consist of stiff elastic muscle fibers embedded in a soft elastic tissue matrix.

The deformation of the tissue is described by the deformation gradient tensor, **F**, which maps an infinitesimal material vector in the reference state, $d\mathbf{x}_0$, to a material vector, $d\mathbf{x}$, in the deformed state (18):

$$d\mathbf{x} = \mathbf{F} \bullet d\mathbf{x}_0. \qquad [3]$$

The Green-Lagrange strain, **E**, is related to **F** by

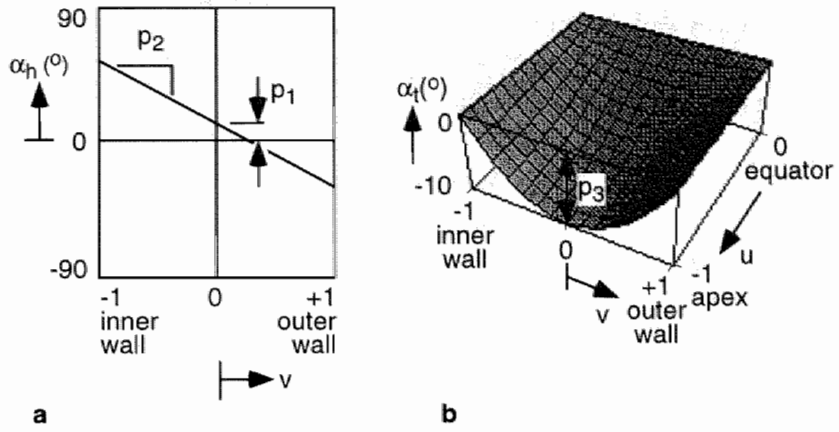

fig. 3. Variation of the fiber angles over the LV wall: (a) the helix fiber angle, α_h, changes linearly between inner and outer walls with intercept p_1 and slope p_2; (b) the transverse fiber angle, α_t, changes quadratically in transmural direction and sinusoidally in equator-to-apex direction. Parameter p_3, the depth of the valley, is used to optimize α_t.

$$\mathbf{E} = \frac{1}{2}(\mathbf{F}^T \bullet \mathbf{F} - \mathbf{I}), \qquad [4]$$

where **I** is the identity tensor and superscript *T* stands for transpose. Strains are expressed with respect to a local coordinate system: one of the coordinate axes points in the fiber direction, $\mathbf{e}_f$, and the other two are perpendicular to it. With respect to this fiber-bound coordinate system the Green-Lagrange strain tensor, **E**, has components E_{ij}. E_{11} is the strain in the fiber direction. The sarcomeres are aligned with the fiber direction (20). Sarcomere length, l_s (μm), is related to strain in the fiber direction, E_{11}, by

$$l_s = l_{s,0}\,(2E_{11} + 1)^{1/2}, \qquad [5]$$

where $l_{s,0}$ (μm) is sarcomere length in the reference state.

The total second Piola-Kirchhoff stress, **S**, in the tissue is the sum of a passive component, $\mathbf{S}_p$, that arises from deformation of passive myocardial tissue and a uniaxial first Piola-Kirchhoff stress, T_a^0, along the fiber direction, $\mathbf{e}_f$, arising from muscle fiber contraction:

$$\mathbf{S} = \mathbf{S}_p + T_a^0\,\mathbf{e}_f\mathbf{e}_f \bullet \left(\mathbf{F}^{-1}\right)^T. \qquad [6]$$

The passive myocardial tissue was assumed to be elastic and transversely isotropic. The strain energy density, W(**E**), of the passive tissue is related to the strain components E_{ij} (adapted from (5)):

$$W(\mathbf{E}) = a_0\left(\exp(a_1 I_E^2 + a_2 II_E + a_3\, \mathbf{e}_f \bullet \mathbf{E} \bullet \mathbf{e}_f) - 1\right) + a_4\left(\det(2\mathbf{E}+\mathbf{I}) - 1\right)^2, \quad [7]$$

where $I_E = \text{trace}(\mathbf{E})$,

$$II_E = \frac{1}{2}\left(\text{trace}\left(\mathbf{E} \bullet \mathbf{E}^T\right) - I_E^2\right),$$

and a_0, a_1, a_2, a_3, and a_4 are material parameters. The second Piola-Kirchhoff stress in the passive tissue, $\mathbf{S}_p$, is obtained by differentiation of equation [7] with respect to **E**:

$$\mathbf{S}_p = \partial W(\mathbf{E}) / \partial \mathbf{E}. \quad [8]$$

The passive second Piola-Kirchhoff stress, $\mathbf{S}_p$, is zero in the unstrained state and increases exponentially with strain.

Muscle fiber contraction in the real LV depends on sarcomere length, sarcomere velocity of shortening, time and extracellular calcium concentration (8). In the finite element simulations the first Piola-Kirchhoff fiber stress, T_a^0 (kPa) depended linearly on sarcomere length, l_s (μm), and active stiffness, K (kPa μm^{-1}):

$$T_a^0 = K(l_s - l_{s,0}). \quad [9]$$

For physiological circumstances such a linear relationship is quite an accurate description throughout the cardiac cycle (30). In the reference state sarcomeres have a uniform length, $l_{s,0}$ (μm), while cavity pressure is zero and cavity-to-wall-volume ratio corresponds to mid-diastole. In this state the left ventricular wall is stress-free, regardless of active stiffness, K. To obtain the stress state at beginning of ejection, the stiffness, K, was estimated such that at the cavity pressure of beginning of ejection a physiologically realistic cavity-to-wall-volume ratio resulted.

Equations solved. Calculations of fiber stresses and strains in the LV wall were based on the law of conservation of momentum (18). Neglecting inertial (21, 26) and gravitational effects, conservation of momentum expresses the static equilibrium of forces in the wall due to blood pressure in the cavity and internal stresses in the wall:

$$\nabla \bullet \left(\mathbf{S} \bullet \mathbf{F}^T \right) = \mathbf{0}. \qquad [10]$$

Solution method. In principle the solution to the equations can be expressed in terms of the displacements of all points in the wall. A Galerkin-based finite element method, implemented in the package DIANA-5.1 (Diana Analysis B.V., Delft, The Netherlands), was used to calculate the displacements of a finite number of points, so-called nodes. Quadratic interpolation was used to determine the displacements of points in between the nodes. Nodes are grouped into elements which constitute the building blocks of the LV wall. To reduce the computational effort, we used the rotational symmetry of the LV wall in the model. The LV wall mesh comprised only the 1/8th-section of the LV in the region ($x \geq 0$, $y \geq 0$, $z \leq 0$) (fig. 2). The mesh consisted of 27 twenty-node brick elements with 3 element layers in the transmural direction and 5 in the equator-to-apex direction. Kinematic boundary conditions on the through-wall faces of the mesh allowed cavity volume changes and torsion to occur. The LV inner wall surface was loaded perpendicularly by cavity pressure while the outer wall surface experienced no external forces.

Design of finite element simulations. Finite element simulations started in the reference state of deformation, corresponding to approximately mid-diastole. The state of deformation and stress at the beginning of ejection was obtained by applying a cavity pressure of 10.64 kPa (80 mm Hg). The stiffness, K, was chosen such that after application of the cavity pressure loading, the cavity-to-wall-volume ratio was about 0.6. This volume ratio and pressure were considered representative for the beginning of ejection (10).

Quantification of mechanical load. Regional mechanical load was quantified as fiber strain at the beginning of ejection. The LV wall mesh was divided into 729 regions with similar volumes. Sarcomere length at the central point of a region was considered representative for that region. For region i, fiber strain, $\varepsilon_{f,i}$, is given by

$$\varepsilon_{f,i} = \frac{l_{s,i} - l_{s,0}}{l_{s,0}}, \qquad [11]$$

where $l_{s,i}$ is the instantaneous sarcomere length in the region and $l_{s,0}$ is the sarcomere length in the reference state.

Optimization procedure

Fiber orientation was optimized to make regional differences in mechanical load as small as possible. The optimization consists of minimizing an objective function, G, defined as the variance of fiber strain at beginning of ejection normalized to the average fiber strain at beginning of ejection:

$$G(\mathbf{p}) = \sum_i w_i \left(\frac{\varepsilon_{f,i} - \varepsilon_{f,av}}{\varepsilon_{f,av}} \right)^2 . \qquad [12]$$

G depends on the fiber orientation parameters p_1, p_2, and p_3 which are stored in the vector $\mathbf{p}$. Region i, representing a fraction w_i of the total wall volume, has a representative fiber strain at beginning of ejection, $\varepsilon_{f,i}$. The average fiber strain at beginning of ejection, $\varepsilon_{f,av}$, is the wall volume-weighted sum of the regional fiber strains.

Most optimization methods require many evaluations of the objective function. Since evaluation of G with the finite element model is computationally expensive, the concept of sequential approximate optimization was used (4). For a given set of fiber orientation parameters, $\mathbf{p}_k$, a finite element analysis was performed to evaluate regional fiber strains, $\varepsilon_{f,i}$, at beginning of ejection. By perturbing the fiber orientation parameters one at a time by 1° and using the already available state of deformation and stress as a first estimate, the regional fiber strains for the perturbed set of fiber orientation parameters were computed, with little additional computational effort. Hence, finite difference derivatives of regional fiber strains with respect to $\mathbf{p}$ at $\mathbf{p}_k$ were obtained. Regional fiber strains, $\hat{\varepsilon}_{f,i}$, were estimated for arbitrary $\mathbf{p}$ by performing a first order Taylor series expansion on $\varepsilon_{f,i}$ around the value $\mathbf{p}_k$:

$$\hat{\varepsilon}_{f,i}(\mathbf{p}) = \varepsilon_{f,i}(\mathbf{p}_k) + \sum_{j=1}^{n} (p_j - p_{k,j}) \frac{\partial}{\partial p_j} \varepsilon_{f,i}(\mathbf{p}_k), \qquad i=1,2,...,N \qquad [13]$$

where $p_{k,j}$ and p_j are the j^{th} components of $\mathbf{p}_k$ and $\mathbf{p}$ respectively. The partial derivatives $\partial/\partial p_j$ were calculated as finite difference derivatives. The numbers n and N refer to the number of fiber orientation parameters, and to the number of regions in the LV wall mesh (N=729) respectively. By substitution of equation [13] in [12], an approximation model, $\hat{G}$, is obtained which gives an estimate of the objective function, G, for an arbitrary set of fiber orientation parameters:

$$\hat{G}(\mathbf{p}) = \sum_i w_i \left(\frac{\hat{\varepsilon}_{f,i} - \hat{\varepsilon}_{f,av}}{\hat{\varepsilon}_{f,av}} \right)^2 . \qquad [14]$$

Repeated evaluation of $\hat{G}$ is very efficient due to the explicit dependence on $\mathbf{p}$. The function, $\hat{G}$, is minimized by a sequential quadratic programming algorithm (31). This algorithm requires limits on the parameter values. The parameters p_1, p_2, and

p_3 were allowed to vary in the range (-90°,+90°), (-90°,0°) and (-90°,+90°) respectively. The result of the optimization of the approximation model is a new set of fiber orientation parameters, $\mathbf{p}_{k+1}$. Two checks are performed to evaluate whether convergence has occurred. The finite element evaluations of the objective function of the current and previous iterations, $G(\mathbf{p}_k)$ and $G(\mathbf{p}_{k-1})$, should agree to within a tolerance of δ:

$$\left|(G(\mathbf{p}_k) - G(\mathbf{p}_{k-1}))/G(\mathbf{p}_k)\right| \leq \delta, \qquad [15]$$

where δ=0.0001. Furthermore, the optimum of the approximation model based on parameters $\mathbf{p}_k$, $\hat{G}_{opt,\mathbf{p}_k}$, should coincide with the finite element evaluation of the objective function at $\mathbf{p}_k$, to the same tolerance of δ:

$$\left|\left(G(\mathbf{p}_k) - \hat{G}_{opt,\mathbf{p}_k}\right)/G(\mathbf{p}_k)\right| \leq \delta. \qquad [16]$$

If convergence has not occurred a new approximation model is set up around the parameters $\mathbf{p}_{k+1}$ and the process is repeated. Because the optimization results may depend on the starting values, it is expedient to perform optimizations with several starting values.

Applied parameter values in finite element model

Wall geometry in reference state. In potassium-arrested canine left ventricles cavity volume and wall mass were reported to be 40±9 ml and 145±19 g (19). Assuming a tissue density of 1.05 g cm^{-3} measured wall volume is 138 ml. In the model we have used a cavity volume of 42 ml, and a cavity-to-wall volume ratio of 0.3. The ratio of midwall long-to-short axes was set to 2.08 (37). From preliminary calculations of fiber stress and strain we found that fiber stress was most homogeneous if we chose the ratio of equatorial-to-apical wall thickness to be 3.0. Parameter values are summarized in table 1.

Sarcomere length in reference state. In rat LVs that were formalin-fixed at zero transmural pressure, sarcomere lengths have been measured as 2.04±0.02 μm (mean±sd) (11, corrected for 4.2% shrinkage) and as 1.83±0.06 μm (29). In formalin-fixed dog LVs at zero transmural pressure, sarcomere lengths have been measured as 2.00 μm (32, corrected for shrinkage). In the model, sarcomere length in the reference state, $l_{s,0}$, was set to 1.95 μm for all sarcomeres in the LV wall.

Constitutive behavior. The values of passive material parameters a_0, a_1, a_2 and a_3 were taken from (5) (table 1). Equibiaxial stretching experiments on sheets of passive canine myocardium (44) indicate that the ratio of fiber to cross-fiber

LV wall geometry		Passive material behavior		Contractile material behavior	
V_{lv}	40 ml	a_0	0.5 kPa	$l_{s,0}$	1.95 μm
VR	0.3	a_1	3	K	77.0 kPa/μm
WTR	3.0	a_2	6		
MAR	2.08	a_3	3		
		a_4	500 kPa		

Table 1. Parameter values for model of left ventricular (LV) wall mechanics. Wall geometry in the reference state was chosen so that the following parameters had given values: cavity volume (V_{lv}), ratio of cavity-to-wall-volume (VR), ratio of equatorial-to-apical-wall-thickness (WTR), and ratio of midwall-long-to-short-axis (MAR). Passive material properties are described by parameters a_0, a_1, a_2, a_3, a_4 (equation [7]). Sarcomere length in the reference state is denoted by $l_{s,0}$. Active fiber stiffness at beginning of ejection is denoted by K (equation [9]).

stress ranges from 1.10 to 2.95. In the present model the values of parameters a_1, a_2 and a_3 were set such that the ratio is 2.0 under equibiaxial loading. The absolute values of a_0 and a_1 were chosen so that calculated passive pressure-volume curves agreed with experiments on canine hearts (23). The volume of the myocardium may change by a few percent as a result of changes in coronary inflow and outflow during the cardiac cycle (16, 43). For simplicity, we have assumed that the LV wall is near-incompressible. The value of a_4 was chosen large enough so that in the simulations numerical stability was maintained and LV wall volume changed by less than 2%.

In experiments (40), the sarcomere length at which no contractile force can be generated has been measured as about 1.6 μm. For simplicity of calculation we have chosen a zero-force length equal to $l_{s,0}$, so that the reference state is stress-free, regardless of the instantaneous active stiffness, K. Using the finite element model, the stiffness of the fibers was chosen so that fiber stress at beginning of ejection was physiological. This resulted in a value of 77.0 kPa μm^{-1} for K.

Finite element mesh. The size of the elements was not changed to investigate their influence on the computed stress and strain distributions. However, for a given distribution of fiber orientation the predicted stress and strain distributions were similar to those predicted by an independently developed finite element model of LV wall mechanics by Huyghe *et al.* (15).

Performed optimizations

Two sets of optimizations, optim1 and optim2, were carried out. In optim1 regional differences in mechanical loading were minimized by optimizing only the

helix fiber angle parameters p_1 and p_2 for the case without any fiber cross-over (p_3=0°). Three optimizations were performed in which the starting values in degrees for (p_1, p_2) were (0,0), (0,-90), and (90,0). In optim2 the fiber cross-over parameter p_3 was included. Seven different sets of starting values were tried for (p_1, p_2, p_3): (0,0,0), (0,-90,0), (90,0,0), (0,0,90), (0,-90,-90), (0,-90,90), and (0,0,-90). The optimizations required between 5 and 16 finite element evaluations of mechanical load. Each finite element analysis required about one CPU-hour on a Sun SPARC-ELC workstation with 24 MB RAM.

Results

In optim1 a single minimum in inhomogeneity of mechanical load was found, with optimized values of p_1 and p_2 of respectively 22.57° and -58.41°. For a wide range of starting values a fiber orientation resulted in which subendocardial fiber paths resembled a right-handed and subepicardial fiber paths a left-handed helix. At the optimum, fiber strain, ε_f, at the beginning of ejection was 0.103±0.013 (mean±sd), if 6 % of the LV wall volume near the apex was excluded (information from the three elements in the mesh adjoining the apex). The coefficient of variation of fiber strain at beginning of ejection, defined as the standard deviation divided by the mean, was 12.5 %. For the whole LV wall, fiber strain at the beginning of ejection was 0.102±0.020 and the coefficient of variation 20.0 %.

In optim2 a single optimum was also found: p_1=20.96°, p_2=-69.21° and p_3=15.33°. For the computed optimum, fiber strain at the beginning of ejection was 0.111±0.011 and the coefficient of variation 9.5 %, if 6 % of the wall volume near the apex was excluded. For the whole LV the fiber strain at the beginning of ejection (fig. 4) was 0.111±0.016 and the coefficient of variation 14.4 %.

Discussion

A finite element model of LV wall mechanics has been developed in which regional mechanical load can be calculated for given fiber orientation, LV cavity pressure, wall geometry and material properties. Regional mechanical load was quantified as fiber strain at the beginning of ejection. Regional differences in mechanical load have been successfully minimized by proper adjustment of fiber orientation. A helical arrangement of fibers in the LV wall formed automatically for a wide range of starting values of the parameters describing the distribution of fiber orientation. Inclusion of fiber cross-over between inner and outer wall surfaces in

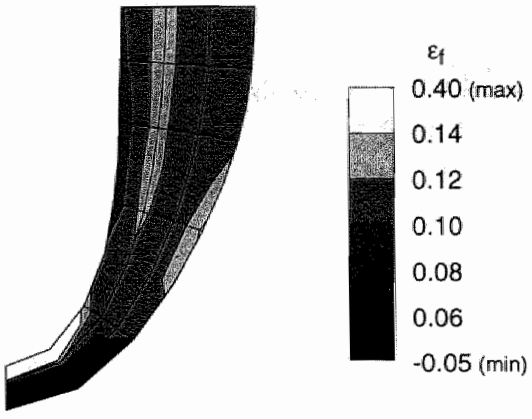

fig. 4. Distribution of fiber strain at the beginning of ejection after optimization of fiber orientation parameters p_1, p_2 and, p_3. Fiber strain over whole LV wall is 0.111±0.016 (mean±sd).

the optimization further reduced load inhomogeneity.

For simplicity, residual load has not been incorporated in the present finite element model of LV wall mechanics. Residual circumferential strain in the unloaded LV wall (zero transmural pressure) has been revealed in the rat heart by making a longitudinal-transmural cut in the LV wall, upon which the wall opens (24). Several studies have emphasized the importance of residual load for accurate prediction of passive mechanical behavior (17), as a potential mediator during cardiac morphogenesis (39), and for its potential effect on systolic wall stress (38). Experiments in the rat heart indicate that circumferential residual strain leads to a transmural gradient in sarcomere length in the unloaded LV of the rat, with sarcomeres in the subepicardium being longer than those in the subendocardium (29). At positive filling pressures, sarcomere length becomes more uniformly distributed over the LV wall of the rat (11), indicating that residual strain may contribute to homogeneity of fiber strain at beginning of ejection.

Solving optimization problems requiring stress analyses by the finite element method easily leads to unacceptably large computational efforts. Computational efficiency can be manipulated by the number of elements in the finite element mesh and by the number of time steps during the cardiac cycle included in the evaluation of the objective function. We have tried to limit the computational effort in three main ways. First, the number of finite element analyses was reduced by using a suitable optimization strategy, namely sequential approximate optimization (4). Second, we quantified mechanical load as regional fiber strain at the beginning of ejection relative to the diastolic reference state. Hence, evaluation of the objective

function by the finite element method required only strain information at the beginning of ejection, not throughout the whole cardiac cycle. Other finite element simulations of LV wall mechanics (5) show that the distribution of fiber stress at beginning of ejection gives a good approximation of the stress distribution during the entire ejection phase. In our model of LV wall mechanics, cardiac tissue is elastic and the stiffness uniform so that homogeneity of fiber stress automatically implies homogeneity of fiber strain. Therefore, by making fiber strain at the beginning of ejection as homogeneous as possible, we expect, to a good approximation, to have made fiber strain homogeneous during the entire ejection phase. Third, we chose a simplified constitutive law for contracting cardiac tissue in which the zero-force sarcomere length equals the sarcomere length in the reference state. As a direct computational gain, the reference state is then stress-free regardless of the active stiffness so that the state of beginning of ejection can be reached by merely loading the endocardial surface with cavity pressure. To make fiber stresses at beginning of ejection physiological the active fiber stiffness was chosen such that cavity pressure and volume had physiological values (1). Following optimization of fiber orientation, fiber stress at beginning of ejection is both physiological and homogeneous (with a coefficient of variation less than 10 %). In conclusion, the measures we have taken to restrict computational effort have made the optimization problem more manageable.

Fiber strains near the apex remain inhomogeneous (fig. 4), despite optimization of fiber orientation. Others (26) who have calculated left ventricular fiber orientation in a mathematical model have ignored the apex on the basis that apical fibers are an integral part of the right ventricle (41). We have included the apex in our model, but recognize that the description of its mechanics is probably erroneous due to an inadequate description of fiber orientation, wall geometry and possibly also material properties. After all, the apex itself is a singular point in the mathematical description of the distribution of fiber orientation. As a consequence we have presented the results of optimizing fiber orientation in the whole LV wall both with and without information from the three elements (6% of wall volume) adjoining the apex.

The choice of the number and nature of the fiber orientation parameters in the model is somewhat arbitrary. Our aim was to use as few parameters as possible that still allowed a reasonable description of measured fiber angles. Within limits, more parameters would result in more homogeneous loading of the wall as indicated in this study by the improvement in load homogeneity when adding transverse fiber angle parameter, p_3, to the two helix angle parameters. Additional helix fiber angle parameters can be chosen on the basis of anatomical measurements which reflect that (1) helix fiber angle is a nonlinear function of

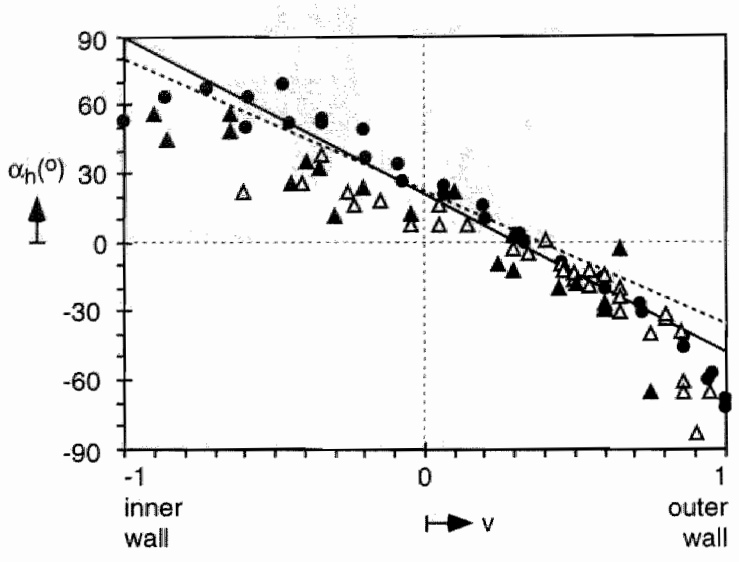

fig. 5. Comparison of measured and computed helix fiber angle, α_h, as a function of transmural position in the wall, v. Measurements: (●) Streeter (33), from equatorial region of human LV, (▲) Nielsen *et al.* (22), from equatorial region of canine LV, (▲) Nielsen *et al.* (22), from adjacent more apical region of canine LV. Computations: (.....) optimization of parameters p_1 and p_2, (——) optimization of parameters p_1, p_2 and p_3.

transmural position, especially close to the wall boundaries (22, 33, 36) and (2) helix fiber angle increases towards the apex (34). Inclusion of fiber angle parameters in the optimization that allow such behavior are likely to further improve load homogeneity.

To assess the physiological relevance of the computed transmural course of helix fiber angle, comparisons were made with reported measurements (22, 33) and model predictions (2, 5, 26). The anatomical measurements were performed in the equatorial and adjacent more apical regions of human and canine left ventricles (22, 33) (fig. 5). For a quantitative comparison, the root mean square (RMS) difference between the computed transmural course of helix fiber angle and a measured data set was determined (table 2). Since the ability to describe the measured data with a straight line is limited by inherent scatter, the RMS differences of linear regression lines to the measurements were also determined. Table 2 shows that the RMS differences of the computed transmural course of helix angle are only slightly larger (range: 11.9° to 18.4°) than those of the linear regression lines (11.4° to 12.1°). Notably, the optimized helix fiber angle distribution of optim2 agrees better with the measurements than that of optim1. Also shown in table 2 are

Measurement	Root Mean Square Difference (degrees)					
	linear fit	optim1	optim2	Boven-deerd 1992	Peskin 1989	Arts 1994
Streeter 1979	11.4	14.4	11.6	10.6	23.8	14.7
Nielsen 1991A	12.1	18.4	15.0	11.0	15.5	13.8
Nielsen 1991B	11.4	18.5	18.3	12.2	14.4	13.2

Table 2. Root mean square (RMS) differences of computed transmural course of helix fiber angle with respect to measurements. Sources of measurements: Streeter (33), from equatorial region of human LV; Nielsen *et al.* (22), A and B, from equatorial and adjacent more apical regions of canine LV respectively. Other columns show RMS differences in degrees for computed transmural course of helix fiber angle: a) best linear fit to measurements, b) optim1: when optimizing parameters p_1 and p_2 only, c) optim2: when additionally optimizing p_3, d) Bovendeerd *et al.* (5), e) Peskin (26), and f) Arts *et al.* (2).

RMS differences for predictions of helix fiber angle distributions of several mathematical models. In a finite element model of LV wall mechanics by Bovendeerd *et al.* (5) equatorial fiber stress, averaged over the ejection period, was made as homogeneous as possible by making trial and error changes in the transmural course of helix fiber angle. The transmural course of helix fiber angle was described by four parameters in three piecewise continuous polynomials up to second order. Arts *et al.* (2) computed a transmural distribution of helix fiber angle in a cylindrical model of LV wall mechanics. The helix fiber angle distribution was the result of a simulated process of cardiac remodeling in which muscle fibers could adapt their orientations to achieve a required amount of shortening during ejection. A helical fiber orientation formed automatically. Finally, Peskin (26) computed a transmural course of fiber angle (angle between fiber and circumferential directions) that followed an inverse sine relation with extreme values of 90° and -90° at the inner and outer wall surfaces. This result was derived from mechanical equilibrium of the LV wall and from the condition that the cross-sectional area of a group of muscle fibers is constant along its length. In conclusion, judging by the RMS differences, the transmural course of helix fiber angle computed in optim1 and optim2 agrees quite well with measurements and also with predictions by mathematical models.

Comparison of computed transverse fiber angle with measurements is more difficult due to the scarcity of experimental data. The transverse fiber angle is positive above the equator and negative below but more accurate latitude-dependence could not be detected (35). Mean through-wall values have been

measured as -4.6±0.8° (mean±SEM) near the equator and -3.5±0.6° near the apex (33). In our model the spatial average of α_t below the equator is -6.5° which compares reasonably well with these measurements. Reported predictions of fiber orientation by mathematical models are another available source to compare the computed transverse fiber angle field with. In a mathematical model to calculate left ventricular fiber orientation (26), transverse fiber angle was zero at the inner and outer wall surfaces and greatest in the middle of the wall. The midwall transverse fiber angle was 0° at the equator position and increased towards the apex to about 18°. In conclusion, there is too little experimental data available to make a quantitative evaluation of the computed transverse fiber angle. Qualitatively, our predictions do not conflict with either available measurements or other model predictions.

The finding that an anatomically realistic distribution of fiber orientation results in rather homogeneous mechanical loading of the wall at the beginning of ejection is in agreement with other (3, 5, 15), but not all, model studies. Results of a finite element model of LV wall mechanics by Guccione *et al.* (13) showed there was considerable regional heterogeneity of end systolic fiber stress. The latter model incorporated measured wall geometry and fiber orientation. Unfortunately, in their study, Guccione *et al.* did not present a sensitivity analysis of the model parameters. It may well be that small changes in fiber orientation within the anatomical range lead to more homogeneous fiber stress over the wall.

Conclusions

A finite element model of LV wall mechanics has been set up. Fiber orientation in the model, quantified by the helix and transverse fiber angles, was described by up to three parameters. Fiber orientation was optimized to make regional differences in fiber strain at the beginning of ejection as small as possible. A single optimum in fiber orientation was found when helix fiber angle was optimized for a wide range of starting values of the fiber orientation parameters. The standard deviation of the fiber strain at beginning of ejection, divided by the mean fiber strain was 12.5 %. Inclusion of the transverse fiber angle in the optimization reduced this measure of inhomogeneity to less than 10 %. The computed transmural course of helix fiber angle has RMS errors with respect to measurements ranging from 11.6° to 18.5°. Linear regression lines through the same measurement data have RMS errors between 11.4° and 12.1°. The agreement between computed and measured fiber orientations suggests that the structure of the left ventricular wall is designed for maximum homogeneity of fiber

strain during ejection.

Acknowledgments

The authors thank Prof. K. Schittkowski for providing an implementation of the sequential quadratic programming algorithm, NLPQL.

References

1. Arts, T., P. H. M. Bovendeerd, F. W. Prinzen, and R. S. Reneman. Relation between left ventricular cavity pressure and volume and systolic fiber stress and strain in the wall. *Biophys J* 59: 93-102, 1991.
2. Arts, T., F. W. Prinzen, L. H. E. H. Snoeckx, J. M. Rijcken, and R. S. Reneman. Adaptation of cardiac structure by mechanical feedback in the environment of the cell: a model study. *Biophys J* 66: 953-961, 1994.
3. Arts, T., and R. S. Reneman. Dynamics of left ventricular wall and mitral valve mechanics - a model study. *J Biomech* 22: 261-271, 1989.
4. Barthelemy, J.-F. M., and R. T. Haftka. Approximation concepts for optimum structural design - a review. *Structural optimization* 5: 129-144, 1993.
5. Bovendeerd, P. H. M., T. Arts, J. M. Huyghe, D. H. van Campen, and R. S. Reneman. Dependence of local left ventricular wall mechanics on myocardial fiber orientation: a model study. *J Biomech* 25: 1129-1140, 1992.
6. Carew, T. E., and J. W. Covell. Fiber orientation in the hypertrophied canine left ventricle. *Am J Physiol* 236: H487-H493, 1979.
7. Cooper IV, G., R. L. Kent, C. E. Uboh, E. W. Thompson, and T. A. Marino. Hemodynamic versus adrenergic control of cat right ventricular hypertrophy. *J Clin Invest* 75: 1403-1414, 1985.
8. de Tombe, P. P., and H. E. D. J. ter Keurs. Sarcomere dynamics in cat cardiac trabeculae. *Circ Res* 68: 588-596, 1991.
9. Delhaas, T., T. Arts, F. W. Prinzen, and R. S. Reneman. Regional fiber stress-fiber strain area as estimate of regional oxygen demand in the canine heart. *J Physiol* 477: 481-496, 1994.
10. Douglas, A. S., E. K. Rodriguez, W. O'Dell, and W. C. Hunter. Unique strain history during ejection in canine left ventricle. *Am J Physiol* 260: H1-H15, 1991.
11. Grimm, A. H., H.-L. Lin, and B. R. Grimm. Left ventricular free wall and intraventricular pressure-sarcomere length distributions. *Am J Physiol* 239: H101-H107, 1980.
12. Grossman, W., D. Jones, and L. P. McLaurin. Wall stress and patterns of hypertrophy in the human left ventricle. *J Clin Invest* 56: 56-64, 1975.
13. Guccione, J. M., K. D. Costa, and A. D. McCulloch. Finite element stress analysis of left ventricular mechanics in the beating dog heart. *J Biomech* 28: 1167-1177, 1995.
14. Huisman, R. F., G. Elzinga, N. Westerhof, and P. Sipkema. Measurement of ventricular wall stress. *Cardiovasc Res* 14: 142-153, 1980.
15. Huyghe, J. M., T. Arts, D. H. van Campen, and R. S. Reneman. Porous medium finite element model of the

beating left ventricle. *Am J Physiol* 262: H1256-H1267, 1992.

16. Judd, R. M., J. R. Resar, and F. C. P. Yin. Effects of barium-induced cardiac contraction on large- and small-vessel intramyocardial blood volume. *Circ Res* 68: 217-225, 1991.
17. Kang, T., and F. C. P. Yin. The need to account for residual strains and composite nature of heart wall in mechanical analysis. *Am J Physiol* 271, 1996.
18. Malvern, L. E. *Introduction to the mechanics of a continuous medium.* London: Prentice-Hall, Inc., 1969.
19. McCulloch, A. D., B. H. Smaill, and P. J. Hunter. Regional left ventricular epicardial deformation in the passive dog heart. *Circ Res* 64: 721-733, 1989.
20. McLean, M., and J. Prothero. Determination of relative fiber orientation in heart muscle: methodological problems. *Anat Rec* 232: 459-465, 1992.
21. Moskowitz, S. E. Effects of inertia and viscoelasticity in late rapid filling of the left ventricle. *J Biomech* 14: 443-445, 1981.
22. Nielsen, P. M. F., I. J. Le Grice, B. H. Smaill, and P. J. Hunter. Mathematical model of geometry and fibrous structure of the heart. *Am J Physiol* 260: H1365-H1378, 1991.
23. Nikolic, S., E. L. Yellin, K. Tamura, H. Vetter, T. Tamura, J. S. Meisner, and R. W. M. Frater. Passive properties of canine left ventricle: diastolic stiffness and restoring forces. *Circ Res* 62: 1210-1222, 1988.
24. Omens, J. H., and Y.-H. Fung. Residual strain in rat left ventricle. *Circ Res* 66: 33-45, 1990.
25. Pearlman, E. S., K. T. Weber, J. S. Janicki, G. G. Pietra, and A. P. Fishman. Muscle fiber orientation and connective tissue content in the hypertrophied human heart. *Lab Invest* 46: 158-164, 1982.
26. Peskin, C. S. Fiber architecture of the left ventricular wall: an asymptotic analysis. *Commun Pure Appl Math* 42: 79-113, 1989.
27. Prinzen, F. W., E. C. Cheriex, T. Delhaas, M. F. M. van Oosterhout, T. Arts, H. J. J. Wellens, and R. S. Reneman. Asymmetric thickness of left ventricular wall resulting from asynchronous electric activation: A study in dogs with ventricular pacing and in patients with left bundle branch block. *Am Heart J* 130: 1045-1053, 1995.
28. Prinzen, T. T., T. Arts, F. W. Prinzen, and R. S. Reneman. Mapping of epicardial deformation using a video processing technique. *J Biomech* 19: 263-273, 1986.
29. Rodriguez, E. K., J. H. Omens, L. K. Waldman, and McCulloch. Effect of residual stress on transmural sarcomere length distributions in rat left ventricle. *Am J Physiol* 264: H1048-H1056, 1993.
30. Sagawa, K. The ventricular pressure-volume diagram revisited. *Circ Res* 43: 677-687, 1978.
31. Schittkowski, K. NLPQL: A fortran subroutine solving constrained nonlinear programming problems. *Ann Op Res* 5: 485-500, 1986.
32. Spotnitz, H. M., E. H. Sonnenblick, and D. Spiro. Relation of ultrastructure to function in the intact heart: sarcomere structure relative to pressure volume curves of intact left ventricles of dog and cat. *Circ Res* 18: 49-66, 1966.
33. Streeter, D. D., Jr. Gross morphology and fiber geometry of the heart. In: *Handbook of physiology - The cardiovascular system I*, edited by R. M. Berne Am. Physiol. Soc., Bethesda, MD, 1979, p. 61-112.
34. Streeter, D. D., Jr., and W. T. Hannah. Engineering mechanics for successive states in canine left ventricular myocardium. 2. Fiber angle and sarcomere length. *Circ Res* 33: 656-664, 1973.

35. Streeter, D. D., Jr., W. E. Powers, M. A. Ross, and F. Torrent-Guasp. Three-dimensional fiber orientation in the mammalian left ventricular wall. In: *Cardiovascular System Dynamics*, edited by J. Baan, A. Noordergraaf and J. Raines. Cambridge, Mass.: M.I.T. Press, 1978, p. 73-84.
36. Streeter, D. D., Jr., H. M. Spotnitz, D. P. Patel, J. Ross Jr., and E. H. Sonnenblick. Fiber orientation in the canine left ventricle during diastole and systole. *Circ Res* 24: 339-347, 1969.
37. Streeter, D. D. J., and W. T. Hanna. Engineering mechanics for successive states in canine left ventricular myocardium. 1. Cavity and wall geometry. *Circ Res* 33: 639-655, 1973.
38. Taber, L. A. On a nonlinear theory for muscle shells: part II - application to the beating left ventricle. *J Biomech Eng* 113: 63-71, 1991.
39. Taber, L. A., N. Hu, T. Pexieder, E. B. Clark, and B. B. Keller. Residual strain in the ventricle of the stage 16-24 chick embryo. *Circ Res* 72: 455-462, 1993.
40. ter Keurs, H. E. D., W. H. Rijnsburger, R. van Heuningen, and M. J. Nagelsmit. Tension development and sarcomere length in rat cardiac trabeculae: evidence of length-dependent activation. *Circ Res* 46: 703-714, 1980.
41. Thomas, C. E. The muscular architecture of the ventricles of hog and dog hearts. *Am J Anat* 101: 17-57, 1957.
42. Waldman, L. K., D. Nosan, F. Villareal, and J. W. Covell. Relation between transmural deformation and local myofiber direction in canine left ventricle. *Circ Res* 63: 550-562, 1988.
43. Yin, F. C. P., C. C. H. Chan, and R. J. Judd. Compressibility of passive myocardium. *Am J Physiol* 271: H1864-H1870, 1996.
44. Yin, F. C. P., R. K. Strumpf, P. H. Chew, and S. L. Zeger. Quantification of the mechanical properties of noncontracting canine myocardium under simultaneous biaxial loading. *J Biomech* 20: 577-589, 1987.

Appendix - Wall geometry

To specify wall geometry in the reference state a spherical coordinate system as well as the rectangular coordinate system of fig. 2 were used. Given the coordinates of a point with respect to the spherical coordinate system, (r,θ,ϕ), its coordinates in the rectangular system, (x,y,z) are

$$\begin{bmatrix} x \\ y \\ z \end{bmatrix} = r \begin{bmatrix} \sin(\theta)\cos(\phi) \\ \sin(\theta)\sin(\phi) \\ \cos(\theta) \end{bmatrix} \qquad \text{(A1)}$$

The LV wall was assumed to be rotationally symmetric. The shape of the wall was defined by specifying a midwall surface and a wall thickness perpendicular to the midwall. A point on the midwall surface at a distance r_m from the origin has position vector $\mathbf{r}_m$ given by

$$\mathbf{r}_m(\theta,\phi) = r_m(\theta)\begin{bmatrix}\sin(\theta)\cos(\phi) & \sin(\theta)\sin(\phi) & \cos(\theta)\end{bmatrix}\begin{bmatrix}\mathbf{e}_x\\ \mathbf{e}_y\\ \mathbf{e}_z\end{bmatrix}, \qquad \text{(A2)}$$

where $\mathbf{e}_x$, $\mathbf{e}_y$, $\mathbf{e}_z$ are unit vectors along the cartesian coordinate axes. The shape of the midwall surface is described by the function $r_m(\theta)$ which depends on two parameters, a_m and b_m:

$$r_m(\theta) = \left(a_m + b_m\cos(2\theta)\right)^{-1/2} \qquad \text{(A3)}$$

The wall thickness perpendicular to the midwall is specified by the function $t(\theta)$, which depends on three parameters, a_t, b_t, and c_t:

$$t(\theta) = a_t + b_t\cos(2\theta) + c_t\cos(4\theta) \qquad \text{(A4)}$$

The unit outward normal vector to the midwall surface is given by $\mathbf{n}_m$:

$$\mathbf{n}_m(\theta,\phi) = \left|\frac{\partial \mathbf{r}_m}{\partial\theta}\right|^{-1}\left(\left(r_m\sin(\theta) - \frac{dr_m}{d\theta}\cos(\theta)\right)\left(\cos(\phi)\mathbf{e}_x + \sin(\phi)\mathbf{e}_y\right) + \left(r_m\cos(\theta) + \frac{dr_m}{d\theta}\sin(\theta)\right)\mathbf{e}_z\right) \qquad \text{(A5)}$$

Hence the position vector, $\mathbf{r}$, of a point in the LV wall is given by

$$\mathbf{r}(\theta,\phi) = \mathbf{r}_m(\theta,\phi) + v\,t(\theta)\mathbf{n}_m(\theta,\phi) \qquad \text{(A6)}$$

The parameter v varies linearly with transmural position from -1 at the endocardium to +1 at the epicardium. The used values of a_m, and b_m were 0.109 and -0.0680 cm^{-2} respectively and those of a_t, b_t, and c_t were 0.643, -0.289 and -0.0643 cm respectively.

Chapter 3

Optimization of cardiac fiber orientation for homogeneous fiber strain during ejection

J. Rijcken[1], P.H.M. Bovendeerd[2], A.J.G. Schoofs[2], D.H. van Campen[2], T. Arts[1]

[1]Department of Biophysics, Cardiovascular Research Institute Maastricht, Maastricht University, Maastricht, The Netherlands,
[2]Department of Mechanical Engineering, Eindhoven University of Technology, Eindhoven, The Netherlands.

submitted

Abstract

The strain of muscle fibers in the heart is likely to be distributed uniformly over the cardiac walls during systole. Mathematical models of left ventricular (LV) wall mechanics have shown that the distribution of fiber strain is sensitive to the orientation of muscle fibers in the wall. In the presented study, we tested the hypothesis that fiber orientation in the LV wall is such that systolic fiber strain is as homogeneous as possible.

A finite element model of LV wall mechanics was set up to compute the distribution of fiber strain at beginning and end of the ejection period of the cardiac cycle. The distribution of fiber orientation over the LV wall, quantified by 3 parameters, was systematically varied to minimize regional differences in mean fiber strain and in fiber shortening during ejection.

A well-defined optimum in the distribution of fiber orientation was found which was not significantly different from anatomical measurements. After optimization, mean fiber strain and difference in fiber strain during ejection, referred to the unloaded state were 0.025±0.011 (mean±sd) and 0.214±0.018 respectively. The results indicate that the LV structure is designed for maximum homogeneity of fiber strain during ejection.

Keywords: left ventricle, finite element analysis

Introduction

Measurements in the left ventricular wall of the heart indicate that regional differences in systolic fiber strain (7, 19, 26) and sarcomere length (10) are not significant, with a possible exception at the junction of left and right ventricles (19). However, the measurements are not comprehensive enough to make statements about the fiber strain distribution over the whole left ventricle (LV). Distributions of systolic fiber stress and strain have also been predicted using mathematical models of LV wall mechanics (2, 4, 5, 9, 11). Model studies by Huyghe *et al.* (11) and Bovendeerd *et al.* (5) showed that the distribution of systolic fiber stress and strain is very sensitive to the transmural course of fiber orientation. Transmural courses of fiber orientation within the reported anatomical range could be chosen that yielded transmural distributions of systolic fiber stress that were either uniform or varied by more than a factor 2. Considering the predicted sensitivity of fiber strain distribution to fiber orientation and the possible homogeneity of fiber strain indicated by measurements, we hypothesized that fiber orientation in the LV wall is such that fiber strain over the ejection period is as homogeneous as possible.

To test this hypothesis a finite element model of LV wall mechanics was developed to calculate the distribution of fiber stress and strain over the wall at beginning and end of ejection for given distributions of fiber orientation. In an optimization procedure an objective function, expressing the summed inhomogeneity of mean fiber strain and of fiber shortening during ejection, was minimized by systematic adjustment of fiber orientation. The predicted fiber orientation was compared with anatomical findings. Also, the parameters defining fiber orientation were varied over a wide range to study the uniqueness of the calculated optimal fiber orientation. In subsequent simulations the relative weight of fiber shortening in the objective function was varied to evaluate its effect on optimal fiber orientation and fiber strain homogeneity.

Methods

Finite element model of left ventricular wall mechanics

Wall geometry in reference state . The deformation-free reference state in the finite element model was defined as the situation in which transmural pressure across the LV wall and the stresses in the wall were 0 kPa. The reference state corresponds approximately to mid-diastole. The LV wall is considered thick-walled and point-symmetric with respect to the center of the equatorial plane. Consequently, only the mechanics of the region between the apex and equator was

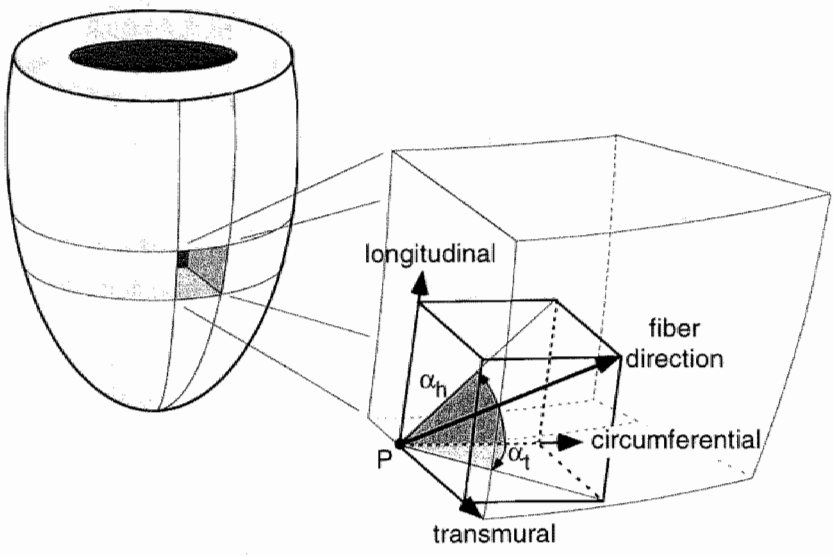

fig. 1. Illustration of the helix (α_h) and transverse (α_t) fiber angles in the rotationally symmetric LV. The fiber angles at a point P are defined with respect to the local transmural, longitudinal and circumferential directions.

considered. LV wall shape in the reference state was defined by a prolate spheroidal midwall surface. Wall geometry was chosen so that cavity and wall volume and long and short axes matched those of the real LV. The course of wall thickness between equator and apex was adapted so that for an anatomically realistic fiber orientation mean through-wall fiber stress at beginning of ejection was similar at all latitudes between equator and apex. The choice of the parameter values used in the finite element model are given in a separate section below.

Fiber orientation in reference state. Fiber orientation in the reference state was quantified by the helix and transverse fiber angles (22) measured with respect to the local transmural, circumferential and longitudinal directions (fig. 1). To be able to define the local transmural and longitudinal directions, we first define a wall-bound coordinate system (u,v) (fig. 2); the coordinate u decreases from 0 at the equator to -1 at the apex in direct proportion with distance along the midwall surface in the equator-to-apex direction; the coordinate v increases from -1 at the endocardium to +1 at the epicardium in direct proportion with distance in the

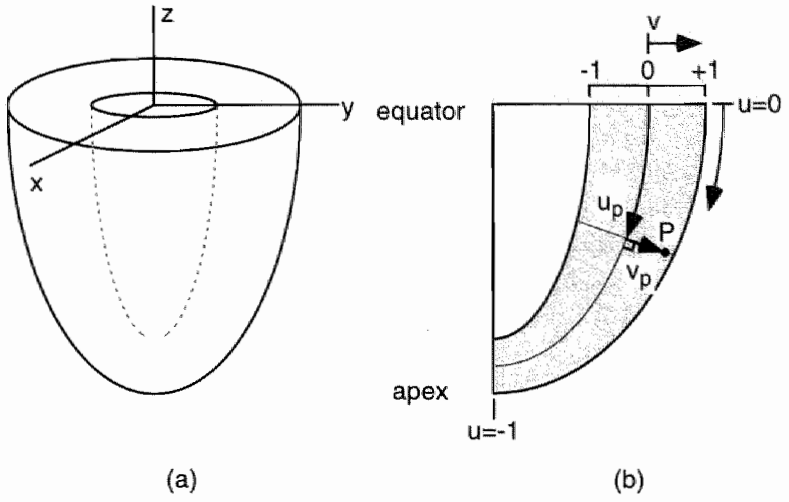

fig. 2. Diagram showing rotationally symmetric LV geometry and coordinate systems: (a) cartesian coordinate system (x,y,z) and (b) wall-bound coordinate system (u,v): point P has coordinates (u_p,v_p). Both u and v vary linearly with distance.

direction perpendicular to the midwall surface. The local transmural direction was then defined as the outward normal to a surface of constant v. The local longitudinal direction is orthogonal to both the transmural and circumferential directions. The helix fiber angle (fig. 1) was defined as the angle between the local circumferential direction and the projection of the fiber direction on the plane perpendicular to the local transmural direction. The transverse fiber angle was defined as the angle between the local circumferential direction and the projection of the fiber direction on the plane perpendicular to the local longitudinal direction. It determines the degree to which fibers cross over between inner and outer wall surfaces. The spatial distributions of the helix and transverse fiber angles are specified with respect to the wall-bound coordinate system (u,v). The helix fiber angle, α_h, varies with v according to:

$$\alpha_h(v) = p_1 + p_2\, v, \qquad [1]$$

where p_1 and p_2 are parameters whose optimal values are to be determined. The transverse fiber angle, α_t, is zero at the wall boundaries, i.e. fibers are assumed not to end here. In accordance with experimental observations (23), α_t is an odd function in coordinate u. To satisfy the latter conditions, we used the following equation:

$$\alpha_t(u,v) = p_3\, u(1-v^2)\,, \qquad [2]$$

where parameter p_3 has to be optimized.

Constitutive behavior. In the finite element model, cardiac tissue was considered to consist of stiff fibers embedded in a soft tissue matrix. The total Cauchy stress tensor, **T**, in the tissue is the sum of a passive component, $\mathbf{T}_p$, that arises from deformation of passive myocardial tissue and an active component, $\mathbf{T}_a$, arising from muscle fiber contraction during systole:

$$\mathbf{T} = \mathbf{T}_p + \mathbf{T}_a\,. \qquad [3]$$

The passive myocardial tissue was assumed to be elastic and transversely isotropic with respect to the fiber direction. The Cauchy stress $\mathbf{T}_p$ in the passive tissue was derived from a strain energy density function, W:

$$\mathbf{T}_p = \frac{1}{\det(\mathbf{F})}\mathbf{F}\bullet\frac{\partial W(\mathbf{E})}{\partial \mathbf{E}}\bullet\mathbf{F}^T\,, \qquad [4]$$

where **F** and **E** are the deformation gradient tensor and the Green-Lagrange strain tensor respectively and superscript *T* denotes a tensor transpose (12). The strain energy density function, W, was chosen as:

$$W(\mathbf{E}) = a_0\left(\exp(a_1 I_E^2 + a_2 II_E + a_3\,\mathbf{e}_f\bullet\mathbf{E}\bullet\mathbf{e}_f) - 1\right) + a_4\left(\det(2\mathbf{E}+\mathbf{I}) - 1\right)^2 \qquad [5]$$

where $I_E = \mathrm{trace}(\mathbf{E})$,

$$II_E = \frac{1}{2}\left(\mathrm{trace}\left(\mathbf{E}\bullet\mathbf{E}^T\right) - I_E^2\right),$$

a_0, a_1, a_2, a_3, and a_4 are material parameters, and $\mathbf{e}_f$ is a unit vector in fiber direction. The passive Cauchy stress, $\mathbf{T}_p$, is zero in the reference state of deformation and increases exponentially with strain.

The muscle fibers contain sarcomeres, contractile protein units, that are assumed to generate a uniaxial force in the fiber direction during systole. The contractile force in the real LV depends on sarcomere length, sarcomere velocity of shortening, time and extracellular calcium concentration (6). Experimental data on active muscle fiber stress are usually presented as active force per unit undeformed cross-sectional area of the muscle, i.e. in terms of the first Piola-Kirchhoff stress. In the finite element simulations the first Piola-Kirchhoff active fiber stress, T_a^0 (kPa),

depended linearly on sarcomere length, l_s (μm), and on active stiffness, K (kPa):

$$T_a^0 = K\frac{l_s - l_x}{l_{s,0}}, \qquad [6]$$

where l_x is the sarcomere length at which no contractile force can be generated, and $l_{s,0}$ is the sarcomere length in the reference state. The active stiffness depended on the phase of the cardiac cycle. It was zero in the reference state and during diastole and increased during systole to a maximum value at the end of ejection. The first Piola-Kirchhoff active fiber stress, T_a^0, is related to the active stress tensor $\mathbf{T}_a$ by the relation:

$$\mathbf{T}_a = \frac{1}{\det(\mathbf{F})}\mathbf{F} \bullet T_a^0 \mathbf{e}_f \mathbf{e}_f. \qquad [7]$$

Design of finite element simulations. Calculations of fiber stresses and strains in the LV wall were based on the law of conservation of momentum (12), expressing static equilibrium of forces in the wall due to both blood pressure in the cavity and internal stresses in the wall. A Galerkin-type finite element method , implemented in the package Diana 5.1 (Diana Analysis B.V., Delft ,The Netherlands), was used to convert the equations of conservation of momentum into a 20-node three-dimensional brick element formulation. Quadratic interpolation was used to determine the displacement field in between nodes of an element. The finite element mesh comprised the sector of the LV in the region ($x \geq 0$, $y \geq 0$, $z \leq 0$). It consisted of a total of 27 elements with 3 element layers in the transmural direction, 5 in the equator-to-apex direction, and 2 in the circumferential direction (except at the apex where there was only 1 element in circumferential direction). The endocardial surface was loaded with LV cavity pressure while the epicardium remained unloaded. Kinematic boundary conditions on the through-wall faces of the mesh allowed cavity volume changes and torsion to occur.

Finite element simulations started in the reference state of deformation defined above. Cavity pressure and active stiffness were prescribed during the cardiac cycle. The beginning of ejection was defined by a cavity pressure of 12.3 kPa, and an active stiffness of 111.5 kPa corresponding to a cavity-to-wall-volume ratio of approximately 0.65. The end of ejection was defined by a cavity pressure of 17.5 kPa and an active stiffness of 557.7 kPa corresponding to a cavity-to-wall-volume ratio of approximately 0.13.

Quantification of fiber strain for optimization. The LV wall mesh was divided into 729 regions with similar volumes. Sarcomere length at the central point of a

region was considered representative for that region. For region i, fiber strain, ε_i, is given by:

$$\varepsilon_i = \frac{l_{s,i} - l_{s,0}}{l_{s,0}}, \qquad [8]$$

where $l_{s,i}$ is the instantaneous sarcomere length in the region and $l_{s,0}$ is the sarcomere length in the reference state.

Optimization procedure

The optimization consists of the minimization of an objective function, G, expressing inhomogeneity in fiber strain during ejection:

$$G(\mathbf{p}) = \text{variance}(\varepsilon_{be} + \varepsilon_{ee}) + w\,\text{variance}(\varepsilon_{be} - \varepsilon_{ee}), \qquad [9]$$

where ε_{be} and ε_{ee} are fiber strains at beginning and end of ejection respectively, and w is a weighting factor. The objective function depends, albeit implicitly, on the fiber orientation parameters p_1, p_2, and p_3 which are stored in the vector **p**. The contributions of regional fiber strains at beginning and end of ejection to the variances in equation [9] were weighted with the volume of the region. The first variance in equation [9] expresses the demand that mean fiber strain be as homogeneous as possible while the second variance demands that fiber shortening be made homogeneous.

To minimize the objective function, the optimization strategy of sequential approximate optimization was used (3). For a given set of fiber orientation parameters, $\mathbf{p}_k$, regional fiber strains, $\varepsilon_{be,i}$ and $\varepsilon_{ee,i}$ at beginning and end of ejection respectively, were determined by the finite element model. Regional fiber strains at beginning and end of ejection were also computed when fiber orientation parameters were perturbed one at a time by 1°. This was done with little additional computational effort by using the already computed states of deformation and stress as first estimates. Hence finite difference derivatives of regional fiber strains with respect to **p** were determined at $\mathbf{p}_k$ for both beginning and end of ejection. This allowed estimation of regional fiber strains at beginning of ejection, $\hat{\varepsilon}_{be,i}$, for arbitrary **p,** from a Taylor series expansion on $\varepsilon_{be,i}$ around the value $\mathbf{p}_k$:

$$\hat{\varepsilon}_{be,i}(\mathbf{p}) = \varepsilon_{be,i}(\mathbf{p}_k) + \sum_{j=1}^{n} (p_j - p_{k,j}) \frac{\partial}{\partial p_j} \varepsilon_{be,i}(\mathbf{p}_k), \qquad i=1,2,...,N \qquad [10]$$

where $p_{k,j}$ and p_j are the j^{th} components of $\mathbf{p}_k$ and **p** respectively, n is the number of

fiber orientation parameters, and N is the number of regions. Estimates of regional fiber strains at end of ejection, $\hat{\varepsilon}_{ee,i}$, were made in analogous manner. By substitution of the linear estimates for $\hat{\varepsilon}_{be,i}$ and $\hat{\varepsilon}_{ee,i}$ in equation [9], a quadratic approximation model, $\hat{G}$, was obtained which gave an estimate of the objective function, G, for an arbitrary set of fiber orientation parameters:

$$\hat{G}(\mathbf{p}) = \text{variance}(\hat{\varepsilon}_{be} + \hat{\varepsilon}_{ee}) + w\,\text{variance}(\hat{\varepsilon}_{be} - \hat{\varepsilon}_{ee}) \qquad [11]$$

Repeated evaluation of $\hat{G}$ is efficient due to the explicit dependence on $\mathbf{p}$. The function $\hat{G}$ was minimized by Powell's method (18), which is a standard direction-set method for unconstrained minimization of a function. The result of the optimization is a new set of fiber orientation parameters $\mathbf{p}_{k+1}$.

Convergence was defined to occur when the following 2 conditions were satisfied. Firstly, finite element evaluations of the objective function of the current and previous iterations, $G(\mathbf{p}_k)$ and $G(\mathbf{p}_{k-1})$, should agree to within a tolerance of δ:

$$(G(\mathbf{p}_{k-1}) - G(\mathbf{p}_k))/G(\mathbf{p}_k) \le \delta, \qquad [12]$$

where δ=0.0001. Secondly, the minimum of the approximation model based on parameters $\mathbf{p}_k$, $\hat{G}_{opt,\mathbf{p}_k}$, should coincide with the finite element evaluation of the objective function at $\mathbf{p}_k$, to the same tolerance of δ:

$$\left(G(\mathbf{p}_k) - \hat{G}_{opt,\mathbf{p}_k}\right)/G(\mathbf{p}_k) \le \delta \qquad [13]$$

If convergence has not occurred, new approximation models are set up around the parameters $\mathbf{p}_{k+1}$ and the process is repeated.

Applied parameter values in finite element model

Wall geometry in reference state. The choice of cavity and wall volume was based on experimental measurements in arrested canine left ventricles (13). Given that the base extends above the equator by a distance of half the semi-major axis (24), the chosen LV wall geometry corresponds to a cavity volume of 42 ml and cavity-to-wall-volume ratio of 0.3. The ratio of midwall long to short axes was set to 2.08 (24). The ratio of equatorial to apical wall thickness was set to 3.0.

Sarcomere length in reference state. In the model, sarcomere length in the reference state, $l_{s,0}$, was set to 1.95 μm for all sarcomeres in the LV wall, based on the average of measurements in left ventricles of rats (8, 20) and dogs (21).

Constitutive behavior. For the passive material the relative values of a_1:a_2:a_3

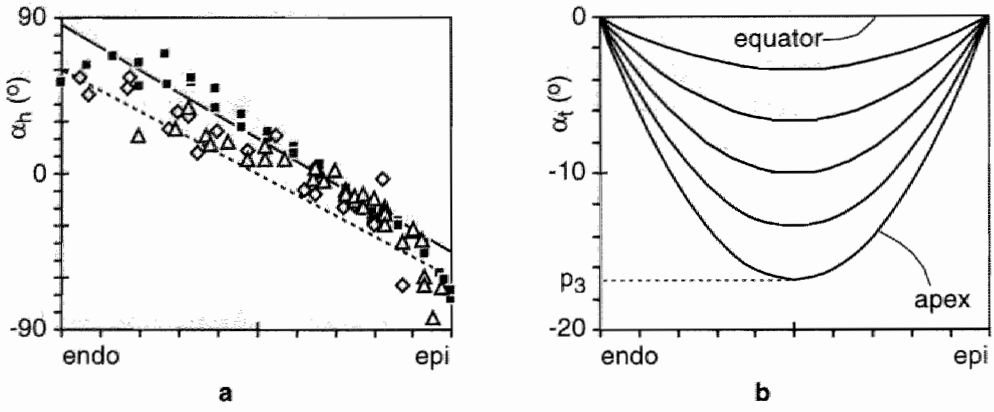

fig. 3. (a) Transmural course of helix fiber angle (α_h) before (....) and after (___) optimization REF. The following measurements are also shown: (▪) Streeter, (22), equatorial region of human LV; (Δ) Nielsen *et al.* (15), equatorial region of canine LV; (◇) Nielsen et al. (15), adjacent more apical region of canine LV. (b) Transmural course of transverse fiber angle (α_t) at various latitudes (u=0.0,-0.2,-0.4,-0.6,-0.8,-1.0) after optimization REF. Before optimization α_t=0°.

in equation [5] were set to 1:2:1, so that the ratio of fiber-to-cross-fiber-stress is 2.0 for an equibiaxially loaded sheet of tissue (27). The absolute values of a_0 and a_1 were set to 0.5 kPa and 3.0 respectively so that calculated passive pressure-volume curves agreed with measurements in canine hearts (16). The value of a_4 was set to 500.0 kPa so that LV wall volume changed by less than 2% in the simulations.

The active material parameter l_x, the zero-force sarcomere length, was set to 1.62 μm, based on experiments in rat cardiac trabeculae (25). The active stiffness, K, at end ejection was estimated as 557.7 kPa, from studies in tetanically contracting rat cardiac trabeculae at an external calcium concentration of 2.5 mM (25). The active stiffness at beginning of ejection was chosen to be 111.5 kPa so that a cavity pressure of 12.3 kPa resulted in a physiologically realistic cavity volume.

Performed simulations

Optimizations were carried out with three different values of the weighting factor, w, in the objective function of equation [9]. In the first optimization (optimization REF), the weighting factor was set to unity. The initial guess for the parameters (p_1, p_2, p_3) was (0°, -60°, 0°). In 2 additional optimizations the weighting factor was set to 0.1 and to 10.0 respectively. The initial guess for these optimizations was the optimum found for the case w=1.0. The uniqueness of the optimum was studied for the case w=1.0: the objective function was evaluated with

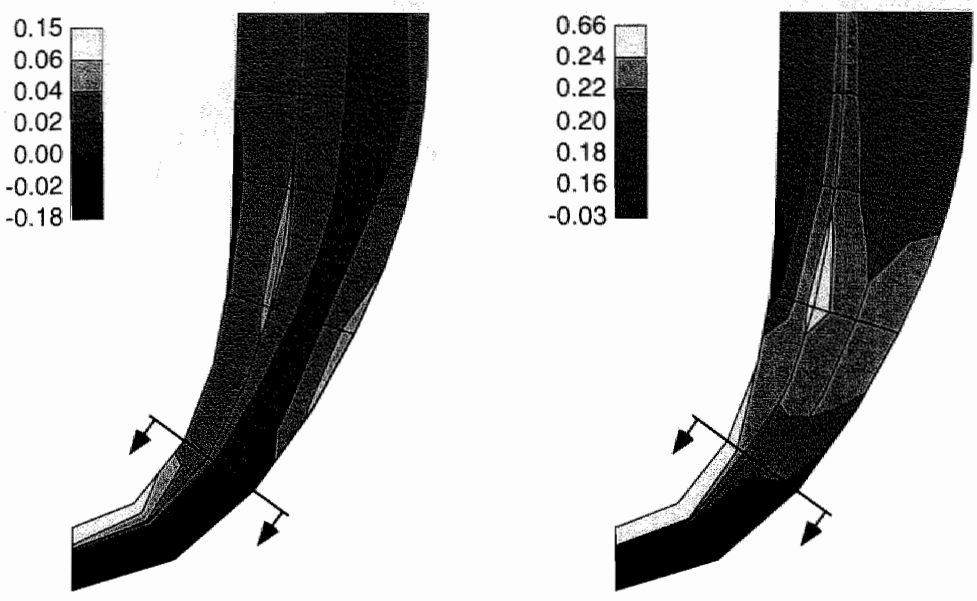

fig. 4. Distribution of fiber strains over the LV wall following optimization REF: (a) mean of fiber strain at beginning and end of ejection, $(\varepsilon_{be}+\varepsilon_{ee})/2$, (b) difference in fiber strain during ejection, $\varepsilon_{be}-\varepsilon_{ee}$. The apical region, indicated by the arrows, was excluded in the quantification of inhomogeneity of fiber strain (see results).

the finite element model for a wide range of the parameters p_1 and p_2 while p_3 was held at its optimal value. Subsequently the objective function was evaluated with p_1 and p_2 set to their optimal values while p_3 was varied.

Results

In optimization REF an optimal fiber orientation was found in which p_1=20.25°, p_2=-65.75°, and p_3=16.73° (fig. 3). The corresponding spatial distribution of mean fiber strain and fiber shortening during ejection is shown in fig. 4. Despite optimization large gradients in fiber strains and shortening were observed near the apex. For the quantification of inhomogeneity in fiber strains and shortening, 6% of LV wall volume near the apex was excluded (information from the three elements in the mesh adjoining the apex). Mean fiber strain during ejection was 0.025±0.011 (mean±sd) while the difference in fiber strain at beginning and end of ejection was 0.214±0.018 (for the whole LV wall volume these values

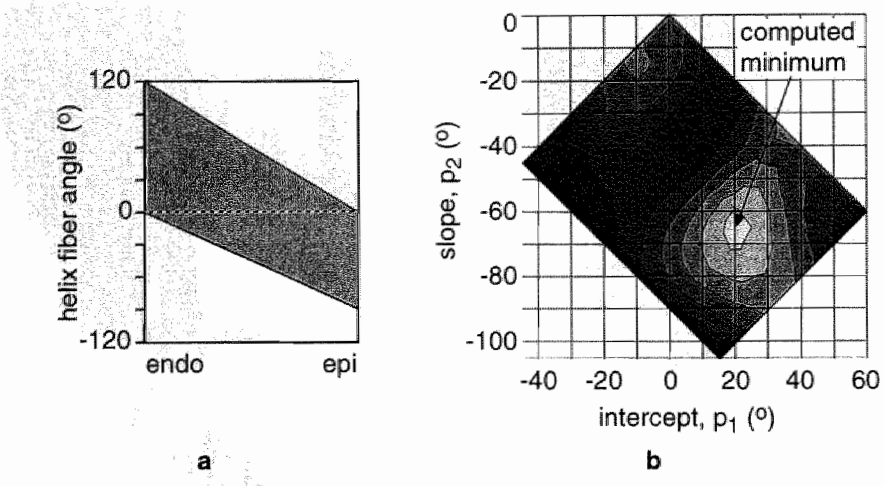

fig. 5. Parameter variation of helix fiber angle parameters p_1 and p_2 for optimized transverse fiber angle parameter (p_3=16.73°) of optimization REF. The objective function was evaluated with the finite element model for 130 combinations of p_1 and p_2 in the range indicated by the shaded region in panel (a). Panel (b) shows contour lines along which the objective function value is constant. Contours are drawn at intervals of 2.63×10^{-3}, between 2.63×10^{-3} and 23.67×10^{-3}. Objective function value along ridge between the 2 minima is approximately 8 times that in computed minimum.

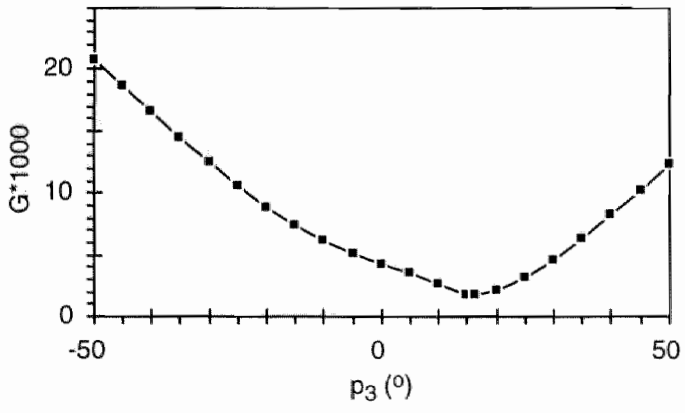

fig. 6. Objective function, G, as function of transverse fiber angle parameter, p_3, at optimized values of helix fiber angle parameters (p_1=20.25°, p_2=-65.75°) for optimization REF. The calculated optimum is at p_3=16.73°.

were 0.023±0.016 and 0.213±0.027 μm respectively). Extensive variation of helix fiber angle parameters p_1 and p_2 at p_3=16.73° showed that the objective function

has at least one other minimum at approximately p_1=-10°, p_2=-15°, though not as deep as the one that was found in optimization REF (fig. 5). Variation of transverse fiber angle parameter p_3 at p_1=20.25°, p_2=-65.75° indicated a single minimum of the objective function (fig. 6).

Tenfold changes in the factor, w, weighing the importance of fiber shortening in the objective function of equation [9], gave rise to changes of less than ±5% in optimized fiber angle parameters, with respect to values obtained in optimization REF (table 1). Variation of the weighting factor, w, gave expected changes in homogeneity of mean fiber strain and of fiber shortening. Compared to optimization REF, the standard deviation of fiber shortening, (ε_{be}-ε_{ee}), decreased for the case w=10.0 and increased for the case w=0.1. Similarly, the standard deviation of mean fiber strain, (ε_{be}+ε_{ee})/2, increased for the case w=10.0 and decreased for the case w=0.1. Also, the standard deviation of mean fiber strain was always lower than that of fiber shortening. For the case w=0.1, the spatial distributions of fiber strain and shortening were almost identical to that for w=1.0 (fig. 4). Compared to optimization REF, optimization with w=10.0 resulted in mean fiber strains that were greater in the endocardial region halfway between equator and apex (not shown).

Discussion

A finite element model of LV wall mechanics has been developed with which regional fiber strain and fiber shortening during ejection could be calculated. The finite element model was incorporated in an optimization procedure in which inhomogeneity of fiber strain and shortening during ejection were minimized by appropriately adapting fiber orientation. Variation of fiber orientation parameters over a wide range indicated that the calculated optimal fiber orientation gave the greatest homogeneity of fiber strain and shortening. Changes in the weighting factor, w, of the objective function (equation [9]), to change the relative contribution of regional differences in mean fiber strain and in fiber shortening, had little effect on the resulting optimal fiber orientation.

To assess the transmural course of helix fiber angle, comparisons were made with reported measurements in the equatorial region of the human LV (22) and in equatorial and adjacent more apical regions of the canine LV (15). The computed transmural course of helix fiber angle lies within the measured range of helix fiber angles over the majority of the wall thickness (fig. 3). For a quantitative comparison, the root mean squared (RMS) difference between the computed transmural course of helix fiber angle and several measurement series was determined. The RMS differences were ±11.9°, ±17.3° for measurements at the

	w=0.1		REF (w=1.0)	w=10.0	
p_1 (°)	20.53	(-1.4%)	20.25	19.82	(-2.1%)
p_2 (°)	-66.97	(-1.8%)	-65.75	-62.29	(+5.2%)
p_3 (°)	16.94	(+1.3%)	16.73	16.17	(-3.3%)
mean[$(\varepsilon_{be}+\varepsilon_{ee})/2$]	0.0256		0.0251	0.233	
sd[$(\varepsilon_{be}+\varepsilon_{ee})/2$]	0.010	(-2.5%)	0.011	0.014	(+27.1%)
mean[$\varepsilon_{be}-\varepsilon_{ee}$]	0.214		0.214	0.214	
sd[$\varepsilon_{be}-\varepsilon_{ee}$]	0.019	(+6.1%)	0.018	0.016	(-10.4%)

Table 1. Effect of weighting factor, w, in objective function, on optimized fiber angle parameters p_1, p_2, p_3 and on inhomogeneity of fiber strain. Symbols: ε_{be}, ε_{ee}=fiber strain at beginning and end of ejection respectively. Figures in parantheses indicate percentage change with respect to REF.

equator by Streeter (22) and Nielsen *et al.* (15), respectively, and ±15.1° closer to the apex (15). Best linear fits to each of the measurement series had RMS differences ranging from ±11.4° to ±12.1°, which are only slightly smaller than RMS differences between the measured and predicted transmural course. In conclusion, both qualitative and quantitative comparisons of computed transmural course of helix fiber angle with measurements indicate that the predicted helix angle is not significantly different from the measurements.

Comparison of the computed spatial distribution of transverse fiber angle with measurements is more difficult due to the scarcity of experimental data. Mean through-wall values have been measured as -4.6±0.8° (mean±sem, n=12) near the equator and -3.5±0.6° (n=15) near the apex (22). In our model the spatial average of α_t below the equator is -5.6° which is not in contradiction with these measurements. In a mathematical model to calculate left ventricular fiber orientation (17), the transverse fiber angle was zero at the inner and outer wall surfaces and greatest in the middle of the wall. The midwall transverse fiber angle was 0° at the equatorial position and decreased to approximately -18° at a position corresponding to u=-0.75. At this position we predict a transverse angle of -12.5°. In conclusion, only limited information is available for quantitative evaluation of the computed transverse fiber angle. Our predictions do not conflict with this information.

In the optimization strategy used in this study the obtained minimum may depend on the initial guess of the fiber orientation parameters. To investigate whether there were other minima in the neighborhood of the computed minimum, the objective function was evaluated over a wide range of the fiber orientation parameters. From the parameter variation, it can be concluded that for a given

value of the transverse fiber angle parameter of p_3=16.73°, the helix fiber angle parameters resulting from the standard optimization REF give the lowest minimum in objective function (fig. 5(b)). Furthermore, for given helix fiber angle parameters of p_1=20.25°, p_2=-65.75° the transverse fiber angle parameter resulting from optimization REF gives the lowest minimum (fig. 6). Figs. 5 and 6 show that the computed minimum of the objective function is well-defined; there are no other local minima visible in the close neighborhood. Although it is not proved, the performed parameter variation indicates it is likely that the computed minimum is the lowest minimum in the anatomical range.

Conclusions on the basis of the present study regarding a mechanism for cardiac adaptation must be considered with caution. Our results support the hypothesis that fibers are oriented in the LV wall such that fiber strain during ejection is as homogeneous as possible. However, the applied optimization strategy, in which information about fiber strain from all over the LV wall is used to adapt regional fiber orientation, is unlikely to be the basis of a physiological adaptation mechanism. Cardiac adaptation is more likely to be controlled in the environment of the cell (1), as has also been proposed for bone adaptation (14).

In conclusion, an objective function expressing inhomogeneity of mean fiber strain and fiber shortening during ejection has been minimized by optimization of fiber orientation. A well-defined minimum in the objective function was found for which mean fiber strain during ejection and the difference in fiber strain between beginning and end of ejection were 0.025±0.011 (mean±sd) and 0.214±0.018 respectively. After optimization the helix fiber angle varied from 86.0° at the endocardium to -45.5° at the epicardium. Comparison with anatomical measurements shows that the optimized transmural course of helix fiber angle is not significantly different. Moreover, the optimizations predict that fibers have a significant transmural component, quantified by the transverse angle, with a spatial average between equator and apex of -5.6°. The results indicate that the structure of the left ventricle may be designed for maximum homogeneity of fiber strain during ejection.

References

1. Arts, T., F. W. Prinzen, L. H. E. H. Snoeckx, J. M. Rijcken, and R. S. Reneman. Adaptation of cardiac structure by mechanical feedback in the environment of the cell: a model study. *Biophys J* 66: 953-961, 1994.
2. Arts, T., and R. S. Reneman. Dynamics of left ventricular wall and mitral valve mechanics - a model study. *J Biomech* 22: 261-271, 1989.
3. Barthelemy, J.-F. M., and R. T. Haftka. Approximation concepts for optimum

structural design - a review. *Structural optimization* 5: 129-144, 1993.

4. Beyar, R., and S. Sideman. Left ventricular mechanics related to the local distribution of oxygen demand throughout the wall. *Circ Res* 58: 664-677, 1986.
5. Bovendeerd, P. H. M., T. Arts, J. M. Huyghe, D. H. van Campen, and R. S. Reneman. Dependence of local left ventricular wall mechanics on myocardial fiber orientation: a model study. *J Biomech* 25: 1129-1140, 1992.
6. de Tombe, P. P., and H. E. D. J. ter Keurs. Sarcomere dynamics in cat cardiac trabeculae. *Circ Res* 68: 588-596, 1991.
7. Delhaas, T., T. Arts, P. H. M. Bovendeerd, F. W. Prinzen, and R. S. Reneman. Subepicardial fiber strain and stress as related to left ventricular pressure and volume. *Am J Physiol* 264: H1548-H1559, 1993.
8. Grimm, A. H., H.-L. Lin, and B. R. Grimm. Left ventricular free wall and intraventricular pressure-sarcomere length distributions. *Am J Physiol* 239: H101-H107, 1980.
9. Guccione, J. M., K. D. Costa, and A. D. McCulloch. Finite element stress analysis of left ventricular mechanics in the beating dog heart. *J Biomech* 28: 1167-1177, 1995.
10. Guccione, J. M., W. G. O'Dell, A. D. McCulloch, and W. C. Hunter. Anterior and posterior left ventricular sarcomere lengths behave similarly during ejection. *Am J Physiol* 272: H469-H477, 1997.
11. Huyghe, J. M., T. Arts, D. H. van Campen, and R. S. Reneman. Porous medium finite element model of the beating left ventricle. *Am J Physiol* 262: H1256-H1267, 1992.
12. Malvern, L. E. *Introduction to the mechanics of a continuous medium.* London: Prentice-Hall, Inc., 1969.
13. McCulloch, A. D., B. H. Smaill, and P. J. Hunter. Regional left ventricular epicardial deformation in the passive dog heart. *Circ Res* 64: 721-733, 1989.
14. Mullender, M. G., R. Huiskes, and H. Weinans. A physiological approach to the simulation of bone remodeling as a self-organizational control process. *J Biomechanics* 27: 1389-1394, 1994.
15. Nielsen, P. M. F., I. J. Le Grice, B. H. Smaill, and P. J. Hunter. Mathematical model of geometry and fibrous structure of the heart. *Am J Physiol* 260: H1365-H1378, 1991.
16. Nikolic, S., E. L. Yellin, K. Tamura, H. Vetter, T. Tamura, J. S. Meisner, and R. W. M. Frater. Passive properties of canine left ventricle: diastolic stiffness and restoring forces. *Circ Res* 62: 1210-1222, 1988.
17. Peskin, C. S. Fiber architecture of the left ventricular wall: an asymptotic analysis. *Commun Pure Appl Math* 42: 79-113, 1989.
18. Press, W. H., B. P. Flannery, S. A. Teukolsky, and W. T. Vetterling. *Numerical Recipes. The art of scientific computing.* Cambridge: Cambridge University Press, 1986.
19. Rademakers, F. E., W. J. Rogers, W. H. Guier, G. M. Hutchins, C. O. Siu, M. L. Weisfeldt, J. L. Weiss, and E. P. Shapiro. Relation of regional cross-fiber shortening to wall thickening in the intact heart. Three-dimensional strain analysis by NMR tagging. *Circ* 89: 1174-1182, 1994.
20. Rodriguez, E. K., J. H. Omens, L. K. Waldman, and McCulloch. Effect of residual stress on transmural sarcomere length distributions in rat left ventricle. *Am J Physiol* 264: H1048-H1056, 1993.
21. Spotnitz, H. M., E. H. Sonnenblick, and D. Spiro. Relation of ultrastructure to function in the intact heart: sarcomere structure relative to pressure volume curves of intact left ventricles of dog and cat. *Circ Res* 18: 49-66, 1966.
22. Streeter, D. D., Jr. Gross morphology and fiber geometry of the heart. In:

Handbook of physiology - The cardiovascular system I, edited by R. M. Berne Am. Physiol. Soc., Bethesda, MD, 1979, p. 61-112.

23. Streeter, D. D., Jr., W. E. Powers, M. A. Ross, and F. Torrent-Guasp. Three-dimensional fiber orientation in the mammalian left ventricular wall. In: *Cardiovascular System Dynamics*, edited by J. Baan, A. Noordergraaf and J. Raines. Cambridge, Mass.: M.I.T. Press, 1978, p. 73-84.
24. Streeter, D. D. J., and W. T. Hanna. Engineering mechanics for successive states in canine left ventricular myocardium. 1. Cavity and wall geometry. *Circ Res* 33: 639-655, 1973.
25. ter Keurs, H. E. D., W. H. Rijnsburger, R. van Heuningen, and M. J. Nagelsmit. Tension development and sarcomere length in rat cardiac trabeculae: evidence of length-dependent activation. *Circ Res* 46: 703-714, 1980.
26. Waldman, L. K., D. Nosan, F. Villareal, and J. W. Covell. Relation between transmural deformation and local myofiber direction in canine left ventricle. *Circ Res* 63: 550-562, 1988.
27. Yin, F. C. P., R. K. Strumpf, P. H. Chew, and S. L. Zeger. Quantification of the mechanical properties of noncontracting canine myocardium under simultaneous biaxial loading. *J Biomech* 20: 577-589, 1987.

Chapter 4

Measurement of transmural component of muscle fiber direction in left ventricle by diffusion tensor imaging

J. Rijcken[1], K. Nicolay[2], P.H.M. Bovendeerd[3], D.H. van Campen[3], T. Arts[1]

[1]Department of Biophysics, Cardiovascular Research Institute Maastricht, Maastricht University, Maastricht, The Netherlands,
[2]Department of *in vivo* NMR Spectroscopy, Bijvoet Center for Biomolecular Research, Utrecht University, Utrecht, The Netherlands,
[3]Department of Mechanical Engineering, Eindhoven University of Technology, Eindhoven, The Netherlands.

submitted

Abstract

AIM: Mathematical models of cardiac mechanics predict that muscle fibers in the left ventricular (LV) wall have a small but significant transmural component. Experimental data to test such model predictions are scarce and not comprehensive. Our aim was the development of a method to accurately measure the transmural component of fiber direction. METHODS: Using diffusion tensor imaging, local diffusion tensors of water were determined in the post-mortem canine heart. The direction of highest diffusivity, defined by the eigenvector corresponding to the largest eigenvalue of the diffusion tensor, was assumed to coincide with local fiber direction. Assuming rotational symmetry of the LV wall, diffusion tensors in annular regions of 13 short-axis planes through the LV were averaged. Fiber directions were determined from average diffusion tensors. For each short-axis plane the radius, R_0, was determined at which fibers lie in the short-axis plane. The transmural component of fiber direction at R_0 was quantified by the angle, $\alpha_{t,0}$, between circumferential and fiber directions. RESULTS: The angle $\alpha_{t,0}$ varied linearly with apex-base distance, from approximately 8° at the base to -10° at one-third of the long LV axis from the apex. The estimated accuracy of the measurement was ±1.6° (sd), which is sufficient to determine the transmural component of fiber direction in the post-mortem LV.

Index terms: diffusion-weighted MRI, transverse angle, fiber imbrication

Introduction

The complex distribution of muscle fiber direction in the cardiac walls is an important determinant of the distribution of mechanical load (3). Accurate knowledge of the distribution of fiber direction is therefore needed for reliable analysis of stresses and strains in the cardiac walls. Fibers are usually thought to be helically wound in layers parallel to the epicardium, with the pitch in a layer depending sharply on depth in the wall. However, blunt anatomical dissections (17) and morphometric measurements (13, 14) indicate that fiber direction is likely to have a transmural component of a few degrees with the epicardial surface. Such a transmural component has also been predicted in a mathematical model of the mechanics of the left ventricular (LV) wall (10). In the latter study, the principle was used that stress in the muscle fibers is uniformly distributed during systole. In another mathematical model of LV wall mechanics (4) it was shown that the introduction of a small transmural component of fiber direction has significant effects on the radial-circumferential shear deformation of the LV wall. Despite the potential functional significance of the transmural component of fiber direction, little effort has been made to quantify it.

In this study, fiber direction in the LV wall was quantified in terms of a helix and a transverse angle. The helix angle describes the helical organization of the muscle fibers. In a cylindrical coordinate system (r,ϕ,z), in which the z-axis coincides with the long LV axis, the helix angle was defined as the angle between the circumferential direction and the projection of fiber direction on the ϕ-z plane. The transverse angle represents the transmural component of fiber direction. This angle is spanned between the circumferential direction and the projection of fiber direction on the r-ϕ plane. Typically, the helix angle changes by about 120^{o} between inner and outer LV wall surfaces, while the changes in transverse angle are likely to be much smaller, of the order of a few degrees (13).

Current methods to measure fiber angles rely either on anatomical dissection or on diffusion tensor imaging. Dissection techniques include 1) blunt dissection, in which macroscopic muscle fiber bundles are followed through the cardiac wall by tearing of the tissue (17), 2) morphometry, (7, 12, 13) in which through-wall blocks of cardiac tissue are excised and prepared as histological sections for the measurement of fiber directions under a microscope, and 3) measurement of macroscopic fiber directions on surfaces parallel to the epicardium (9). Recently, diffusion tensor imaging (DTI) has been used to make comprehensive and fully 3-dimensional reconstructions of material anisotropy in the heart, both *in vitro* (6) and *in vivo* (11). With DTI, local apparent diffusion coefficients of water, measured in 6 directions, are used to determine the local diffusion tensor (2, 8). The direction in

which water diffusivity is highest is defined by the eigenvector corresponding to the largest eigenvalue of the diffusion tensor. Experiments in cardiac (11) and skeletal muscle (5, 18) confirm that the direction of highest diffusivity corresponds closely to local fiber direction, as determined by anatomical measurements.

A problem with current measurement techniques is their limited accuracy. The standard deviation in the measurement of fiber direction with DTI, for example, appeared to be approximately $\pm 10^{o}$ (11). In morphometric studies (12, 15) this standard deviation in a single histological section was also approximately $\pm 10^{o}$. Since the accuracy of the present techniques is similar to the magnitude of the transverse angle itself, it is difficult to assess whether the transverse angle is significantly different from zero.

We propose a new method to determine the transverse angle by DTI in the post-mortem canine left ventricle. To improve the accuracy we averaged the diffusion tensor components, before calculating the eigenvectors. The main assumption underlying the averaging approach was rotational symmetry of the distribution of fiber direction in the LV. Following DTI measurements in 13 short-axis planes of the LV, diffusion tensor components in annular regions of each plane were averaged. Fiber directions and angles were calculated from average diffusion tensors. In each short-axis plane the radius was determined at which the helix angle was zero (i.e. the radius at which fibers lie in the short-axis plane). At this radius, the transverse angle was determined. Thus, we obtained the base-to-apex course of the transverse angle in the mid-wall region of the LV wall.

Methods

Experimental preparation. An adult healthy husky dog was used, that was to be sacrificed for an unrelated orthopedic experiment. The dog, weighing approximately 30 kg, was fully heparinized. Under sodium thiopental anesthesia a left lateral thoracotomy was performed. The pericardium was opened. A ligature was placed loosely around the ascending aorta. The ligature was tied while 100 ml of a 10% KCl solution was rapidly injected into the left ventricle causing immediate cardiac arrest. The heart was excised and submerged in a calcium-free solution containing: NaCl (138 mM), KCl (4 mM), $MgCl_2.6H_2O$ (1 mM), HEPES (11.6 mM), glucose.H_2O (11 mM), and NaOH (to obtain pH 7.4). The right atrium was punctured to allow free outflow of blood during retrograde perfusion of the heart. A perfusion system was attached to the aorta. The coronary circulation was perfused for 2 minutes at 13 kPa with the calcium-free solution to wash out calcium and prevent contraction of the heart. Subsequently the heart was submerged in a

solution of 3.6% formaldehyde in phosphate-buffered saline and perfused with formaldehyde at 13 kPa for 30 minutes. After removal of the atria the heart was stored in formaldehyde.

Diffusion tensor imaging. ^{1}H DTI measurements were performed at 200 MHz on a SIS Co. (Palo Alto, USA) NMR Spectrometer. The instrument was equipped with a self-shielded gradient (inner diameter 33 cm) that provided a maximal gradient strength of 32 mT m^{-1} (rise time 600 µs). The heart was wrapped in plastic foil to prevent dehydration, securely fastened, and placed in the center of the magnet bore. The long LV axis was visually aligned with the center line of the cylindrical magnet bore. Diffusion-weighted images were collected with a spin-echo MRI sequence in which the dephasing lobe of the read-out gradient was placed immediately prior to the data acquisition window to minimize cross-talk between the imaging gradients and the diffusion-sensitizing gradients. Diffusion data were measured in 13 short-axis slices, each with a thickness of 2.75 mm and a slice center line separation of 5.5 mm. Other parameter values were: echo time TE, 100 ms; repetition time TR, 4 s; diffusion gradient pulse duration, 25 ms; diffusion gradient pulse separation, 50 ms; number of transients, 1; field-of-view, 11 x 11 cm; data matrix, 128 x 128 points (giving an in-plane image resolution of 0.086 x 0.086 cm). At each point of the data matrix in a slice, the apparent diffusion coefficient (ADC) of tissue water was determined in each of 6 directions. Determination of the ADCs was based on reported procedures (2). Briefly, diffusion sensitizing gradients were applied separately in the directions (1,0,0), (0,1,0), (0,0,1), $\sqrt{2}/2$(1,1,0), $\sqrt{2}/2$(0,1,1), and $\sqrt{2}/2$(1,0,1), in an (X,Y,Z) coordinate system with the Z-axis along the center line of the magnet bore. For each direction, 5 different magnitudes of the sensitizing gradient were applied, ranging from 0 to 25 mT m^{-1}, yielding b-values (2) between 0 and 1165 s mm^{-2}. For each direction and for each point of the data matrix, the b-values and ratios of attenuated to unattenuated NMR-signals (i.e. with and without sensitizing gradients respectively) were determined. The ADC in a given diffusion sensitizing gradient direction was determined as the negated slope of a linear regression line to the logarithm of the ratio of NMR-signals versus b-value. If the correlation coefficient of the logarithm of the ratio of NMR-signals and b-value was less than 0.9, the ADC was deemed unreliable and set to zero. The signal-to-noise ratio (SNR) of unattenuated signals ranged from 18.5 to 19.0 dB while the SNR of maximally attenuated signals ranged from 14.9 to 15.7 dB. The measurements were performed at an ambient temperature of 20 °C and took approximately 5 hours to complete.

Processing of raw diffusion data. Raw diffusion data consisted of 6 apparent diffusion coefficients per sample point (voxel), one for each diffusion sensitizing gradient direction. Apparent diffusion coefficients for given slices and directions of

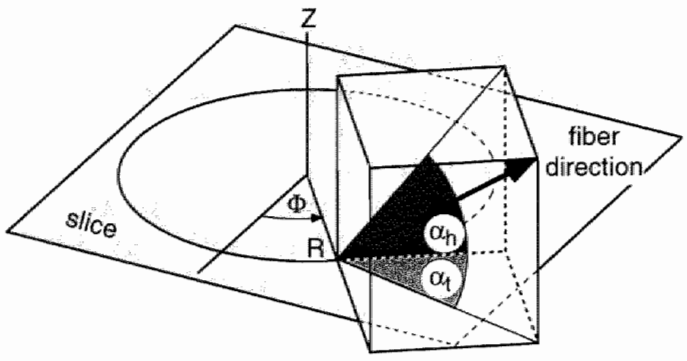

fig. 1. The manually selected left ventricular center in each slice is the origin of a cylindrical coordinate system (R,Φ,Z). Fiber direction is quantified by the helix angle, α_h, and the transverse angle, α_t.

measurement were displayed in histograms. Apparent diffusion coefficients outside the interval 0.2-1.5 $x10^{-9}$ m^2 s^{-1}, comprising approximately 2% of the data, were considered unrealistic and were excluded from further processing. Finally, only voxels with a complete set of 6 apparent diffusion coefficients were accepted for further analysis.

Determination of slice coordinate system. For each slice, the apparent diffusion coefficients in the X-direction accepted for determination of fiber angles were displayed on a computer terminal. In each slice the center of the LV outer contour was selected manually with a cursor, and a cylindrical coordinate system, (R,Φ,Z), was defined (fig. 1). The Z-axis is perpendicular to the plane of the slice, and is parallel to the center line of the magnet bore.

Circumferential averaging of diffusion tensors. Per slice, 4 contiguous annular regions of interest (ROI) together covering the majority of the LV wall were selected with a cursor. The innermost radius was chosen such that papillary muscles were not part of an ROI. For each accepted voxel in a ROI, a symmetric diffusion matrix was determined in the rectangular laboratory reference frame (X,Y,Z) from the measured apparent diffusion coefficients (1, 2). The diffusion matrices were converted to the cylindrical coordinate system of the slice. Diffusion matrix components within each ROI were averaged. Thus, per slice a diffusion matrix was obtained at 4 different radii.

Determination of fiber angles. For each of the 4 averaged diffusion matrices in a slice, eigenvalues and unit eigenvectors were computed. Fiber direction was defined by the eigenvector corresponding to the largest eigenvalue, i.e. fibers were defined to be parallel to the direction in which the diffusivity of water was highest. Fiber direction was quantified by the helix angle, α_h, and the transverse angle, α_t

(fig. 1). The helix angle is defined as the angle between the circumferential direction and the projection of the fiber direction on the Φ-Z plane. The transverse angle is defined as the angle between the circumferential direction and the projection of the fiber direction on the R-Φ plane. At each of the 4 radial positions in a slice the fiber angles α_h and α_t were calculated. In each slice the radius, R_0, was determined at which $\alpha_h=0^o$. This was done by linear interpolation between two adjacent helix angles that bracketed the value 0^o. Finally, in each slice the transverse angle, $\alpha_{t,0}$, at radius R_0 was determined by linear interpolation between two adjacent transverse angles bracketing the value R_0.

Error analysis. The effects of two potential error sources in the determination of the transverse angle, $\alpha_{t,0}$, in a slice were estimated: 1) inter-observer variability in manual selection of the LV center, and 2) misalignment of the long LV axis and the center line of the magnet bore. To enable estimation of the errors, a model of the LV fiber field was designed. In a simulated thick-walled cylinder, the helix angle depended linearly on radial distance with a value of 0.0 radians at radius 1.0 units and a slope of -5.0 radians per unit distance in radial direction. The transverse angle had a constant value of 0.1 radians throughout the field. In the model, a plane of observation, representing a slice, was defined, whose center was either displaced by a distance r* from the axis of symmetry or whose normal made an angle γ (radians) with the axis of symmetry of the fiber field. In the defined slice the radius R_0 and the transverse angle at R_0 were determined, analogous to the procedure described above for the measurements.

A realistic estimate of inter-observer variability in manual selection of LV center was obtained as follows. Seven volunteers were asked to select the LV center in a short-axis image of apparent diffusion coefficients in the X-direction of the real LV (fig. 2a). The mean LV center position was determined. Inter-observer variability was defined as the mean distance, r*, of the individual LV center positions from the mean LV center position, normalized to the estimated mid-wall radius. A value of r*=0.08 was obtained. The angle, γ, representing the misalignment between the long LV axis and the center line of the magnet bore, was estimated to be less than 0.26 radians (or 15^o). Values of γ and r* were varied separately to investigate their effects on the error in transverse angle.

Results

The histograms of the apparent diffusion coefficients had similar shapes for all diffusion-sensitizing directions. For a typical slice the apparent diffusion coefficients were 0.74±0.36 (mean±sd), 0.73±0.35, 0.72±0.37, 0.74±0.38,

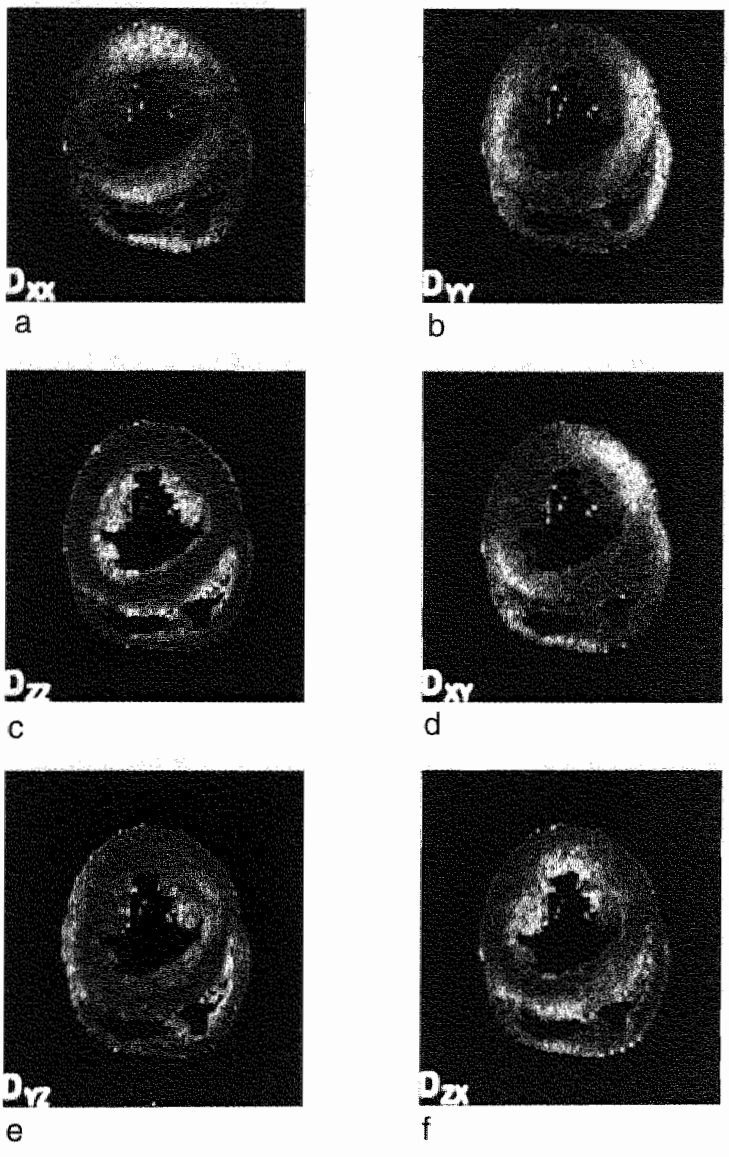

fig. 2. Gray-value images of measured apparent diffusion coefficients D_{XX}, D_{YY}, D_{ZZ}, D_{XY}, D_{YZ}, and D_{ZX} of equatorial slice that were accepted for determination of fiber angles. The X-axis runs from left to right, the Y-axis from top to bottom and the Z-axis out of the paper away from the reader. Diffusivity increases with brightness.

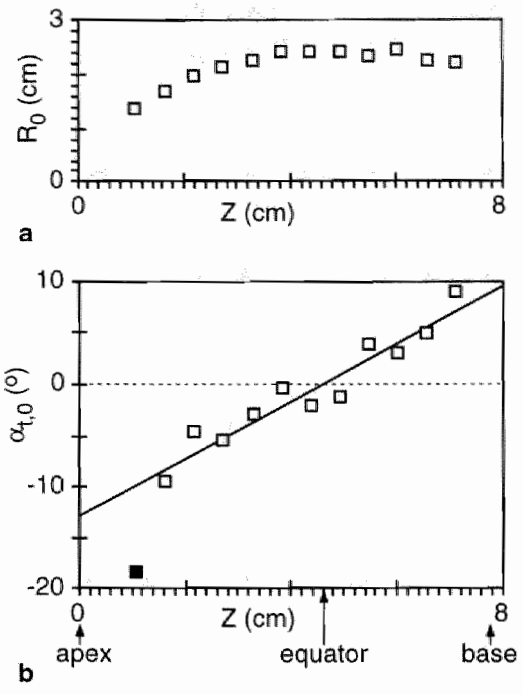

fig. 3. (a) The radius, R_0, at which the helix angle is 0 radians, as function of apex-base distance, Z. (b) The transverse angle, $\alpha_{t,0}$, at radius R_0 as function of Z. Also shown is a regression line to the data (—), determined after the most apical measurement, denoted by (■), was excluded. The position of the equator is indicated by a zero-transverse angle. The indicated positions of base and apex were estimated from slice spacing and thickness.

0.76±0.34, and 0.74±0.36 $x10^{-9}$ m^2 s^{-1} in the X-, Y-, Z-, XY-, YZ-, and ZX-directions respectively. Of all the voxels containing at least one apparent diffusion coefficient in the interval 0.2-1.5 $x10^{-9}$ m^2 s^{-1}, 88% contained all 6 apparent diffusion coefficients. In the most basal slice, the LV wall contained too few voxels from which 6 apparent diffusion coefficients were accepted, to be able to reliably select the LV center and the regions of interest. Therefore, the most basal slice was excluded from the analysis. In the most apical slice the LV cavity could barely be distinguished. Gray-value images of apparent diffusion coefficients of a typical slice that were accepted for determination of fiber angles are shown in fig. 2. A sense of the distribution of fiber direction can be obtained from the individual panels of fig. 2. A high diffusivity, indicated by brightness, is observed in all panels of fig. 2 in regions where the expected fiber direction has a large component parallel to the diffusion sensitizing gradient direction.

In all slices the helix angle was positive towards the endocardium and negative towards the epicardium. The radius, R_0, at which the (interpolated) helix angle was zero followed the LV mid-wall shape, increasing from the apex to the equator and subsequently decreasing (fig. 3). The transverse angle at radius R_0 decreased nearly linearly with apex-base distance from approximately 8° near the base to 0° at the equator and to -19° near the apex (fig. 3). The most apical measurement of transverse angle appeared to deviate strongly from the practically linear course found in the remainder of the left ventricle. If the most apical slice was excluded, the standard deviation between the transverse angle data and a linear regression line was ±1.6°. On inclusion of the most apical slice, the standard deviation between the transverse angle data and a linear regression line was ±2.8°. The residual deviation between the transverse angle in the most apical slice and the latter regression line was more than twice the residual standard deviation.

Error Analysis. The inter-observer variability in manual selection of LV center was represented by the value $r^*=0.08$. Under these circumstances the observed transverse angle, $\alpha_{t,0}$, was 0.096 radians, resulting in an error of -4.1% relative to the true value of 0.1 radians. If the slice was tilted by an angle $\gamma=0.26$ radians, the observed transverse angle, $\alpha_{t,0}$, was 0.098 radians, resulting in an error of -2.1%. The error in observed transverse angle increased approximately quadratically both with r^* and γ.

Discussion

A method has been developed to measure the transmural component of fiber direction by diffusion tensor imaging (DTI) in the post-mortem heart. The DTI technique was used to determine local diffusion tensors of water in short-axis planes through the heart by magnetic resonance. Local fiber direction was defined as the direction of highest diffusivity, as determined from the local diffusion tensor. To enhance the accuracy of the DTI approach, the LV fiber structure was considered to be rotationally symmetric. The diffusion tensor components in the LV were averaged in circumferential direction in each short-axis plane, before determining fiber directions. The radius was determined at which fibers lay in the short-axis plane. At this radius, the transverse angle (fig. 1) was determined. In a single canine LV the transverse angle thus determined showed a nearly linear dependence on apex-base distance.

It is difficult to determine the random error in the determination of the transverse angle by the present method. From the practically linear apex-base variation of the transverse angle (fig. 3), it is clear that the method is sufficiently

accurate to conclude that the transverse angle is significantly different from zero. Assuming that fiber direction changes smoothly through the wall, the deviation of the measurements from a smooth line gives an indication of the accuracy of the method. The standard deviation of the measured transverse angle data set with respect to a linear regression line was ±1.6° if the most apical measurement was excluded. Thus, the random error in the determination of the transverse angle by the proposed method is likely to be less than ±1.6° (sd) over most of the wall, or less than 10% of the observed range of the transverse angle (fig. 3).

The implemented averaging of diffusion tensor components may be expected to increase the accuracy of the method. For the averaging procedure rotational symmetry of the distribution of fiber direction in the LV wall was assumed. Anatomical measurements in canine hearts (9) support this contention, indicating that circumferential variations in helix angle are small except at the junctions of left and right ventricles. Averaging was carried out in as early a stage as possible to minimize the accumulation of errors due to nonlinear data operations. Therefore, instead of averaging transverse angles themselves, the diffusion tensor components were averaged.

In the present study the transverse and helix angles were defined with respect to a cylindrical coordinate system (fig. 1). It is more common to define the fiber angles with respect to the local longitudinal, local transmural and circumferential directions (9, 12, 13). The helix fiber angle is then defined as the angle between the local circumferential direction and the projection of fiber direction on the plane normal to the local transmural direction (fig. 4a). The transverse fiber angle, α_{t^*}, is defined as the angle between the local circumferential direction and the projection of fiber direction on the plane normal to the local longitudinal direction. At the radius, R_0, at which the measured helix angle is zero, the relation between the transverse fiber angle, $\alpha_{t^*,0}$, and the measured transverse angle, $\alpha_{t,0}$, is given by:

$$\alpha_{t^*,0} = \tan^{-1}\left(\tan\alpha_{t,0}\cos\beta\right), \qquad [1]$$

where β is the angle between the local longitudinal direction and the long LV axis. Thus, at the equator, where β=0, the definitions of α_t and α_{t^*} agree exactly but further towards the apex and base their difference increases. The angle β was estimated from a second order polynomial fitted to the measured apex-base course of R_0 (fig. 3a). Hence, for each measured transverse angle $\alpha_{t,0}$, the angle $\alpha_{t^*,0}$ was determined. Fig. 4b shows that the difference between $\alpha_{t^*,0}$ and the measured transverse angle $\alpha_{t,0}$ is negligible except at the most apical site where it is 2.1°.

The results indicate that an alternative, more accurate, definition of the

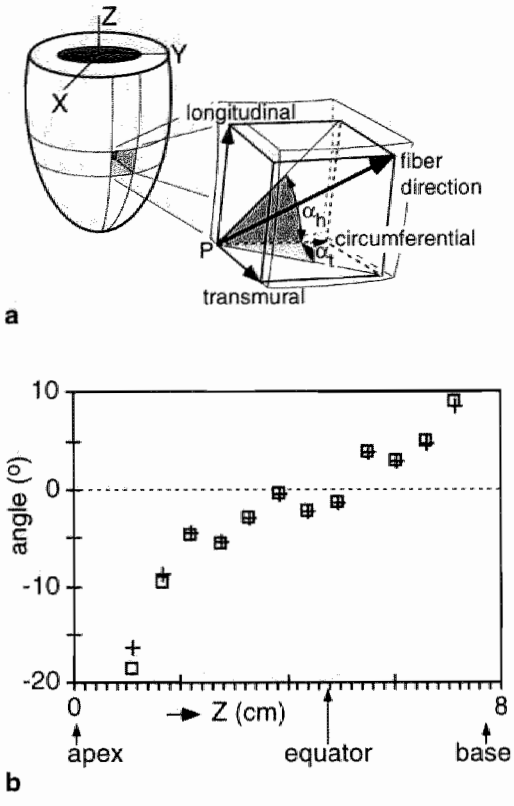

fig. 4. (a) Definition of the more commonly used helix (α_{h^*}) and transverse (α_{t^*}) angles with respect to local longitudinal, circumferential, and transmural directions. (b) The estimated transverse fiber angle, $\alpha_{t^*,0}$, (+) at radius R_0 as function of Z. Also shown is the measured transverse angle, $\alpha_{t,0}$ (□). The difference between $\alpha_{t^*,0}$ and $\alpha_{t,0}$ is small except close to the apex.

equator is possible. The equator is usually defined as the latitude at which the epicardial LV radius is greatest (13). From anatomical measurements in canine hearts (16) the ratio of apex-equator to equator-base distance was thus found to be approximately 2:1. However, in the neighborhood of the equator, the LV wall is almost cylindrical, the rate of change of LV wall radius with latitude being close to zero. Therefore, determination of the equator on the basis of maximum radius may be difficult. The practically linear latitude dependence of the transverse angle, $\alpha_{t,0}$ (fig. 3), allows a more accurate definition of the equator as the latitude at which the transverse angle is zero. This definition is in agreement with predictions of the distribution of fiber directions by mathematical models of LV wall mechanics (10). In

the single dog heart, the thus defined equator occurs in the region with the largest LV wall radius (fig. 3), which corresponds closely to the definition by Streeter (13).

These are the first measurements of the transmural component of muscle fiber direction throughout a major part of the post-mortem left ventricle. In one other study (13) the transmural component of fiber direction was quantified by a morphometric technique in a single normal human heart in the LV free wall at the equator and at a site approximately halfway between equator and apex. Through-wall averages of transverse angle were found to be -4.6±0.8° (mean±sem, n=12) at the equator and -3.5±0.6° (n=15) further towards the apex. Through-wall averages can also be estimated from our measurements, assuming as a first approximation a quadratic transmural course of transverse angle, going through zero at the wall surfaces and reaching an extreme value of $\alpha_{t,0}$. Thus, estimated through-wall averages are 0° at the equator and -4° halfway between equator and apex (see fig. 3). However, since both studies are based on single hearts, conclusions regarding the differences in observed transverse angle are premature.

In conclusion, we have developed a method using diffusion tensor imaging to measure the transmural component of fiber direction in the post-mortem left ventricle. In one dog heart the transmural component of fiber direction in the mid-wall region of the LV, quantified by the transverse angle, showed a nearly linear dependence on apex-base distance. The transverse angle could be quantified with a random error of ±1.6° (sd) over the majority of the LV wall. The error represents approximately 10% of the observed range of the transverse angle. Therefore, the developed method is sufficiently accurate to resolve the transmural component of fiber direction.

Acknowledgments

The authors thank Hans de Nijs for implementation of the method in MATLAB and for processing much of the data. The MRI-studies were performed at the Netherlands *in vivo* NMR facility (Bijvoet Center, Utrecht University) which was supported by the Netherlands Organization for Scientific Research (NWO).

References

1. Basser, P. J., J. Mattiello, and D. LeBihan. estimation of the effective self-diffusion tensor from the NMR spin echo. *J MR series B* 103: 247-254, 1994.
2. Basser, P. J., J. Mattiello, and D. LeBihan. MR Diffusion tensor spectroscopy and imaging. *Biophys J* 66: 259-267, 1994.
3. Bovendeerd, P. H. M., T. Arts, J. M.

Huyghe, D. H. van Campen, and R. S. Reneman. Dependence of local left ventricular wall mechanics on myocardial fiber orientation: a model study. *J Biomech* 25: 1129-1140, 1992.

4. Bovendeerd, P. H. M., J. M. Huyghe, T. Arts, D. H. van Campen, and R. S. Reneman. Influence of endocardial-epicardial crossover of muscle fibres on left ventricular wall mechanics. *J Biomech* 27: 941-951, 1994.
5. Drost, M. R., G. C. van Donkelaar, L. J. G. Kretzers, and K. Nicolay. A comparison of local muscle fiber direction measured by diffusion tensor imaging with muscle fiber direction as determined in an actual section. *Fifth scientific meeting of the International Society of Magnetic Resonance in Medicine*, Vancouver, 1997, p. 1717.
6. Garrido, L., V. J. Wedeen, K. K. Kwong, U. M. Spencer, and H. L. Kantor. Anisotropy of water diffusion in the myocardium of the rat. *Circ Res* 74: 897-793, 1994.
7. Greenbaum, R. A., Y. H. Siew, D. G. Gibson, A. E. Becker, and R. H. Anderson. Left ventricular fibre architecture in man. *Br Heart J* 45: 248-263, 1981.
8. Le Bihan, D., and R. Turner. Diffusion and perfusion nuclear magnetic resonance imaging. In: *Magnetic resonance angiography*, edited by E. J. Potchen, J. E. Siebert, E. M. Haacke and A. Gottschalk. St Louis, Missouri, USA: Mosby, 1993, p. 323-333.
9. Nielsen, P. M. F., I. J. Le Grice, B. H. Smaill, and P. J. Hunter. Mathematical model of geometry and fibrous structure of the heart. *Am J Physiol* 260: H1365-H1378, 1991.
10. Peskin, C. S. Fiber architecture of the left ventricular wall: an asymptotic analysis. *Commun Pure Appl Math* 42: 79-113, 1989.
11. Reese, T. G., R. M. Weisskoff, R. N. Smith, B. R. Rosen, R. E. Dinsmore, and V. J. Wedeen. Imaging myocardial fiber architecture in vivo with magnetic resonance. *Magn Reson Med* 34: 786-791, 1995.
12. Ross, M. A., and D. D. Streeter Jr. Nonuniform subendocardial fiber orientation in the normal macaque left ventricle. *Eur J Cardiol* 3: 229-247, 1975.
13. Streeter, D. D., Jr. Gross morphology and fiber geometry of the heart. In: *Handbook of physiology - The cardiovascular system I*, edited by R. M. Berne Am. Physiol. Soc., Bethesda, MD, 1979, p. 61-112.
14. Streeter, D. D., Jr., W. E. Powers, M. A. Ross, and F. Torrent-Guasp. Three-dimensional fiber orientation in the mammalian left ventricular wall. In: *Cardiovascular System Dynamics*, edited by J. Baan, A. Noordergraaf and J. Raines. Cambridge, Mass.: M.I.T. Press, 1978, p. 73-84.
15. Streeter, D. D., Jr., H. M. Spotnitz, D. P. Patel, J. Ross Jr., and E. H. Sonnenblick. Fiber orientation in the canine left ventricle during diastole and systole. *Circ Res* 24: 339-347, 1969.
16. Streeter, D. D. J., and W. T. Hanna. Engineering mechanics for successive states in canine left ventricular myocardium. 1. Cavity and wall geometry. *Circ Res* 33: 639-655, 1973.
17. Torrent-Guasp, F. *The cardiac muscle*. Madrid: Fundacin Juan, 1973.
18. van Doorn, A., P. H. M. Bovendeerd, K. Nicolay, M. R. Drost, and J. D. Janssen. Determination of muscle fibre orientation using diffusion-weighted MRI. *Eur J Morphol* 34: 5-10, 1996.

Chapter 5

Left ventricular muscle fiber orientation is optimal for homogeneous fiber strain during ejection

J. Rijcken[1], P.H.M. Bovendeerd[2], R.S. Reneman[3], D.H. van Campen[2], T. Arts[1]

[1]Department of Biophysics, Cardiovascular Research Institute Maastricht, Maastricht University, The Netherlands,
[2]Department of Mechanical Engineering, Eindhoven University of Technology, Eindhoven, The Netherlands,
[3]Department of Physiology, Cardiovascular Research Institute Maastricht, Maastricht University, The Netherlands.

Abstract

AIM: Our aim was to test whether characteristic details of the measured distribution of muscle fiber orientation could be predicted, based on the hypothesis that the distribution of fiber orientation in the left ventricular (LV) wall is such that systolic fiber strain is as homogeneous as possible. METHODS: A finite element model of LV wall mechanics, incorporating thick-walled rotationally symmetric wall geometry and nonlinear anisotropic constitutive behavior, was used to compute systolic fiber strain. Fiber orientation was quantified by the helix and transverse angles, expressing the directional components in the planes perpendicular to the local transmural direction and the base-apex direction, respectively. The distributions of fiber angles over the LV wall were optimized to minimize regional differences in systolic fiber strain. RESULTS: After optimization, fiber strain referred to mid-diastole was 0.133±0.013 (mean±sd) and -0.082±0.007 at the beginning and end of ejection, respectively. At equatorial latitude the helix angle changed from 64.1° to -45.3° between inner and outer wall surfaces. The transmural course of helix angle was distinctly nonlinear in the subendocardium. The helix angle increased towards the apex. The mid-wall transverse angle changed practically linearly from zero at the equator to -7.7° halfway between equator and apex. The computed distributions of fiber angles over the wall were consistent with reported measurements. CONCLUSIONS: The successful prediction of the measured distribution of fiber orientation supports the hypothesis that systolic muscle fiber strain is homogeneous in the heart.

Index terms: structural optimization; finite element analysis; functional anatomy

Introduction

Mechanical load in the left ventricular (LV) wall is likely to be uniformly distributed. Measurement of mechanical load, in the form of stress or strain, is difficult. The measurement of stress or force in the cardiac wall with a force transducer is unreliable because the transducer damages the tissue at the site of measurement (12). Strain in the cardiac wall has been measured by several methods (2, 7, 20, 24, 33, 34). Muscle fiber strain or sarcomere length has been determined in only a few studies at a limited number of sites in the LV wall (5, 11, 21, 34). In the latter studies, regional differences in fiber strain or sarcomere length were found to be not significant during the ejection period, except perhaps at the junction of right and left ventricles (21).

In view of the incompleteness of experimental data, mathematical models have been developed to predict the distribution of stress and strain over the LV wall. Recent mathematical models (1, 4, 10, 13) incorporate increasingly accurate cardiac geometry, nonlinear anisotropic material behavior of cardiac tissue, sometimes the effects of residual stress (10), and allow for the large deformations observed in the heart. Models of LV wall mechanics indicate that the distributions of fiber stress and strain over the LV wall during ejection are sensitive to the distribution of muscle fiber orientation (4, 13). it was found (4, 13) that it was possible to choose a distribution of fiber orientation within the anatomical range that yielded transmural distributions of systolic fiber stress that were either practically uniform or varied by more than a factor two.

In this study, fiber orientation was quantified by the helix and transverse fiber angles (fig. 1). For definition of the fiber angles, a nested set of shells was defined in the LV wall, with the inner and outer shells forming the endocardial and epicardial surfaces. The fiber angles at a point in the LV wall were specified with respect to the local, mutually orthogonal circumferential, longitudinal, and transmural directions of a shell. The helix fiber angle was defined as the angle between the circumferential direction and the projection of fiber direction on the plane perpendicular to the local transmural direction. The transverse fiber angle was defined as the angle between the circumferential direction and the projection of fiber direction on the plane perpendicular to the local longitudinal direction. Anatomical measurements in the human (8, 29, 30), canine (17), and macaque (26) LV indicate that the transmural course of the helix fiber angle is distinctly nonlinear near the inner and outer wall surfaces. Moreover, the measurements indicate that towards the apex, fiber direction has a larger longitudinal component (30). Also, measurements in the dog (23) indicate that the transverse fiber angle in the mid-wall region is practically proportional to base-apex distance, except near the apex.

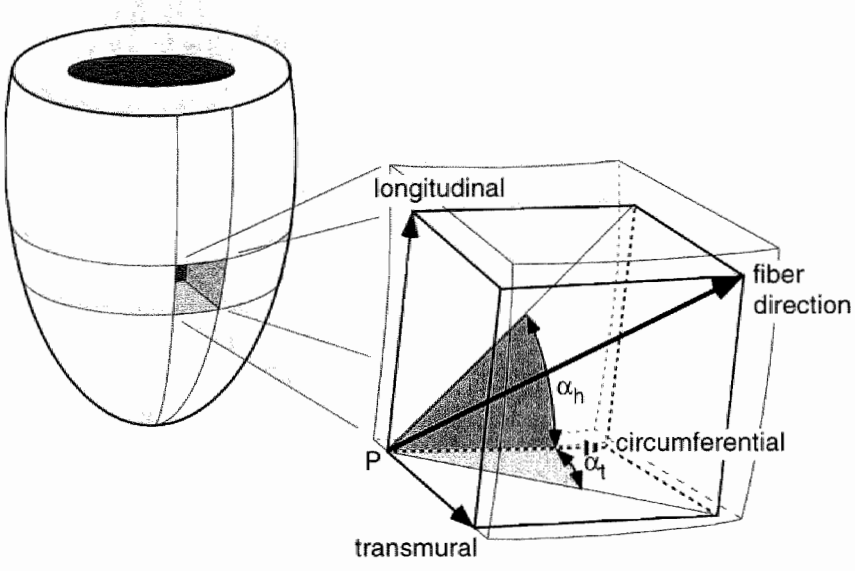

fig. 1. Illustration of the helix (α_h) and transverse (α_t) fiber angles in the rotationally symmetric LV. The fiber angles at a point P are defined with respect to the local transmural, local longitudinal and circumferential directions.

The aim of the present study was to investigate whether the observed characteristic details of the fiber angle distributions over the LV wall could be predicted on the basis of the hypothesis that the spatial distribution of muscle fiber orientation is such that systolic fiber strain is as homogeneous as possible. Earlier (22), this hypothesis was used to calculate the gross features of the observed distribution of muscle fiber orientation. However, because the spatial distribution of muscle fiber orientation was quantified by only 3 parameters no details were visible. Therefore, in this study the number of parameters describing the spatial distributions of the helix and transverse fiber angles was extended to a total of 12 to enable more detailed prediction of the observed variation of fiber angles with position in the wall. A finite element model was used to compute the distribution of fiber strain at the beginning and end of ejection. The model was embedded in an optimization procedure in which fiber strain at the beginning and end of ejection was made as homogeneous as possible by proper adjustment of the distribution of the 12 fiber angle parameters. The computed fiber angle distributions over the LV

wall were compared with those reported in anatomical measurements.

Methods

The design of the finite element model of LV wall mechanics and of the optimization strategy, as described earlier (22), are recapitulated, and changes and additions made in this study are indicated.

Finite element model of left ventricular wall mechanics

LV wall geometry in reference state . The reference state of no deformation in the finite element model of LV wall mechanics corresponded approximately to mid-diastole. In that state transmural pressure across the LV wall and stress in the wall were set to 0 kPa.

The LV wall was considered to be thick-walled and rotationally symmetric. Wall geometry was point-symmetric with respect to the center of the equatorial plane. Consequently, only the mechanics of the region between the apex and equator was considered for analysis. Wall geometry was chosen so that cavity and wall volume and long and short axes matched those of the canine LV. The choice of all parameter values used in the finite element model are given below in a separate section .

Fiber orientation in reference state. Fiber orientation in the reference state was quantified by the helix and transverse fiber angles as defined in relation to fig. 1. To be able to quantify the spatial distributions of the fiber angles a wall-bound coordinate system (u, v) was defined (fig. 2); the coordinate u decreases from 0 at the equator to -1 at the apex in direct proportion with distance along the midwall surface in the equator-to-apex direction; the coordinate v increases from -1 at the endocardium to +1 at the epicardium in direct proportion with distance in the direction perpendicular to the midwall surface.

The helix fiber angle, α_h, varies with u and v according to:

$$\begin{aligned}\alpha_h(u,v) = \; & (1+h_{u2}P_2(u)+h_{u4}P_4(u))(h_{v0}P_0(v)+h_{v1}P_1(v) \\ & +h_{v2}P_2(v)+h_{v3}P_3(v)+h_{v4}P_4(v)),\end{aligned} \qquad [1]$$

where h_{u2}, h_{u4} (dimensionless), and h_{v0}, h_{v1}, h_{v2}, h_{v3}, and h_{v4} (radians) are parameters the optimal values of which are to be determined, and $P_j(u)$ and $P_j(v)$ are Legendre polynomials (14) of order j in u and v, respectively. The uneven Legendre polynomials in u were excluded so that point symmetry with respect to the center of the equatorial plane was satisfied.

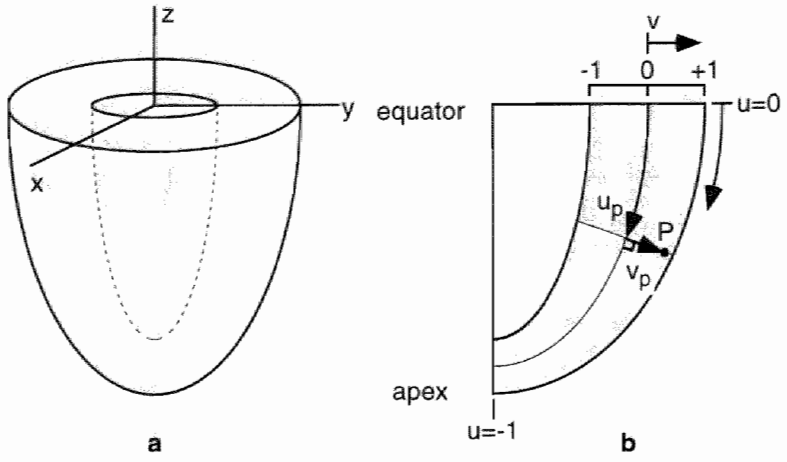

fig. 2. Diagram showing rotationally symmetric LV geometry and coordinate systems: (a) cartesian coordinate system (x, y, z) and (b) wall-bound coordinate system (u, v): point P has coordinates (u_p, v_p). Both u and v vary linearly with distance.

The transverse fiber angle, α_t, is zero at the wall boundaries, i.e. fibers are assumed not to end here. To satisfy point symmetry with respect to the center of the equatorial plane, α_t is an odd function of u. We described the spatial distribution of α_t by:

$$\alpha_t(u,v) = \left(t_{u1}P_1(u) + t_{u3}P_3(u) + t_{u5}P_5(u)\right)\left(1 + t_{v1}P_1(v) + t_{v2}P_2(v)\right)\left(1 - v^2\right), \qquad [2]$$

where parameters t_{u1}, t_{u3}, t_{u5}, (radians) and t_{v1}, and t_{v2} (dimensionless) have to be optimized.

Constitutive behavior. In the finite element model, cardiac tissue was considered to be a composite material of stiff fibers embedded in a compliant, but nearly incompressible tissue matrix. The total Cauchy stress tensor, **T**, in the tissue is the sum of a passive component, $\mathbf{T}_p$, arising from deformation of passive myocardial tissue, and an active component, $\mathbf{T}_a$, arising from muscle fiber contraction during systole:

$$\mathbf{T} = \mathbf{T}_p + \mathbf{T}_a. \qquad [3]$$

Passive myocardial tissue was assumed to be elastic and transversely isotropic with respect to the fiber direction. The Cauchy stress $\mathbf{T}_p$ in the passive

tissue was derived from a strain energy density function, W:

$$\mathbf{T}_p = \frac{1}{\det(\mathbf{F})}\mathbf{F}\bullet\frac{\partial W(\mathbf{E})}{\partial \mathbf{E}}\bullet\mathbf{F}^T, \qquad [4]$$

where **F** and **E** are the deformation gradient tensor and the Green-Lagrange strain tensors referred to the reference state, respectively, and superscript *T* denotes a tensor transpose (15). The strain energy density function, W, was chosen as:

$$W(\mathbf{E}) = a_0\left(\exp(a_1 I_E^2 + a_2 II_E + a_3\,\mathbf{e}_f\bullet\mathbf{E}\bullet\mathbf{e}_f) - 1\right) + a_4\left(\det(2\mathbf{E}+\mathbf{I}) - 1\right)^2, \quad [5]$$

where $I_E = \text{trace}(\mathbf{E})$,

$$II_E = \frac{1}{2}\left(\text{trace}\left(\mathbf{E}\bullet\mathbf{E}^T\right) - I_E^2\right),$$

a_0, a_1, a_2, a_3, and a_4 are material parameters, $\mathbf{e}_f$ is a unit vector in fiber direction, and trace is the sum of the diagonal elements.

The muscle fibers contain sarcomere units that are assumed to generate a uniaxial force in the fiber direction during systole. Experimental data on active muscle fiber stress are usually presented in terms of the first Piola-Kirchhoff stress. In the finite element simulations the first Piola-Kirchhoff active fiber stress, T_a^0 (kPa), depended linearly on sarcomere length, l_s (μm), and on active stiffness, K (kPa):

$$T_a^0 = K\frac{l_s - l_x}{l_{s,0}}, \qquad [6]$$

where l_x is the sarcomere length at which no contractile force can be generated, and $l_{s,0}$ is the sarcomere length in the reference state. Instantaneous sarcomere length, l_s, is related to the component of Green-Lagrange strain in the fiber direction, E_{11}, by: $l_s = l_{s,0}(1+2E_{11})^{1/2}$. The active stiffness, K, depended on the phase of the cardiac cycle. It was zero in the reference state and increased during systole to a maximum value at the end of ejection (27). The first Piola-Kirchhoff active fiber stress, T_a^0, is related to the active stress tensor $\mathbf{T}_a$ by the relation:

$$\mathbf{T}_a = \frac{1}{\det(\mathbf{F})}\mathbf{F}\bullet T_a^0\mathbf{e}_f\mathbf{e}_f. \qquad [7]$$

Finite element method. Calculations of fiber stresses and strains in the LV wall were based on the law of conservation of momentum (15), expressing static

equilibrium of forces in the wall due to both blood pressure in the cavity and internal stresses in the wall. The equations of conservation of momentum were converted into a Galerkin-type finite element formulation, implemented in the package Diana 5.1 (Diana Analysis B.V., Delft, The Netherlands). The finite element mesh consisted of twenty-seven 20-node brick elements comprising the sector of the LV in the region ($x \geq 0$, $y \geq 0$, $z \leq 0$). The endocardial surface was loaded with LV cavity pressure while the epicardium remained unloaded. Kinematic boundary conditions on the through-wall faces of the mesh allowed cavity volume changes and torsion to occur.

Finite element simulations. Finite element simulations started in the reference state of deformation (fig. 3). Cavity pressure and active stiffness were prescribed to obtain states of stress and deformation corresponding to the beginning and end of ejection. The beginning of ejection was defined by a cavity pressure of 12.3 kPa, and an active stiffness of 110 kPa corresponding to a cavity-to-wall-volume ratio of approximately 0.65. The end of ejection was defined by a cavity pressure of 17.5 kPa and an active stiffness of 560 kPa corresponding to a cavity-to-wall-volume ratio of approximately 0.13.

Output of a finite element simulation was fiber strain at the beginning and end of ejection in N=729 contiguous regions covering the LV wall mesh. For region i, fiber strain, ε_i, is given by:

$$\varepsilon_i = \frac{l_{s,i} - l_{s,0}}{l_{s,0}}, \qquad [8]$$

where $l_{s,i}$ is the instantaneous sarcomere length in the central point of the region and $l_{s,0}$ is the sarcomere length in the reference state.

Optimization of fiber orientation

The optimization consists of the minimization of an objective function, G, defined as the average over LV wall volume, V_w, of the deviation of regional fiber strains at the beginning and end of ejection from their respective mean values:

$$G(\mathbf{p}) = \sum_{i=1}^{N} \frac{\Delta V_i}{V_w} \left(\left(\varepsilon_{be,i} - \varepsilon_{be,av} \right)^2 + \left(\varepsilon_{ee,i} - \varepsilon_{ee,av} \right)^2 \right), \qquad [9]$$

where ΔV_i is the wall volume of region i, $\varepsilon_{be,i}$ and $\varepsilon_{ee,i}$ are regional fiber strains at the beginning and end of ejection, respectively, $\varepsilon_{be,av}$ and $\varepsilon_{ee,av}$ are average fiber strains over the LV wall at the beginning and end of ejection, respectively, and N=729 is the total number of regions into which the LV wall was divided. The

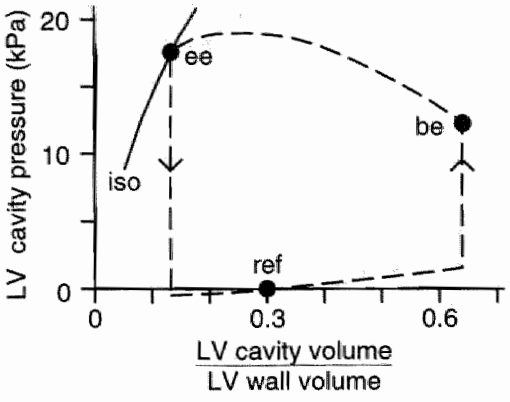

fig. 3. Schematic pressure-volume (p-V) diagram of LV during cardiac cycle. In the finite element simulations the point 'ref' is the stress-free reference state. The state of stress and deformation is computed at the beginning (be) and end (ee) of the ejection period. The point ee is located on the isovolumic (iso) curve.

objective function depends on the fiber angle parameters h_{u2}, h_{u4}, h_{v0}, h_{v1}, h_{v2}, h_{v3}, h_{v4}, t_{u1}, t_{u3}, t_{u5}, t_{v1}, and t_{v2} which are stored in the vector **p**. The first and second terms on the right hand side of equation [9] express the condition that fiber strain at the beginning and at the end of ejection, respectively, be as homogeneous as possible. The optimization strategy implemented to minimize the objective function of equation [9] was sequential approximate optimization (3).

Applied parameter values in finite element model

LV wall geometry in reference state. The choice of cavity and wall volume was based on experimental measurements in arrested canine left ventricles (16). Given that the base extends above the equator by a distance of half the semi-major axis (31), the LV wall geometry chosen corresponds to a cavity volume of 42 ml and a cavity-to-wall-volume ratio of 0.3. The ratio of mid-wall long to short axes was set to 2.08 (31). The course of wall thickness between equator and apex was adjusted so that mean through-wall fiber stress at the beginning of ejection was similar at all latitudes between equator and apex. In the resulting wall shape the ratio of equatorial to apical wall thickness was 3.0.

Sarcomere length in reference state. In the model, sarcomere length in the reference state, $l_{s,0}$, was set to 1.95 μm for all sarcomeres in the LV wall, a value based upon the average of values obtained in left ventricles of rats (9, 25) and dogs (28).

Constitutive behavior. For the passive material the relative values of a_1:a_2:a_3

in equation [4] were set to 1:2:1, so that the ratio of fiber to cross-fiber stress is 2.0 for an equibiaxially loaded sheet of tissue (36). The absolute values of a_0 and a_1 were set to 0.5 kPa and 3.0, respectively, so that calculated passive pressure-volume curves agreed with measurements in canine hearts (18). The value of a_4 was set to 500 kPa so that in the finite element simulations the LV wall was almost incompressible (volume changes < 2%) and numerical stability was maintained. In experiments (35) similar changes in volume are observed as a result of an entirely different mechanism, namely changes in vascular volume.

The active material parameter l_x, the zero-force sarcomere length, was set to 1.60 μm, based on experiments in rat cardiac trabeculae (32). The active stiffness, K, at the end of ejection was estimated from measurements of first Piola-Kirchhoff fiber stress and sarcomere length in isometrically contracting rat cardiac trabeculae at an external calcium concentration of 2.5 mM (fig. 6a of (32)). The observed exponential force-length relationship was approximated by a straight line joining the coordinates (l_x μm, 0 kPa) and (2.0 μm, 115 kPa) yielding a stiffness, K, at the end of ejection of 560 kPa. The active stiffness at the beginning of ejection was chosen to be 110 kPa so that a cavity pressure of 12.3 kPa resulted in a physiologically realistic ratio of cavity to wall volume of 0.65 (6).

Performed optimizations

In an initial optimization all 12 fiber angle parameters were optimized simultaneously. As initial guess, the parameters h_{v0}, h_{v1}, and t_{u1} were set to 0.35, -1.15, and 0.29 radians, respectively, in accordance with their optimal values computed earlier (22). The remaining 9 parameters were initialized to zero. Subsequently, optimizations were performed in which one of the highest order parameters h_{u4}, h_{v4}, t_{u5}, and t_{v2} was alternately excluded from the optimization and then re-included. During the process of excluding and including parameters a lowest minimum was found. The results of the optimization OPLOW corresponding to the lowest minimum are presented in detail in the results.

To estimate the contribution of each of the higher order parameters h_{u4}, h_{v4}, t_{u5}, and t_{v2} to the lowest minimum in objective function, found in OPLOW, additional optimizations were carried out in which one of the highest order parameters was excluded. Initial guess in the optimization was the column of values of the fiber angle parameters found in OPLOW. This resulted in a minimum in objective function that was higher than that of OPLOW. The optimized fiber angle parameters served as initial guess in a subsequent optimization in which the highest order parameter was included again (with initial value equal to zero). The latter optimization served to check that re-inclusion of the highest order parameter did not lead to a local minimum lower than that of OPLOW.

parameter	optimum value	ΔG on exclusion	parameter	optimum value	ΔG on exclusion
h_{u2}	0.0984	-	t_{u1} (rad)	0.501	-
h_{u4}	-0.0701	2.76×10^{-6}	t_{u3} (rad)	0.169	-
h_{v0} (rad)	0.362	-	t_{u5} (rad)	0.0304	4.37×10^{-6}
h_{v1} (rad)	-1.16	-	t_{v1}	-0.626	-
h_{v2} (rad)	-0.124	-	t_{v2}	0.502	89.5×10^{-6}
h_{v3} (rad)	0.129	-			
h_{v4} (rad)	-0.0614	0.182×10^{-6}			

Table I. Computed values of helix and transverse fiber angle parameters, as defined in relation to equations [1] and [2]. The values belong to the lowest found minimum OPLOW. the additional column, ΔG, shows the increase in this minimum when excluding the related parameter from the optimization procedure.

Results

The lowest computed minimum in objective function, in optimization OPLOW, was 0.877×10^{-3}. The corresponding fiber angle parameters are listed in table I. The optimized distribution of fiber angles is shown in fig. 4. The helix fiber angle depended almost linearly on transmural position, v, for the major part of the wall. For a given transmural position, v, the helix fiber angle increased in magnitude towards the apex, reaching a maximum at the latitude, u=-0.82. This implies that fiber direction has a larger longitudinal component towards the apex. The transverse fiber angle decreased from 0° at the equator through -21.7° at u=-0.8, to -37.9° at the apex (u=-1.0). At a given latitude the most extreme value of the transmural course of transverse fiber angle occurred on the endocardial side of the wall, at v=-0.44. The spatial distribution of fiber strains and shortening is shown in fig. 5. Fiber strain at the beginning and end of ejection was 0.132±0.019 (mean±sd) and -0.083±0.009, respectively. Fiber shortening during ejection, quantified by the difference in fiber strain between beginning and end of ejection, was 0.215±0.022. Fig. 5 shows that despite optimization, large gradients in fiber strain and shortening remain near the apex. If 6% of LV wall volume near the apex was excluded (information from the elements in the mesh adjoining the apex), fiber strain at the beginning and end of ejection was 0.133±0.013 and -0.082±0.008, respectively, while fiber shortening was 0.216±0.015.

Optimizations in which the parameters h_{u4}, h_{v4}, t_{u5}, and t_{v2} were separately excluded from OPLOW yielded minima in objective function of 0.880×10^{-3},

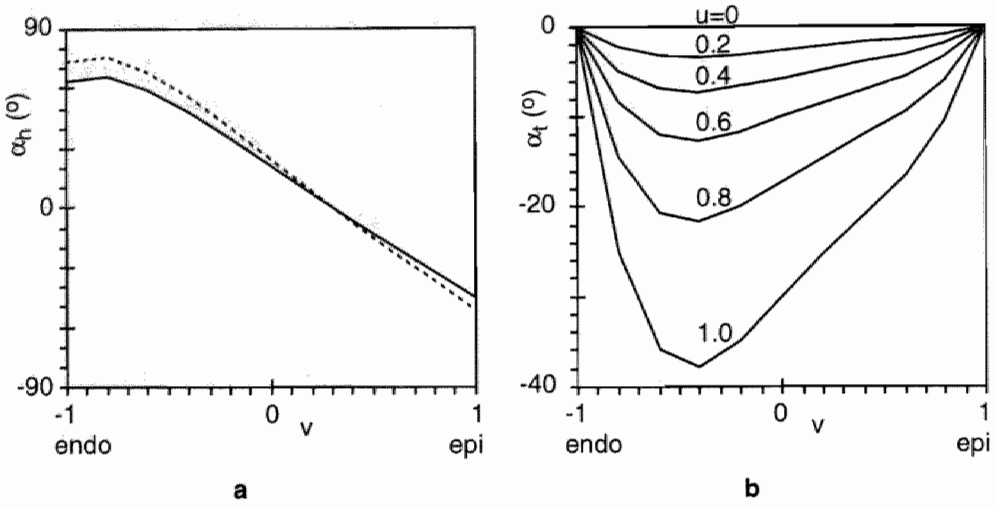

fig. 4. Distributions of helix and transverse fiber angles following optimization OPLOW. (a) Transmural course of helix fiber angle, α_h, at equator, u=0, (___), and at u=-0.82, (...) (see text). (b) Transmural course of transverse fiber angle, α_t, at latitudes u=0,-0.2,-0.4,-0.6,-0.8,-1.0.

0.877×10^{-3}, 0.881×10^{-3}, and 0.966×10^{-3}, respectively. The increase in objective function resulting from exclusion of the parameters h_{u4}, h_{v4}, t_{u5}, or t_{v2} was 2.76×10^{-6} (0.31%), 0.182×10^{-6} (0.02%), 4.37×10^{-6} (0.50%), and 89.5×10^{-6} (10.21%), respectively.

Discussion

We hypothesized that the distribution of muscle fiber orientation in the left ventricular wall is such that fiber strain in this wall at the beginning and end of ejection is as homogeneous as possible. Based on this hypothesis a distribution of fiber orientation was computed which exhibits characteristic features also observed in anatomical measurements, namely the nonlinear transmural course of helix fiber angle in the subendocardium, the increase in longitudinal component of fiber direction towards the apex, and a longitudinal course of mid-wall transverse angle which is practically linear near the equator and increasingly nonlinear towards the apex.

Although the results obtained are promising the present approach has its limitations. Firstly, it is to be expected that in the given parameter space, local minima in the objective function exist. In the implemented optimization strategy, the

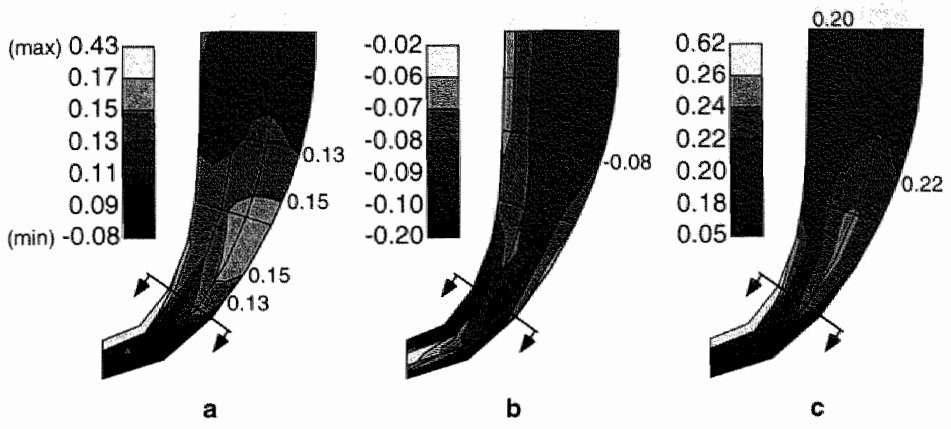

fig. 5. Distribution of systolic fiber strains and shortening over the LV wall after optimization OPLOW: (a) fiber strain at the beginning of ejection, (b) fiber strain at the end of ejection, (c) fiber shortening during ejection, defined as the difference in fiber strain at the beginning and end of ejection. The apical region, indicated by the arrows, was excluded in the quantification of fiber strain (see results).

depth of the minimum found and its location in the parameter space may depend on the initial guess. Therefore, it cannot be guaranteed that the minimum found in optimization OPLOW is the lowest minimum. Secondly, we did not change the size of the elements in the mesh to check the stress, strain or displacement convergence of the solution. However, for a transmural course of helix fiber angle according to anatomical measurements (30), the distributions of sarcomere length and fiber stress were similar to those computed by another independently developed finite element model of LV wall mechanics (13).

The number of fiber angle parameters in the description of the fiber angle fields is somewhat arbitrary. In optimizations in which the parameters h_{u4}, h_{v4}, t_{u5}, and t_{v2} were excluded the objective function, G, increased by 0.31%, 0.02%, 0.50%, and 10.21% from the minimum computed in OPLOW, respectively (table 1). Thus, the contributions to the homogeneity of fiber strain at the beginning and end of ejection by parameters h_{u4}, h_{v4} and t_{u5} are so small that they can safely be ignored in the description of the distribution of fiber orientation. The contribution of t_{v2} to the minimum is significant and extension of the transmural course of the transverse fiber angle with higher order terms may be warranted. We did not investigate the contribution to strain homogeneity of fiber angle parameters of lower order. In an earlier study, the objective function (equation [9]) was minimized with just 3 of the parameters (h_{v0}, h_{v1}, and t_{u1}) (22). The minimum in objective function was reduced by a factor 2.0 when 12 as opposed to 3 fiber angle parameters were optimized.

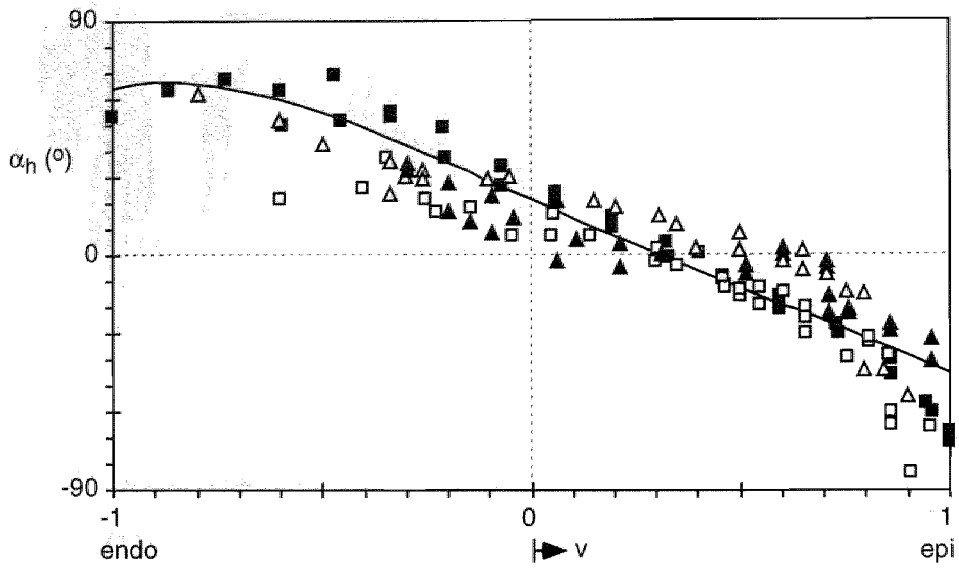

fig. 6. Measured and predicted transmural course of helix fiber angle at equator. Symbols: (■) anatomical measurements in human LV free wall (29); anatomical measurements in dog LV free wall (17) at anterior (△), lateral (□), and posterior (▲) sites; (—) model prediction after optimization OPLOW.

The predicted spatial distribution of helix fiber angle was compared with reported measurements. The transmural course of helix fiber angle at the equator was compared with anatomical measurements in the human (29) and canine LV (17). The computed transmural course of helix fiber angle lies within the range of measurements (fig. 6). In the subendocardium the predicted transmural course of helix fiber angle is distinctly nonlinear in accordance with the experimental data. However, in the subepicardium the predicted transmural course of helix fiber angle is practically linear, unlike the general behavior shown by the experimental data. For a quantitative comparison, the root mean square (RMS) difference between the predicted and each of the measured transmural courses of helix fiber angle was determined. The RMS differences with respect to measurements were 9.8° in the human LV free wall (29) and 15.7°, 14.9°, and 10.4° in the canine LV free wall (17) at lateral, anterior, and posterior sites, respectively. The optimization OPLOW also predicted that towards the apex, the longitudinal component of fiber direction increases (fig. 4). This trend has also been observed in anatomical measurements in the canine LV (30). Thus, both qualitative and quantitative comparisons of the predicted and measured distributions of helix fiber angle indicate that the computed helix fiber angle distribution is not significantly different from measurements.

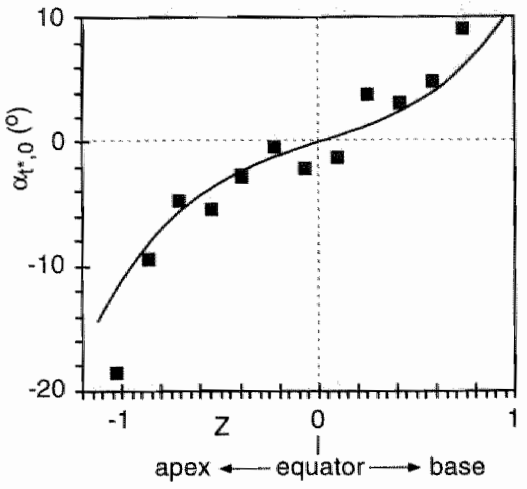

fig. 7. Predicted and measured transmural component, $\alpha_{t^*,0}$, of fiber direction in mid-wall region, as function of normalized base-apex distance, Z (see text). Symbols: (■) measurements in dog heart (23); (—) model predictions by optimization OPLOW. For the measurements, the equator was defined as the latitude at which angle $\alpha_{t^*,0} = 0$, as estimated from a linear regression line to the data (excluding most apical data point). The apex-base distance in model and measurements were normalized to the distance along the long LV axis between equator and the latitude at which mid-wall radius was 60% of equatorial mid-wall radius.

Assessment of the predicted distribution of transverse fiber angle is more difficult due to the scarcity of experimental data. A component of fiber orientation closely related to the transverse fiber angle (differences <2° over the major part of LV wall) has been determined in a single dog heart by diffusion tensor imaging (23). Briefly, in the diffusion tensor imaging experiments, 12 short-axis planes perpendicular to the LV long axis were selected. In each short-axis plane, the radius, R_0, was determined at which mean fiber direction was in the short-axis plane. At the radius R_0 the angle $\alpha_{t^*,0}$ was determined between the fiber and circumferential directions. Thus, the longitudinal course of $\alpha_{t^*,0}$ in approximately the mid-wall region was determined (fig. 7). To compare the predicted transmural component of fiber orientation with the measurements, the angle $\alpha_{t^*,0}$ was also determined in the optimized distribution of fiber orientation, following the same procedure as in (23). The predicted longitudinal course of $\alpha_{t^*,0}$ lies within the range of measurements, except perhaps close to the apex (fig. 7). Both predicted and measured values of $\alpha_{t^*,0}$ decrease from 0° at the equator to approximately -10° at the latitude at which the mid-wall radius is 60% of the equatorial mid-wall radius. Close to the apex, both the measured and predicted longitudinal course of $\alpha_{t^*,0}$

vary nonlinearly with distance along the long LV axis, although for the measurements this nonlinear dependence seems more pronounced. Thus, the predicted longitudinal course of the transmural component of fiber orientation in the mid-wall region of the LV wall is not significantly different from measurements in a single dog heart.

The optimized transverse fiber angle distribution was also compared with predictions by an analytical mathematical model by Peskin (19). In the latter model, the 3-dimensional orientation of fibers was computed, assuming, among others, that systolic fiber stress is uniformly distributed. In the computed fiber field the transverse fiber angle was zero at the inner and outer wall surfaces and largest in the middle of the wall. The mid-wall transverse fiber angle was 0° at the equatorial position and decreased to approximately -18° at a position corresponding to u=-0.75. At this latitude we predict a mid-wall transverse fiber angle of -15.1° and a minimum value of -18.9° at v=-0.44. Therefore, the distributions of transverse fiber angle computed in (19) and in the present study do not seem to be in conflict.

In conclusion, an objective function expressing inhomogeneity of fiber strain over the LV wall at the beginning and end of ejection has been minimized by optimization of the distribution of fiber orientation. A minimum in the objective function was found which was twice as low as that found earlier (22) with a more limited set of fiber angle parameters. The fiber strain at the beginning and end of ejection corresponding to the optimized distribution of fiber orientation was 0.133±0.013 (mean±sd) and -0.082±0.007, respectively. The set of fiber angle parameters used to describe the distributions of helix and transverse fiber angles is sufficiently large: extension of the parameter set may be expected to lower the minimum in objective function by less than 10.2%. We successfully predicted several characteristic features of the observed distribution of fiber orientation. In accordance with reported measurements (8, 17, 26, 29, 30) the predicted helix fiber angle varies nonlinearly with transmural position near the endocardium. Moreover, fiber direction has a larger longitudinal component towards the apex, which has also been observed in dog hearts (30). Finally, the predicted transmural component of fiber direction in the mid-wall region was practically proportional to base-apex distance, except near the apex and not significantly different from measurements (23). Therefore, the results of the present study indicate that the fibrous structure of the LV is designed for homogeneous fiber strain during ejection.

References

1. Arts, T., and R. S. Reneman. Dynamics of left ventricular wall and mitral valve mechanics - a model study. *J Biomech* 22: 261-271, 1989.
2. Azhari, H., J. L. Weiss, W. J. Rogers, C. O. Siu, E. A. Zerhouni, and E. P. Shapiro. Noninvasive quantification of principal strains in normal canine hearts using tagged MRI images in 3-D. *Am J Physiol* 264: H205-H216, 1993.
3. Barthelemy, J.-F. M., and R. T. Haftka. Approximation concepts for optimum structural design - a review. *Structural optimization* 5: 129-144, 1993.
4. Bovendeerd, P. H. M., T. Arts, J. M. Huyghe, D. H. van Campen, and R. S. Reneman. Dependence of local left ventricular wall mechanics on myocardial fiber orientation: a model study. *J Biomech* 25: 1129-1140, 1992.
5. Delhaas, T., T. Arts, P. H. M. Bovendeerd, F. W. Prinzen, and R. S. Reneman. Subepicardial fiber strain and stress as related to left ventricular pressure and volume. *Am J Physiol* 264: H1548-H1559, 1993.
6. Douglas, A. S., E. K. Rodriguez, W. O'Dell, and W. C. Hunter. Unique strain history during ejection in canine left ventricle. *Am J Physiol* 260: H1-H15, 1991.
7. Fann, J. I., G. E. Sarris, N. B. Ingels Jr., M. A. Niczyporuk, K. L. Yun, G. T. Daughters II, G. C. Derby, and D. C. Miller. Regional epicardial and endocardial two-dimensional finite deformations in canine left ventricle. *Am J Physiol* 261, 1991.
8. Greenbaum, R. A., Y. H. Siew, D. G. Gibson, A. E. Becker, and R. H. Anderson. Left ventricular fibre architecture in man. *Br Heart J* 45: 248-263, 1981.
9. Grimm, A. H., H.-L. Lin, and B. R. Grimm. Left ventricular free wall and intraventricular pressure-sarcomere length distributions. *Am J Physiol* 239: H101-H107, 1980.
10. Guccione, J. M., K. D. Costa, and A. D. McCulloch. Finite element stress analysis of left ventricular mechanics in the beating dog heart. *J Biomech* 28: 1167-1177, 1995.
11. Guccione, J. M., W. G. O'Dell, A. D. McCulloch, and W. C. Hunter. Anterior and posterior left ventricular sarcomere lengths behave similarly during ejection. *Am J Physiol* 272: H469-H477, 1997.
12. Huisman, R. F., G. Elzinga, N. Westerhof, and P. Sipkema. Measurement of ventricular wall stress. *Cardiovasc Res* 14: 142-153, 1980.
13. Huyghe, J. M., T. Arts, D. H. van Campen, and R. S. Reneman. Porous medium finite element model of the beating left ventricle. *Am J Physiol* 262: H1256-H1267, 1992.
14. Kreyszig, E. *Advanced engineering mathematics*. New York: John Wiley & Sons, Inc., 1993.
15. Malvern, L. E. *Introduction to the mechanics of a continuous medium*. London: Prentice-Hall, Inc., 1969.
16. McCulloch, A. D., B. H. Smaill, and P. J. Hunter. Regional left ventricular epicardial deformation in the passive dog heart. *Circ Res* 64: 721-733, 1989.
17. Nielsen, P. M. F., I. J. Le Grice, B. H. Smaill, and P. J. Hunter. Mathematical model of geometry and fibrous structure of the heart. *Am J Physiol* 260: H1365-H1378, 1991.
18. Nikolic, S., E. L. Yellin, K. Tamura, H. Vetter, T. Tamura, J. S. Meisner, and R. W. M. Frater. Passive properties of canine left ventricle: diastolic stiffness and restoring forces. *Circ Res* 62: 1210-1222, 1988.
19. Peskin, C. S. Fiber architecture of the left ventricular wall: an asymptotic

analysis. *Commun Pure Appl Math* 42: 79-113, 1989.

20. Prinzen, T. T., T. Arts, F. W. Prinzen, and R. S. Reneman. Mapping of epicardial deformation using a video processing technique. *J Biomech* 19: 263-273, 1986.
21. Rademakers, F. E., W. J. Rogers, W. H. Guier, G. M. Hutchins, C. O. Siu, M. L. Weisfeldt, J. L. Weiss, and E. P. Shapiro. Relation of regional cross-fiber shortening to wall thickening in the intact heart. Three-dimensional strain analysis by NMR tagging. *Circ* 89: 1174-1182, 1994.
22. Rijcken, J., P. H. M. Bovendeerd, A. J. G. Schoofs, D. H. van Campen, and T. Arts. Optimization of cardiac fiber orientation for homogeneous fiber strain during ejection. *submitted*.
23. Rijcken, J., K. Nicolay, P. H. M. Bovendeerd, D. H. van Campen, and T. Arts. Measurement of transmural component of muscle fiber direction in left ventricle by diffusion tensor imaging. *submitted*.
24. Rodriguez, E. K., W. C. Hunter, M. J. Royce, M. K. Leppo, A. S. Douglas, and H. F. Weisman. A method to reconstruct myocardial sarcomere lengths and orientations at transmural sites in beating canine hearts. *Am J Physiol* 263: H293-H306, 1992.
25. Rodriguez, E. K., J. H. Omens, L. K. Waldman, and McCulloch. Effect of residual stress on transmural sarcomere length distributions in rat left ventricle. *Am J Physiol* 264: H1048-H1056, 1993.
26. Ross, M. A., and D. D. Streeter Jr. Nonuniform subendocardial fiber orientation in the normal macaque left ventricle. *Eur J Cardiol* 3: 229-247, 1975.
27. Sagawa, K. The ventricular pressure-volume diagram revisited. *Circ Res* 43: 677-687, 1978.
28. Spotnitz, H. M., E. H. Sonnenblick, and D. Spiro. Relation of ultrastructure to function in the intact heart: sarcomere structure relative to pressure volume curves of intact left ventricles of dog and cat. *Circ Res* 18: 49-66, 1966.
29. Streeter, D. D., Jr. Gross morphology and fiber geometry of the heart. In: *Handbook of physiology - The cardiovascular system I*, edited by R. M. Berne Am. Physiol. Soc., Bethesda, MD, 1979, p. 61-112.
30. Streeter, D. D., Jr., H. M. Spotnitz, D. P. Patel, J. Ross Jr., and E. H. Sonnenblick. Fiber orientation in the canine left ventricle during diastole and systole. *Circ Res* 24: 339-347, 1969.
31. Streeter, D. D. J., and W. T. Hanna. Engineering mechanics for successive states in canine left ventricular myocardium. 1. Cavity and wall geometry. *Circ Res* 33: 639-655, 1973.
32. ter Keurs, H. E. D., W. H. Rijnsburger, R. van Heuningen, and M. J. Nagelsmit. Tension development and sarcomere length in rat cardiac trabeculae: evidence of length-dependent activation. *Circ Res* 46: 703-714, 1980.
33. Villarreal, F. J., and W. Y. W. Lew. Finite strains in anterior and posterior wall of canine left ventricle. *Am J Physiol* 259: H1409-H1418, 1990.
34. Waldman, L. K., D. Nosan, F. Villareal, and J. W. Covell. Relation between transmural deformation and local myofiber direction in canine left ventricle. *Circ Res* 63: 550-562, 1988.
35. Yin, F. C. P., C. C. H. Chan, and R. J. Judd. Compressibility of passive myocardium. *Am J Physiol* 271: H1864-H1870, 1996.
36. Yin, F. C. P., R. K. Strumpf, P. H. Chew, and S. L. Zeger. Quantification of the mechanical properties of noncontracting canine myocardium under simultaneous biaxial loading. *J Biomech* 20: 577-589, 1987.

Chapter 6

Discussion

Discussion

The broad objective of the studies presented in this thesis was to gain insight into mechanisms by which the fibrous structure of the heart is determined. It was hypothesized that muscle fibers in the left ventricular wall are oriented such that the distribution of fiber strain during ejection is as homogeneous as possible. To test the hypothesis, a finite element model of left ventricular wall mechanics was developed incorporating the fibrous structure of the left ventricle, passive and active elastic material properties, approximately prolate spheroidal wall geometry, and large deformations. The finite element model was incorporated in an optimization procedure in which both fiber strain and fiber shortening during ejection were made as homogeneous as possible by proper adjustment of fiber orientation. The thus predicted distribution of fiber orientation was compared with anatomical measurements.

Major results

First, it was shown that minimization of the inhomogeneity of fiber strain at the beginning of ejection is possible by proper variation of the distribution of fiber orientation (chapter 2). The mathematical formulation of the distribution of fiber orientation using 3 parameters allowed a reasonable description of the gross features of the distribution of fiber orientation found in anatomical measurements.

When an extended objective function consisting of the weighted sum of *mean fiber strain during ejection and fiber shortening during ejection* was minimized a well-defined minimum was found (chapter 3). The optimized linear transmural course of helix fiber angle was not significantly different from anatomical measurements. Also, a significant transmural component of fiber orientation was predicted. Variation of the fiber angle parameters indicated that the computed minimum in objective function is the lowest minimum in the anatomical range. A ten-fold increase or decrease of the relative weight of fiber shortening with respect to mean fiber strain in the objective function affected the optimized distributions of fiber angles only a little ($< 0.7^{o}$ change in spatial averages of helix and transverse angles). As expected, increasing or decreasing the relative weight of fiber shortening resulted in an increase or decrease, respectively, of the homogeneity of fiber shortening.

To enable determination of characteristic details of the distribution of fiber orientation we extended the mathematical description of the distribution of fiber orientation from 3 to 12 parameters (chapter 5). Minimization of inhomogeneity in

fiber strain at the beginning and end of ejection resulted in a distribution of helix fiber angle that was in compliance with the observed nonlinear transmural course of helix fiber angle in the subendocardium (13, 20, 22), and with the observed increase in the magnitude of the helix fiber angle towards the apex (23). The nonlinear transmural course of the helix fiber angle in the subepicardium (5, 13, 20, 22) observed in anatomical measurements was not predicted. The optimizations predicted a practically linear course of helix fiber angle in this region.

Comparison of the distribution of transverse fiber angle predicted in chapter 5 with measurements was difficult owing to the sparseness of experimental data. Therefore, a method based on diffusion tensor imaging was developed to measure the longitudinal course of the transverse fiber angle in the mid-wall region (chapter 4). The transverse angle could be determined with an estimated error of $\pm 1.6^{o}$ (sd) which is sufficient to assess whether the measured angle is significantly different from zero. The predicted and measured courses of transverse fiber angle in the mid-wall region agreed to within the estimated measurement error over the whole left ventricular wall except close to the apex.

Discussion of results

Evaluation of the results of chapters 2, 3, and 5, necessitates discussion of the assumptions underlying the finite element model of left ventricular wall mechanics and the optimizations. In the finite element model of left ventricular wall mechanics several simplifying assumptions were made regarding the active constitutive behavior of cardiac muscle, the sequence in which the left ventricular wall is activated, and residual strain.

The active constitutive behavior of cardiac muscle has been simplified. Experiments on isolated cardiac trabeculae (26, 27) indicate that active fiber stress depends on instantaneous sarcomere length, the velocity of sarcomere shortening, and on extracellular calcium concentration. In the studies described in chapters 2, 3, and 5 it was assumed that active fiber stress depends only on sarcomere length and on instantaneous active stiffness. The force-length dependence, in combination with the 'time-varying elastance' concept (21), assumed in the finite element model, has been shown to be adequate for many purposes (9). Simplification of the constitutive behavior is relatively unimportant for the prediction of the distribution of fiber orientation. This is demonstrated in chapters 2 and 3, in which the active constitutive behavior was different but similar optimized distributions of fiber angles over the left ventricular wall were obtained ($<0.9^{o}$ change in spatial averages of helix and transverse fiber angles).

Another effect of active constitutive behavior that has not been taken into account in the finite element model is the sequence in which the left ventricular wall is activated. We have assumed that muscle fibers in the left ventricular wall are all activated at the same time. In the normal heart there is a difference of approximately 40 ms between the activation of the first muscle fibers at the endocardial surface near the apex and the last muscle fibers at the epicardial surface near the base (4). It is difficult to estimate the effect of our choice of simultaneous activation on the optimized distribution of fiber orientation. The heart adapts, e.g. through regional growth, to changes in the activation sequence induced by chronic pacing (17), but changes in the distribution of fiber orientation have not, to our best knowledge, been documented. For simplicity, the activation sequence was not included in the finite element model of left ventricular wall mechanics. Implementation of the activation sequence requires simulation of the isovolumic contraction phase which, considering the associated computational costs, is not warranted in the optimization set-up.

Residual stress and strain were not incorporated in the finite element model of left ventricular wall mechanics. Studies of residual strain have focused mainly on the circumferential component (14, 19, 25). Residual circumferential strain has been shown to lead to a transmural gradient in sarcomere length in the unloaded (zero transmural pressure) left ventricle of the rat, with shorter sarcomeres in the subendocardium (19). The transmural gradient in sarcomere length in the unloaded state may contribute to a more homogeneous sarcomere length at positive filling pressures (6). It is unclear whether more homogeneous end-diastolic sarcomere length also contributes to homogeneity of sarcomere length (and fiber strain) at the beginning of ejection, because considerable redistribution of sarcomere length occurs during the isovolumic contraction phase (18). However, finite element simulations of left ventricular wall mechanics (7) in which sarcomere length in the unloaded state was either chosen to be uniform or to exhibit the transmural gradient measured in (19) showed negligible differences in end-systolic fiber stress distributions. The possible effects of residual strain on the optimization of fiber orientation are worth investigating in the future, because it has not been shown conclusively that residual strain is unimportant, and because implementation of the effects of residual strain in our finite element model is possible at negligible computational costs.

It may be argued that left ventricular wall geometry should be included in the optimization procedure. Model studies have indicated that wall geometry affects the stress and strain distributions (8, 15). Therefore, according to the hypothesis that fiber orientation is such that fiber strain is homogeneous, wall geometry may also affect the distribution of fiber orientation. In several other studies employing

mathematical models of left ventricular wall mechanics (1, 2, 10, 16, chapters 2, 3, 5), the distribution of fiber orientation has been predicted using aspects of mechanics (e.g. homogeneous fiber stress during the ejection phase). Despite the different wall geometries used in the latter studies, the predicted transmural course of helix fiber angle was similar. Other evidence suggesting that the importance of left ventricular wall geometry for homogeneous fiber strain is limited is provided by the rather large variation of geometry parameters, such as the ratio of long to short axis (range 1.4-2.1) in hearts of different species (11, 24). In contrast, the transmural course of helix fiber angle appears to be almost independent of species (5, 13, 20, 22). Thus, summarizing, the effects of wall geometry on the homogeneity of fiber strain during ejection are likely to be secondary to effects of the distribution of fiber orientation.

In model studies (3) it has been found that the transverse fiber angle reduces the radial-circumferential shearing deformation. Additionally, it was found that inclusion of the transverse fiber angle reduced the spatial homogeneity of active muscle fiber stress. These findings suggest that to predict the transverse fiber angle distribution by optimization, the objective function should include a term involving radial-circumferential shearing deformation. Nevertheless, minimization of inhomogeneity of fiber strain leads to a spatial distribution of transverse fiber angle in agreement with anatomical measurements (chapter 5). Moreover, it was shown that for the optimized transmural course of helix fiber angle the inhomogeneity in fiber strain during ejection was sensitive to the spatial distribution of the transverse fiber angle (chapter 3, fig. 6): if in the optimum, the transverse fiber angle is set to zero the objective function increases by a factor of approximately 2. This *interdependence* of the distributions of transverse and helix fiber angles was not investigated by Bovendeerd *et al.* (3), which may explain their finding that inclusion of the transverse fiber angle worsens homogeneity of systolic fiber stress. Thus, it may be concluded that, besides its potential role in limiting shearing deformation, the transverse fiber angle is also important to homogeneity of fiber strain at the beginning of ejection.

It is unlikely that the employed optimization strategy (chapters 2, 3, 5), in which strain information from all over the left ventricular wall is used to make regional changes in fiber orientation, has a physiological basis. Adaptation of biological tissues to their mechanical milieu is more likely to occur in the environment of the cell, as has been proposed for cardiac tissue (1), and for bone tissue (12). However, there is evidence that the computed structure of the biological tissues resulting from a simulated process of cardiac adaptation is similar to that obtained using an optimization strategy of the type of chapters 2, 3, and 5. In a cylindrical model of left ventricular wall mechanics Arts *et al.* (1) simulated the

process of cardiac adaptation, allowing growth and regional re-orientation of muscle fibers to achieve systolic fiber shortening of 15% and end-diastolic sarcomere length of 2.1 μm. The resulting transmural course of helix fiber angle was within the anatomical range and similar to what we computed (chapter 2). Also, the spatial distribution of bone density computed using adaptation mechanisms active in the environment of the cell leads to a final bone structure that is very similar to that computed with an optimization strategy of the type used in this thesis (28). Given the successful prediction of a distribution of muscle fiber orientation by our optimization strategy, it is possible that regional adaptation mechanisms exist in the heart that determine cardiac structure on the basis of deviations of regional sarcomere length or fiber strain during systole from a reference value.

Conclusions

It was shown (chapters 2, 3, 5) that minimization of regional inhomogeneities in fiber strain during ejection is possible with a suitable choice of the distribution of fiber orientation. Moreover the optimized distribution of fiber orientation was found to be in the anatomical range. These findings provide strong support for the hypothesis that the left ventricular fibrous structure is such that fiber strain is as homogeneous as possible during ejection.

It is unlikely that the employed optimization strategy (chapters 2, 3, 5), in which strain information from all over the left ventricular wall is used to make regional changes in fiber orientation, has a physiological basis. Cardiac structure is more likely to be controlled in the environment of the cell, as has been proposed by Arts *et al.* (1). The merit of the presented studies is that they provide support for the existence of regional fiber strain-based or sarcomere length-based mechanisms that determine the fibrous structure of the left ventricle.

Recommendations

To gain further insight into mechanisms by which cardiac structure is determined, the following recommendations are given, regarding enhancement of the finite element model and suggestions for future research.

The effects of residual strain on the optimized distribution of muscle fiber orientation should be investigated. The effects of circumferential residual strain can be incorporated in the finite element model of left ventricular wall mechanics by

assuming a transmural gradient in sarcomere length in the unloaded (zero transmural pressure) state.

Measurements of the transmural component of fiber direction (chapter 4) should be carried out in more hearts to enable better comparison with model predictions. The measurements of the transmural component of fiber direction, should also cover regions other than the mid-wall.

A more physiological strategy for structure formation, based on processes in the environment of the cell, should be implemented in the finite element model. This may eventually result in a fully three-dimensional finite element model of the heart in which various possible responses to chronically altered mechanical load, such as tissue growth and re-orientation of muscle fibers, are implemented at a regional level. This finite element model can be used to investigate the nature of cardiac adaptation processes, thereby furthering insight in the normal heart. Furthermore, it can be used to study cardiac adaptation effects resulting from interventions such as ischemia or pacing.

References

1. Arts, T., F. W. Prinzen, L. H. E. H. Snoeckx, J. M. Rijcken, and R. S. Reneman. Adaptation of cardiac structure by mechanical feedback in the environment of the cell: a model study. *Biophys J* 66: 953-961, 1994.
2. Bovendeerd, P. H. M., T. Arts, J. M. Huyghe, D. H. van Campen, and R. S. Reneman. Dependence of local left ventricular wall mechanics on myocardial fiber orientation: a model study. *J Biomech* 25: 1129-1140, 1992.
3. Bovendeerd, P. H. M., J. M. Huyghe, T. Arts, D. H. van Campen, and R. S. Reneman. Influence of endocardial-epicardial crossover of muscle fibres on left ventricular wall mechanics. *J Biomech* 27: 941-951, 1994.
4. Durrer, D., R. T. van Dam, G. E. Freud, M. J. Janse, F. L. Meyler, and R. C. Arzbaecher. Total excitation of the isolated human heart. *Circ* 41: 899-912, 1970.
5. Greenbaum, R. A., Y. H. Siew, D. G. Gibson, A. E. Becker, and R. H. Anderson. Left ventricular fibre architecture in man. *Br Heart J* 45: 248-263, 1981.
6. Grimm, A. H., H.-L. Lin, and B. R. Grimm. Left ventricular free wall and intraventricular pressure-sarcomere length distributions. *Am J Physiol* 239: H101-H107, 1980.
7. Guccione, J. M., K. D. Costa, and A. D. McCulloch. Finite element stress analysis of left ventricular mechanics in the beating dog heart. *J Biomech* 28: 1167-1177, 1995.
8. Guccione, J. M., A. D. McCulloch, and W. C. Hunter. Three-dimensional finite element analysis of anterior-posterior variations in local sarcomere length and active fiber stress during left ventricular ejection. *Advances in Bioengineering, ASME*, 1993, p. 571-574.
9. Guccione, J. M., L. K. Waldman, and A. D. McCulloch. Mechanics of active contraction in cardiac muscle: Part 2 -

cylindrical models of the systolic left ventricle. *J Biomech Eng* 115: 81-90, 1993.

10. Huyghe, J. M., T. Arts, D. H. van Campen, and R. S. Reneman. Porous medium finite element model of the beating left ventricle. *Am J Physiol* 262: H1256-H1267, 1992.
11. Lee, J. C., J. F. N. Taylor, and S. Evans Downing. Comparison of ventricular weights and geometry in newborn, young, and adult mammals. *J Appl Physiol* 38: 147-150, 1975.
12. Mullender, M. G., R. Huiskes, and H. Weinans. A physiological approach to the simulation of bone remodeling as a self-organizational control process. *J Biomechanics* 27: 1389-1394, 1994.
13. Nielsen, P. M. F., I. J. Le Grice, B. H. Smaill, and P. J. Hunter. Mathematical model of geometry and fibrous structure of the heart. *Am J Physiol* 260: H1365-H1378, 1991.
14. Omens, J. H., and Y.-H. Fung. Residual strain in rat left ventricle. *Circ Res* 66: 33-45, 1990.
15. Pao, Y. C., E. L. Ritman, and E. H. Wood. Finite-element analysis of left ventricular myocardial stresses. *J Biomech* 7: 469-477, 1974.
16. Peskin, C. S. Fiber architecture of the left ventricular wall: an asymptotic analysis. *Commun Pure Appl Math* 42: 79-113, 1989.
17. Prinzen, F. W., E. C. Cheriex, T. Delhaas, M. F. M. van Oosterhout, T. Arts, H. J. J. Wellens, and R. S. Reneman. Asymmetric thickness of left ventricular wall resulting from asynchronous electric activation: A study in dogs with ventricular pacing and in patients with left bundle branch block. *Am Heart J* 130: 1045-1053, 1995.
18. Rodriguez, E. K., W. C. Hunter, M. J. Royce, M. K. Leppo, A. S. Douglas, and H. F. Weisman. A method to reconstruct myocardial sarcomere lengths and orientations at transmural sites in beating canine hearts. *Am J Physiol* 263: H293-H306, 1992.
19. Rodriguez, E. K., J. H. Omens, L. K. Waldman, and McCulloch. Effect of residual stress on transmural sarcomere length distributions in rat left ventricle. *Am J Physiol* 264: H1048-H1056, 1993.
20. Ross, M. A., and D. D. Streeter Jr. Nonuniform subendocardial fiber orientation in the normal macaque left ventricle. *Eur J Cardiol* 3: 229-247, 1975.
21. Sagawa, K. The ventricular pressure-volume diagram revisited. *Circ Res* 43: 677-687, 1978.
22. Streeter, D. D., Jr. Gross morphology and fiber geometry of the heart. In: *Handbook of physiology - The cardiovascular system I*, edited by R. M. Berne Am. Physiol. Soc., Bethesda, MD, 1979, p. 61-112.
23. Streeter, D. D., Jr., H. M. Spotnitz, D. P. Patel, J. Ross Jr., and E. H. Sonnenblick. Fiber orientation in the canine left ventricle during diastole and systole. *Circ Res* 24: 339-347, 1969.
24. Streeter, D. D. J., and W. T. Hanna. Engineering mechanics for successive states in canine left ventricular myocardium. 1. Cavity and wall geometry. *Circ Res* 33: 639-655, 1973.
25. Taber, L. A., N. Hu, T. Pexieder, E. B. Clark, and B. B. Keller. Residual strain in the ventricle of the stage 16-24 chick embryo. *Circ Res* 72: 455-462, 1993.
26. ter Keurs, H. E. D., W. H. Rijnsburger, R. van Heuningen, and M. J. Nagelsmit. Tension development and sarcomere length in rat cardiac trabeculae: evidence of length-dependent activation. *Circ Res* 46: 703-714, 1980.
27. ter Keurs, H. E. D. J., J. J. J. Bucx, P. P. de Tombe, P. Backx, and T. Iwazumi. The effects of sarcomere length and Ca^{++} on force and velocity of shortening in cardiac muscle. *Adv Exp Med Biol* 226: 581-593, 1988.
28. Weinans, H. Bone remodeling: A self-

organizing stiffness optimization? *BMES Trabecular bone symposium*, Boston, MA, 1995.

Summary

The left ventricle (LV) of the heart is a hollow muscle that pumps blood from the lungs into the aorta. The LV wall is composed for an important part (approximately 70% by volume) of muscle fibers that follow helical pathways on approximately toroidal surfaces (fig. 1). Blood is driven out of the LV cavity during the ejection phase of the cardiac cycle as the result of the coordinated contraction of the muscle fibers.

Mathematical models of LV wall mechanics have shown that the distribution of mechanical load over the LV wall during ejection is highly dependent on the chosen distribution of fiber orientation. Measurements indicate that during the ejection phase of the cardiac cycle, regional differences in fiber strain and sarcomere length are not significant. Also, it is clear there are mechanisms in the heart which allow it to adapt to long term changes in mechanical loading. For instance, in response to an increased blood pressure, the whole LV wall thickens while cavity dimensions remain approximately constant. The adaptive growth results in at least a partial return in mechanical loading to the original level. In the light of these findings we hypothesized that the distribution of muscle fiber orientation in the LV wall is such that mechanical load, quantified by fiber strain during ejection referred to the unloaded (mid-diastolic) state, is as homogeneous as possible. In the studies presented in this thesis the hypothesis was tested in 2 steps. Firstly, in a mathematical model of LV wall mechanics a distribution of muscle fiber orientation was computed that made fiber strain during ejection as homogeneous as possible. Subsequently, the predicted distribution of fiber orientation was compared with experimental data from anatomical measurements.

We have developed a mathematical model of LV wall mechanics, based on the theory of continuum mechanics and elaborated by the finite element method. This model was used to calculate the distribution of fiber strain over the wall for a given distribution of fiber orientation. In the model, LV wall geometry was represented by a thick-walled ellipsoid. The model incorporated nonlinear elastic material properties and allowed the large deformations observed in the real heart. Muscle fiber orientation was quantified by the helix and transverse fiber angles in a coordinate system with local transmural (t-), circumferential (c-), and longitudinal (l-) directions perpendicular to the wall, along the circumference, and along the meridian respectively (fig. 2). The helix fiber angle was defined as the angle between the c-direction and the projection of fiber direction on the cl-plane. The transverse fiber angle was defined as the angle between the c-direction and the projection of fiber direction on the ct-plane. The distributions of the helix and transverse fiber angles over the LV wall were represented by a limited number (3 to

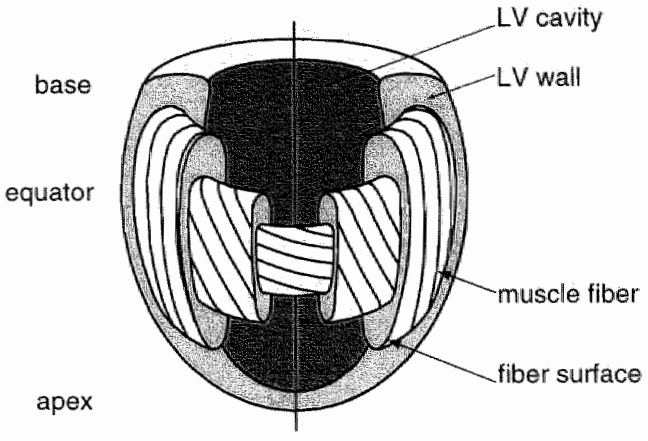

fig. 1. Schematic representation of muscle fiber pathways in the isolated left ventricular wall. The mitral and aortic valves in the basal plane as well as the papillary muscles are not shown. The fibers follow helical pathways on approximately toroidal surfaces. Symbols: LV=left ventricle.

12) of parameters defining polynomials in the l- and t- directions. The finite element model was incorporated in an optimization procedure in which an objective function, expressing inhomogeneity of fiber strain, was minimized by proper choice of the helix and transverse fiber angle parameters.

In a minimum parameter model (chapter 2) a distribution of muscle fiber orientation was computed that made fiber strain at the beginning of ejection as homogeneous as possible. The helix fiber angle was allowed to change linearly with distance in transmural direction, as described by two parameters - a slope and an intercept. The transverse fiber angle was assumed to change quadratically in transmural direction, from zero at the wall surfaces to an extremum in the middle of the wall. Midwall transverse fiber angle was also assumed to increase proportionally with distance from the equator. The proportionality factor was the third parameter used to describe the spatial distribution of muscle fiber orientation. Optimization of the 3 fiber angle parameters for homogeneous fiber strain at beginning of ejection resulted in a well-defined distribution of fiber orientation. Moreover, the computed distribution of fiber orientation was within the anatomical range.

In a subsequent study (chapter 3) more realistic material properties were used. Moreover, the objective function was changed to make both fiber strain at the beginning and at the end of the ejection period as homogeneous as possible. Optimization of the fiber angle parameters resulted in a well-defined minimum in the

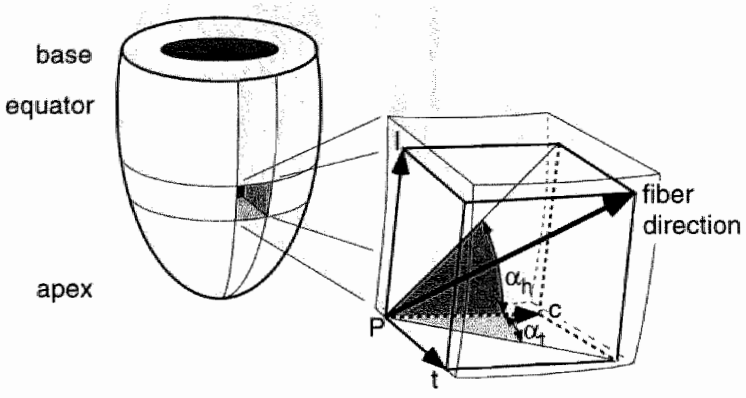

fig. 2. Quantification of muscle fiber orientation in the left ventricular wall. At a point P in the wall muscle fiber orientation is quantified by the helix and transverse fiber angles, α_h and α_t, respectively, measured with respect to the transmural (t-), longitudinal (l-), and circumferential (c-) directions (see text).

objective function. Systematic variation of the fiber angle parameters indicated that the computed minimum in objective function is the lowest minimum. The optimized linear transmural course of helix fiber angle was not significantly different from experimental data. The predicted distribution of transverse fiber angle did not conflict with the scarce published measurement data available.

The assessment of the computed distribution of the transverse fiber angle over the LV wall is difficult due to the scarcity of experimental data. To supplement existing data, a method based on diffusion tensor imaging was developed to measure aspects of the distribution of the transverse fiber angle (chapter 4). In the diffusion tensor imaging technique the regional 3-dimensional diffusion of water present in the tissue is determined. The direction of greatest diffusivity in a region corresponds well with the muscle fiber direction. This technique was applied in the post mortem dog heart. The analysis of data was improved by averaging diffusion data from short-axis slices through the LV wall in circumferential direction, under the assumption of rotational symmetry of the LV wall. Thus, the base-apex course of the transverse fiber angle in the mid-wall region was determined with an estimated measurement error of $\pm 1.6^{o}$ (sd).

Finally, to enable determination of several characteristic details of the distribution of muscle fiber orientation over the LV wall, the mathematical description of the distribution of fiber angles was extended from 3 to 12 parameters

(chapter 5). Minimization of inhomogeneity of fiber strain at the beginning and end of the ejection period resulted in a distribution of helix fiber angle in compliance with both the observed nonlinear transmural course of helix fiber angle in the subendocardium, and with the observed increase in the magnitude of the helix fiber angle towards the apex. In contrast to experimental data, a practically linear transmural course of helix fiber angle was predicted in the subepicardium. The predicted base-apex course of transverse fiber angle in the mid-wall region of the LV wall agreed with measurements (chapter 4) within the measurement error.

In conclusion, the close agreement between measured and computed spatial distributions of muscle fiber orientation supports the hypothesis that the distribution of muscle fiber orientation is such that the spatial distribution of fiber strain during ejection is as homogeneous as possible. We suggest that in future research a mathematical model of LV wall mechanics be developed incorporating adaptation rules that govern regional structure and mass in the environment of the muscle fiber cell. The studies in this thesis indicate that fiber strain or sarcomere length should be considered important for such rules of regional adaptation.

Samenvatting

De linker ventrikel van het hart is een holle spier die bloed afkomstig van de longen de aorta inpompt. De linker ventrikelwand bestaat voor een belangrijk deel (*circa* 70% van het volume) uit spiervezels, die op complexe wijze geordend zijn in de wand (fig. 1). Bloed dat zich in de linker ventrikelholte bevindt wordt tijdens de uitdrijffase van de hartcyclus uitgepompt middels de gecoördineerde samentrekking van de spiervezels.

Computersimulaties van de mechanica van de linker ventrikelwand hebben aangetoond dat de verdeling van mechanische belasting over de wand sterk afhankelijk is van de gekozen verdeling van spiervezeloriëntatie. Metingen geven aan dat in het echte hart regionale verschillen in vezelrek en sarcomeerlengte niet significant zijn tijdens de uitdrijffase van de hartcyclus. Verder is het duidelijk dat het hart zich kan aanpassen, onder andere middels groei, aan veranderingen in mechanische belasting. Een gevolg van hoge bloeddruk bijvoorbeeld is dat er over een periode van weken tot maanden groei van de wand plaatsvindt die leidt tot verdikking van de ventrikelwand bij een even grote ventrikelholte. Echter, er vindt geen verandering plaats in de manier waarop de spiervezels in de wand zijn geordend. De adaptieve groei leidt tot tenminste een gedeeltelijke normalisatie van de mechanische belasting van de ventrikelwand. Deze 3 bevindingen: a) de verdeling van vezelrek over de ventrikelwand is sterk afhankelijk van de verdeling van vezeloriëntatie, b) vezelrek of -lengte tijdens de uitdrijffase is waarschijnlijk homogeen, en c) er zijn adaptatiemechanismen aanwezig in het hart om de mechanische belasting te reguleren, hebben geleid tot de volgende hypothese: de verdeling van spiervezeloriëntatie over de linker ventrikelwand is zodanig dat de verdeling van spiervezelrek tijdens de uitdrijffase van de hartcyclus zo homogeen mogelijk is. In de studies in dit proefschrift werd de hypothese getoetst in 2 stappen. Ten eerste werd met een computermodel van de mechanica van de linker ventrikelwand een verdeling van vezeloriëntatie berekend, waarbij de verdeling van spiervezelrek tijdens de uitdrijffase van de hartcyclus zo homogeen mogelijk was. Vervolgens werd de berekende verdeling van vezeloriëntatie vergeleken met experimentele data uit anatomische metingen.

Een mathematisch model van de mechanica van de linker ventrikelwand is ontwikkeld, gebaseerd op de theorie van de continuümsmechanica en geïmplementeerd middels de eindige-elementen methode. Dit model werd gebruikt als gereedschap om voor gegeven verdeling van vezeloriëntatie over de ventrikelwand de verdeling van vezelrek te berekenen. In het model werd rekening gehouden met de niet-lineair elastische materiaaleigenschappen van hartweefsel en met de grote vervormingen die plaatsvinden in het echte hart. De initiële

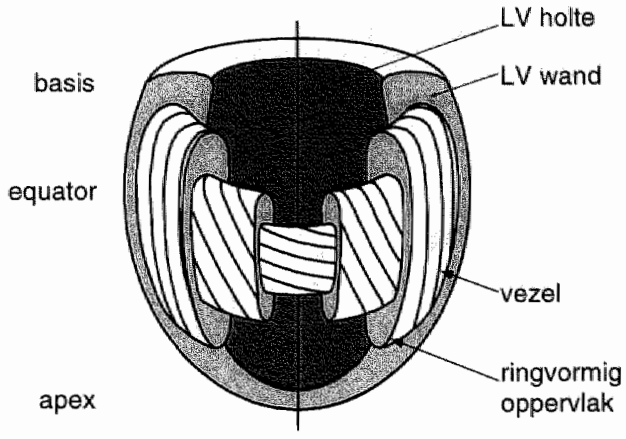

fig. 1. Schematische weergave van het verloop van spiervezels in de linker ventrikelwand. De linker ventrikel (LV) is weergegeven als een dikwandige ellipsoïde. De basis, equator en apex van de ventrikel zijn aangegeven. Vezels zijn gewikkeld op denkbeeldige ringvormige oppervlakken. De spoed waarmee vezels zijn gewikkeld is klein aan de buiten- en binnenwand en groot midden in de wand.

geometrie van de linker ventrikelwand werd beschreven met een dikwandige ellipsoïde. Spiervezeloriëntatie werd gekwantificeerd door de helix- en oversteekhoeken, gedefinieerd ten opzichte van de lokale transmurale (t-), longitudinale (l-), en omtreksrichtingen (c-) (fig. 2). De t-, l-, en c-richtingen lopen respectievelijk loodrecht op de wand, langs een meridiaan, en langs de omtrek evenwijdig aan de equator. De helixhoek werd gedefinieerd als de hoek tussen de c-richting en de projectie van de lokale vezelrichting op het cl-vlak. De oversteekhoek werd gedefinieerd als de hoek tussen de c-richting en de projectie van de lokale vezelrichting op het ct-vlak. De verdelingen van de helix- en oversteekhoeken over de linker ventrikelwand werden beschreven met een beperkt aantal parameters (in totaal tussen 3 en 12). Het eindige-elementen model van linker ventrikelwandmechanica werd ingepast in een optimalisatieprocedure. Een doelfunctie, een maat voor de inhomogeniteit in vezelrek tijdens de uitdrijffase, werd geminimaliseerd door aanpassing van de helix- en oversteekhoek-parameters.

In eerste instantie werd in een model met een minimum aantal parameters (hoofdstuk 2) een verdeling van vezeloriëntatie berekend waarbij vezelrek bij het begin van de uitdrijffase zo homogeen mogelijk was. Het transmurale verloop van de helixhoek werd beschreven met een rechte lijn, gekwantificeerd door 2 parameters - een helling en een intercept. Het transmurale verloop van de

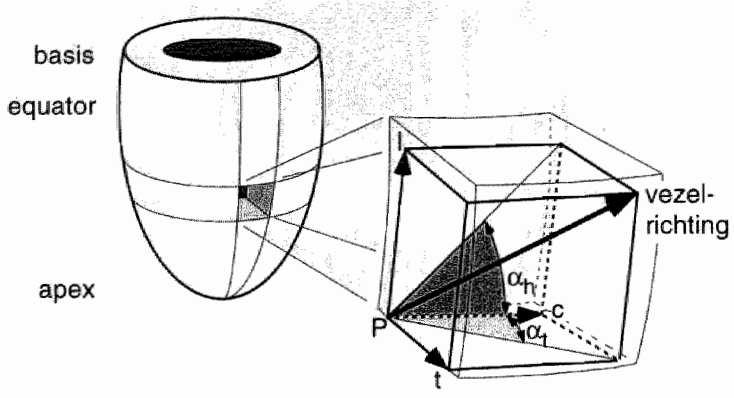

fig. 2. Kwantificatie van vezeloriëntatie in de linker ventrikelwand. Op een punt P in de wand kan de 3-dimensionale oriëntatie van een spiervezel worden gekwantificeerd middels de helix- en oversteekhoeken, α_h en α_t respectievelijk, gedefinieerd ten opzichte van de transmurale (t-), longitudinale (l-), en omtreksrichtingen (c-) (zie tekst).

oversteekhoek is kwadratisch, waarbij de oversteekhoek nul is aan de oppervlakken van de binnen- en buitenwanden en van maximale grootte in het midden van de wand. De grootte van de oversteekhoek in het midden van de wand neemt toe met afstand van de equator. De evenredigheidsconstante voor deze toename was de derde parameter in de beschrijving van de verdeling van vezeloriëntatie. Optimalisatie van de 3 vezeloriëntatieparameters resulteerde in een goed-gedefinieerd minimum in de doelfunctie. De aldus berekende verdeling van vezeloriëntatie kwam redelijk goed overeen met experimentele data van anatomische metingen.

In een volgende studie (hoofdstuk 3) werd een te minimaliseren doelfunctie gebruikt die erop gericht was vezelrek bij zowel het begin als bij het einde van de uitdrijffase zo homogeen mogelijk te maken over de ventrikelwand. Optimalisatie van de vezeloriëntatieparameters resulteerde in een goed-gedefinieerd minimum in de doelfunctie. Bij variatie van de vezeloriëntatieparameters bleek dat er tenminste nog één ander minimum in de doelfunctie is, maar minder diep dan het minimum gevonden in de optimalisatie. Het geoptimaliseerde lineaire transmurale verloop van de helixhoek was niet significant verschillend van experimentele data uit anatomische metingen. De voorspelde verdeling van oversteekhoek over de ventrikelwand was niet strijdig met de schaarse experimentele data hiervan.

Evaluatie van de berekende verdeling van oversteekhoek over de wand is

moeilijk omdat er maar weinig experimentele data hierover beschikbaar is. Ter aanvulling van bestaande data is een methode ontwikkeld, gebaseerd op diffusie-gewogen kernspinresonantie (DTI), om de verdeling van oversteekhoek over de wand te bepalen (hoofdstuk 4). In de DTI-techniek wordt de regionale 3-dimensionale diffusiviteit van water in het hartspierweefsel gemeten. De richting waarin diffusie het gemakkelijkst plaatsvindt komt goed overeen met de lokale spiervezelrichting. De DTI-techniek werd toegepast in het *post mortem* hondenhart. Ter verhoging van de nauwkeurigheid werd de diffusiedata van korte-as doorsneden van de linker ventrikelwand gemiddeld in de omtreksrichting. Hiervoor werd rotatiesymmetrie van de linker ventrikelwand verondersteld. Zodoende werd het basis-apex verloop van de oversteekhoek in het midden van de wand bepaald met een geschatte nauwkeurigheid van $\pm 1.6^{o}$ (sd).

Om een aantal karakteristieke details van de verdeling van vezeloriëntatie te kunnen voorspellen, werd de beschrijving van de verdeling van vezelhoeken over de wand uitgebreid van 3 naar in totaal 12 parameters. De 12 vezeloriëntatieparameters werden geoptimaliseerd voor homogene vezelrek bij zowel het begin als het einde van de uitdrijffase. In overeenkomst met de experimentele data uit anatomische metingen, werd een transmuraal verloop van de helixhoek voorspeld dat niet-lineair was in de buurt van de binnenwand. Ook werd correct voorspeld dat de vezels in de omgeving van de apex een grotere component hebben in basis-apex richting dan de vezels bij de equator. Uit deze studie bleek verder dat de verdeling van oversteekhoek over de ventrikelwand goed kan worden bepaald op basis van optimalisaties voor homogene vezelrek. De overeenkomst tussen de gemeten en berekende verdeling van oversteekhoek was binnen de geschatte meetfout van de meetmethode (hoofdstukken 4, 5).

In dit onderzoek is aangetoond dat het mogelijk is om een verdeling van vezeloriëntatie in de linker ventrikelwand van het hart te voorspellen op basis van de hypothese dat de spiervezels zodanig georiënteerd zijn dat de verdeling van spiervezelrek over de wand tijdens de uitdrijffase van de hartcyclus zo homogeen mogelijk is. Bovendien blijkt dat de op die manier voorspelde verdeling van vezeloriëntatie binnen de meetfout overeenkomt met de gemeten verdeling van vezeloriëntatie. Dit duidt erop dat de linker ventrikelwand zodanig is ontworpen dat alle spiervezels dezelfde rek ondergaan.

Dankwoord

Nu het grote werk is verzet rest mij de plezierige taak een aantal mensen te bedanken voor hun inspanningen, moeite, hulp, stimulering, gezelschap en vriendschap.

Allereerst, Theo. Je hebt de dagelijkse begeleiding op je genomen. Jouw deskundigheid op het gebied van fysiologie en mechanica alsook bij het 'troubleshooten' zijn essentieel geweest voor het project. Onder andere je kritische blik en hang naar eenvoud van expressie zijn zeer leerzaam geweest. Wellicht nog belangrijker, de diepgang waarmee je fysica naar mathematiek vertaalde was voor mij in eerste instantie een nogal verontrustende openbaring ('waar heeft ie 't nou weer over') maar naar gelang de tijd vorderde zeer leerzaam. Dit heeft in belangrijke mate bijgedragen aan mijn groeiende overtuiging dat modellen werken. Beste Peter, jij was er altijd voor een goed gesprek. Je bent een uitstekend didacticus en hebt mij in een aanzienlijk aantal momenten het licht doen zien schijnen. Jouw vermogen om te werken met de gedachtenspinsels van anderen (*c.q.* de mijne) heeft niet alleen aanzienlijk bijgedragen aan dit boekje maar is voor mijzelf ook waardevol en leerzaam geweest. Jouw kennis van hartmechanica, continuümsmechanica, en de eindige-elementen methode waren voor mij een goeie (en nodige) back-up.
Beste Dick, dank voor je toeziend oog. De werkbesprekingen waren zonder uitzondering nuttig voor de structuur en voortgang van het project.
De leden van de beoordelingscommissie, prof. dr. R.S. Reneman, prof. dr. A. Huson, prof. dr. ir. A. Hoeks, dr. K. Nicolay, en dr. ir. A.J.G. Schoofs, dank voor het beoordelen van het manuscript.

Beste Bert, dank voor je ondersteuning op het gebied van optimalisatietechnieken. Jouw kennis van dit vakgebied is in belangrijke mate bepalend geweest voor de keuze van optimalisatiestrategie.
Beste Klaas, dank voor je inzet bij het verrichten van de DTI-metingen.

Mijn kamergenoot Frank wil ik bedanken, voor het meedenken in trage momenten, de prettige sfeer, de lunches in het donkere restaurant, en de oosterse inzichten. Beste Jan, het heeft je niet meegezeten de laatste tijd. Ik wil je bedanken voor het aanhoren van mijn geklaag, met name in mijn beginperiode. Hans, bedankt voor het verzetten van werk waar ik zelf bijna niet meer aan toe kwam. Andere mensen op het lab, Aurelio en Michael, dank voor de hulp, soms onmisbaar, en de prettige sfeer. De rest van de vakgroep wil ik bedanken voor hun commentaar vanaf de

zijlijn: Jean, Léon, Peter, Steven, Arnold, Xander, Roel, Jacqueline, Lucienne en Dick alsook Esther, Victor en Di bedankt voor de gezelligheid. Mensen van de vakgroep bewegingswetenschappen, in het bijzonder Jos, René, Maarten, Matthijs, Paul, dank voor inhoudelijke gesprekken, het voetbal (tot in de gang), de sporadische lunchloop, en de gezelligheid. Ook wil ik Hans Snijders en Dennis Roddeman bedanken voor hun hulp bij Diana problemen. Gerard, je volharding wat betreft je eigen boekje en de wending die je leven, zij het niet geheel uit vrije wil, heeft genomen geven me moed te doen wat belangrijk is. Ik ben blij dat je nog in Maastricht woont. Erik, ook jou doe ik hier geen recht door je simpelweg te bedanken - overigens zou ik niet precies weten waarvoor, in ieder geval voor vriendschap. Matthijs, dank voor gezelligheid en nuttige gesprekken over onderzoek, kids, en het artsenleven.

Familie valt voor mij in een categorie waarbij het uitspreken van dank traditioneel als overbodig wordt beschouwd en soms een zeer onhandig gevoel geeft - beste pa en ma, zonder jullie zou dit natuurlijk niet mogelijk zijn geweest. Oli4 en Kat hebben ook al heel lang bijgedragen aan dit werk. Oli4's concept van de kaft, op zeer korte termijn, wordt zeer op prijs gesteld.
Syl en Gebbe, dit hebben we nu achter de rug.

Curriculum vitae

July 1968	Born in Enschede, The Netherlands
1979-1986	St. Andrew's Secondary School, Blantyre, Malawi
1986-1990	Master of Engineering (Mechanical Engineering) study program at the University of Leeds, Leeds, England
1988-1989	Exchange student in the Department of Mechanical Engineering of the University of Waterloo, Waterloo, Canada
1990-1992	Medical student at the Free University of Amsterdam, Amsterdam, The Netherlands
1992-1997	Research assistant in the Department of Biophysics, Cardiovascular Research Institute Maastricht, Faculty of Medicine, Maastricht University, The Netherlands